INVESTIGATIONS INTO THE VIRUS-LIKE PARTICLE BACTERIOPHAGE Qβ AS A CARRIER PLATFORM IN CONJUGATE VACCINES AGAINST CANCER AND ALZHEIMER'S DISEASE

By

Hunter Sean McFall-Boegeman

A DISSERTATION

Submitted to
Michigan State University
in partial fulfillment of the requirements
for the degree of

Chemistry–Doctor of Philosophy

2022

ABSTRACT

INVESTIGATIONS INTO THE VIRUS-LIKE PARTICLE BACTERIOPHAGE Qβ AS A CARRIER PLATFORM IN CONJUGATE VACCINES AGAINST CANCER AND ALZHEIMER'S DISEASE

By

Hunter Sean McFall-Boegeman

Traditional vaccines are made of either killed or live-attenuated viruses. Killed virus vaccines may suffer from weak immune responses and live attenuation is an inexact science that can take years. There has been an interest in developing alternative vaccine technologies. One class of vaccine technology that has shown promise is the subunit conjugate vaccine. In such vaccines only antigenically relevant portions of infectious agents are conjugated to a carrier capable of stimulating a stronger immune response. The use of virus-like particles as carriers in conjugate vaccines has shown promise, allowing for the targeting on non-traditional vaccine targets. In this dissertation we report on the use of the virus-like particle Qβ as a carrier in conjugate vaccines targeting cancer and Alzheimer's disease.

Cancer's ability to escape the immune response requires a total immune response ensure that cancer does not mutate and return resistant to previously used immunotherapies. Previous use of Qβ-based conjugate vaccines against cancer have focused eliciting humoral responses. Herein we report lessons learned from the attempts to functionalize Qβ to elicit cellular immune response in a manner that would minimize the effect on a potential humoral response.

Alzheimer's disease is one of the most common causes of dementia and is hallmarked by the aggregation of tau. A Qβ-based conjugate vaccine targeting the tau-tau binding sites was synthesized and evaluated. Immunization generated a strong humoral immune response superior to a KLH-based conjugate vaccine targeting the same epitope. Generated antibodies

were able to preferentially recognize disease associate forms of tau and stain tau in human tissue.

To my wife, Sarah McFall-Boegeman, thank you for your unwavering love and support.
And to my son, Derek McFall-Boegeman, you are the fuel that pushed me across the finish line.

ACKNOWLEDGEMENTS

First, I would like to thank my advisor Dr. Xuefei Huang, for giving me the space to go down the rabbit holes I found. His understanding that my passion was in teaching chemistry and allowing me to take the time and opportunities to advance my teaching.

I would like to thank my guidance committee, Dr. Liangliang Sun, Dr. Xiangshu Jin, and Dr. Kevin Walker for their advice and guidance navigating my graduate school career. I would also like to thank all of the support staff and specialists in the Department of Chemistry and Institute for Quantitative Health Science and Engineering for their help navigating the paperwork associated with completing a graduate program and training me to use the department's instrumentation. In particular, Dr. Dan Holmes for his assistance with the NMR; Dr. Anthony Schilmiller for teaching me how to troubleshoot the mass spectrometers; Dr. Matthew Bernard for teaching me the underlying principles of flow cytometry and panel development; and Dr. Kathy Severin for use of the A&P labs' instruments.

My fellow Huang group lab members have my eternal appreciation. Dr. Sherif Ramadan is one of the best teachers of carbohydrate synthesis there is. Dr. Suttipun "Berm" Sungsuwan introduced me to the biological techniques that formed the bases of this thesis. The questions and suggestions from the biological sub-group members, Dr. Xuanjun Wu, Dr. Zahra Rashidijahanabad, Dr. Seyedmehdi Hossaini Nasr, Dr. Jia Gao, Dr. Kunli Liu, Dr. Vincent Shaw, Dr. Setare Nick, Zibin Tan, Shivangi Chugh, Cameron Talbot, Ida Shafiei, Athar Nakisa, and Chia-Wei Yang, were tremendously helpful in analyzing my results and becoming confident in defending my interpretations. For the rest of the Huang group, Dr. Tianlu Li, Dr. Yuetao Zhao, Dr. Weizhun

Yang, Dr. Jicheng Zhang, Dr. Changxin Huo, Dr. Peng Wang, Dr. Kedar Baryal, Dr. Somnath Bhagat, Dr. Dushen Chen, Dr. Xingling Pan, Mengxia Sun, Morgan Mayieka, Po-Han Lin, and Vindula Alwis, the conversations and support over these last 6 years has meant a lot.

Finally, I would like to thank my friends and family. In particular, Dr. Katarina Keel who has been there to commiserate when our syntheses failed and to celebrate exciting breakthroughs by reminding each other to get out of the lab. The biggest thanks though has to go to my amazing wife, Dr. Sarah M^{c}Fall-Boegeman. I know moving to Michigan was scary and hard, but I am so proud of the life we have built here and cannot wait to see what the future holds for our small family.

TABLE OF CONTENTS

LIST OF TABLES x

LIST OF FIGURES xi

LIST OF SCHEMES xvii

KEY TO ABBREVIATIONS xviii

CHAPTER 1 MECHANISMS OF CELLULAR AND HUMORAL IMMUNITY THROUGH THE LENS OF VLP-BASED VACCINES 1

1.1 Introduction 1
1.2 Search Strategy 2
1.3 Virus-Like Particles as Carriers in Conjugate Vaccines 2
1.4 The Innate Immune Response 6
1.4.1 A Primer on the Innate Immune Response 6
1.4.2 Virus-Like Particle-Based Activation of the Immune System 7
1.5 Cellular Immunity 13
1.5.1 A Primer on Cellular Immunity 13
1.5.2 Presentation of Cytotoxic T Cell Epitopes by Antigen Presenting Cells 16
1.6 Humoral Immunity 19
1.6.1 A Primer on Humoral Immunity 19
1.6.2 B Cell Activation 21
1.7 Immunological Memory and Long-Term Efficacy 26
1.7.1 Long-Term Cellular Immunity 26
1.7.2 Long-Term Humoral Immunity 29
1.8 Concluding Thoughts 30
1.9 Potential Future Work 31
REFERENCES 34

CHAPTER 2 FUNCTIONALIZATION OF THE INTERIOR OF BACTERIOPHAGE Qβ WITH T CELL EPITOPES 52

2.1 Introduction 52
2.2 Results and Discussion 53
2.2.1 Covalent Functionalization of the Capsid Interior 53
2.2.1.1 Expression of a Qβ Mutant Containing the Unnatural Amino Acid Azidohomoalanine 53
2.2.1.2 Removal of Packaged RNA From Qβ 54
2.2.1.3 Conjugation With Small Molecule Cargo 55
2.2.1.4 Hydrophobic Epitopes Destabilize the Capsid 56

2.2.2 Covalent Functionalization of the Packaged RNA 57
2.2.2.1 Conjugation to RNA Through Thiosemicarbazides 57
2.2.2.2 Loading Efficiency 58
2.2.2.3 *In Vitro* Testing 59
2.2.2.4 *In Vivo* Testing 62
2.2.3 Non-Covalent Functionalization of the Packaged RNA 64
2.2.3.1 Synthesis of Thiazole Orange-CDM 64
2.3 Conclusions 67
2.4 Future work 68
2.5 Materials and Methods 69
2.5.1 General Experimental Procedures and Methods for Synthesis 69
2.5.2 Expression of wt Qβ 70
2.5.3 Expression of $Q\beta_{T93AHA}$ Mutants by Global Methionine Replacement 70
2.5.4 Purification of Qβ or $Q\beta_{T93AHA}$ 71
2.5.5 Lead Mediated Hydrolysis of Capsid RNA 71
2.5.6 Synthesis of OVA Peptides Used in the Study 72
2.5.7 General CuAAC Click Reaction Conditions 72
2.5.8 Covalent Functionalization of Capsid RNA 73
2.5.9 Bone Marrow-Derived Dendritic Cell (BMDC) Isolation and Culture 74
2.5.10 General Flow Cytometry Protocol 75
2.5.11 Cross-Presentation Assay 75
2.5.12 B3Z T Cell Activation Assay 75
2.5.13 Harvesting of Cells from Spleens and Lymph Nodes (LNs) 76
2.5.14 *In Vivo* CTL Activity Assay 76
2.5.15 Flow Cytometry Analysis of T Cell Populations 77
2.5.16 Synthesis of TO-CDM 77
APPENDIX 82
REFERENCES 109

CHAPTER 3 A VLP-BASED CONJUGATE VACCINE TO PREVENT TAU OLIGOMERIZATION IN ALZHEIMER'S DISEASE 114
3.1 Introduction 114
3.2 Results and Discussion 116
3.2.1 Synthesis and Characterization of Vaccine Constructs 116
3.2.2 Vaccination Induces Long Lasting Immune Responses 117
3.2.3 Antibodies Produced are Capable of Recognizing Hyperphosphorylated, Monomeric, and Oligomeric Tau 120
3.2.4 Immunized Serum Recognizes Tau in Patient Brain Tissue 123
3.2.5 *In Vitro* Protection Testing 125
3.2.6 Examination of a Qβ Mutant as an Improved Carrier 127
3.2.7 *In Vivo* Protection Studies 128
3.2.8 Development of a Monoclonal Nanobody 129
3.3 Conclusions and Future Work 130
3.4 Materials and Methods 131

3.4.1 General Methods 131
3.4.2 Synthesis of Qβ-GMBS-Tau and mQβ-GMBS-Tau 132
3.4.3 Synthesis of KLH-GMBS-Tau 132
3.4.4 Synthesis of BSA-GMBS-Tau 133
3.4.5 Expression and Purification of $Tau_{151-391}$ and 2N4R Tau 133
3.4.6 Western Blotting 134
3.4.7 Immunohistochemistry 135
3.4.8 Immunofluorescence 136
3.4.9 p-Tau Aggregation Assay 136
3.4.10 Immunization of Mice 137
3.4.11 Evaluation of Antibody Titers by ELISA 137
3.4.12 Competitive ELISA 138
3.4.13 Ammonium Sulfate Cut 139
3.4.14 Llama Immunization 139
APPENDIX 141
REFERENCES 147

LIST OF TABLES

Table 1.1. Common VLPS, their natural targets, structural features, production methods, and the antigenic targets explored. 5

LIST OF FIGURES

Figure 1.1. (A) The repetitive surface of virus-like particles (VLPs) first activate antigen-presenting cells (APCs) through toll-like receptor (TLR) 2/6 heterodimers located on the cell surface. This activation causes APCs to enter a temporary state of alert. Following uptake of the VLPs, into the endosome, the capsid is disrupted releasing the VLPs genetic material. The released genetic material can then activate TLR 9 homodimers (DNA) or TLR 7/8 heterodimers (RNA). Activation of APCs through TLR 9 or TLR 8/7 induces a more potent activation of the APCs. (B) Upon injection VLPs can be up taken by APCs which then migrate to the lymph nodes and present the VLPs or their conjugated antigens to the cells of adaptive immune system. VLPs can also efficiently drain from the injection site to the lymph nodes due to their size..... 9

Figure 1.2. In conventional antigen presentation (left) cytosolic proteins are degraded by the proteosome. The resulting short peptides are transported to the endoplasmic reticulum (ER) by transporter associate with antigen processing (TAP) proteins. There the peptides are loaded onto new major histocompatibility complex (MHC) class I molecules and sent to the cell surface by way of the Golgi. During cross-presentation (right) extracellular proteins are phagocytosed. Inside the phagosome, enzymes can degrade the captured protein into small peptides. The peptides can then be loaded onto either recycled MHC class I molecules from the cell surface or new MHC class I molecules delivered to the phagosome by endoplasmic reticulum-Golgi compartments (ERGICs) containing Sec22b. Other pathways include the protein or peptides escaping to the cytosol where they are processed by the proteosome. Following proteasomal processing, the peptides can enter the conventional antigen presentation pathway or return to the phagosome via TAP proteins transported to the phagosome via ERGICs. Regardless of pathway once the MHC class I is loaded with the cytotoxic T lymphocyte epitope (CTLe) it is sent to the cell surface..... 15

Figure 1.3. Organized antigen display is critical for B cell receptor (BCR) cross-linking. (A) Soluble antigens activate BCRs in a random fashion leading to little BCR cross-linking and thus a weak immune response. (B) Conjugation of antigens to a virus-like particle (VLP), such as Qβ, organizes the display of antigens. The organization increases the density of the activated BCRs leading to increased cross-linking and thus a stronger activation signal. This results in a more robust immune response. (C) Creation of immune synapse leading to BCR cross-linking and antigen processing. (1) Unbound BCRs do not interact with the native actin cytoskeleton; (2) BCR recognition of antigens leads to rearrangement of the actin cytoskeleton; (3) Myosin uses the remodeled actin cytoskeleton to pull antigen bound BCRs together; (4) Upon reaching a critical mass of antigen bound BCR, an intracellular vesicle containing a bud from the VLP envelope is formed; (5) The captured viral material is processed, and any captured major histocompatibility complex (MHC) Class II restricted antigens are presented on the B cell surface..... 23

Figure 2.1. (A) RNA (blue ribbon) inside the $Q\beta_{T93AHA}$ capsid (red-to-yellow ribbon) can be removed from the capsid, via lead-mediated hydrolysis, exposing the azide functionality. (B) Removal of the RNA from the capsid results in a change in the 260:280 abs ratio. (C) Native gel electrophoresis of intact $Q\beta_{T93AHA}$ capsids with or without lead treatment. RNA was visualized by ethidium bromide and protein was visualized by Coomassie blue staining. (D) DLS analysis of particle size before and after lead treatment. 55

Figure 2.2. Bone marrow-derived dendritic cells (BMDCs) can cross present SIINFEKL delivered by **vaccine construct 1**. BMDCs were pulsed with **vaccine construct 1** at different amounts. BMDCs were stained with anti-mouse H-$2K^b$ bound to SIINFEKL (Clone 25-D1.16). (A) Percentage of BMDCs that stained positive. Mean fluorescence intensity (MFI) gate for OVA^+ cells was set as the minimal MFI that would exclude 99% of cells from an unlabeled BMDC sample. (B) MFI of samples pulsed with different amounts of **vaccine construct 1**. 60

Figure 2.3. B3Z T cell activation assay. Bone marrow-derived dendritic cells (BMDCs) were co-incubated with varying concentrations of antigen in different forms. Following incubation, antigen loaded BMDCs were co-cultured with B3Z T cells. T cell activation was measured by the development of color from chlorophenol red-β-*D*-galactopyranoside with the absorbance measured at 570nm. All samples were measured in triplicate. *p*-values were calculated by a one-tailed *t*-test. $*p < 0.05$. 61

Figure 2.4. Percent increase in specific killing of $CSFE^{Hi}OVA^+$ splenocytes by mice (N = 3/group) immunized with either FITC-K(N_3)EQLESIINFEKL, an admix of FITC-K(N_3)EQLESIINFEKL and Qβ, or **vaccine construct 1**, compared to naïve mice. No difference was observed between immunization groups. 63

Figure 2.5. Analysis of CTL populations in immunized mice. (A) Immunization timeline. A group of 3 C57BL/6 mice were immunized 3 times bi-weekly with 0.48 µmol of cytotoxic T cell epitope (CTLe) as **vaccine construct 1** with 20 µg of MPLA as adjuvant. On D35, mice were sacrificed, and their spleens and lymph nodes were harvested. (B) Flow cytometry analysis was performed on the harvested cells. Cells were stained for CD45 (lymphocyte marker), CD3 (T cell marker), CD4 (helper T cell marker), CD8 (CTL marker) and tetramers against CTLe specific T cell receptors. Cells were gated for CTLs ($CD45^+CD3^+CD4^-CD8^+$) and the percentage of antigen specific CTLs was examined. Representative result shown. 64

Figure 2.6. The structure of thiazole orange. A small molecule dye capable of binding to RNA. 65

Figure 2.7. Size exclusion chromatography (SEC) traces of wt Qβ (green) and $Q\beta_{T93AHA}$ (Red), showed minimal size change in assembled capsids due to the engineered mutation. 83

Figure 2.8. Deconvoluted ESI-MS Spectrum of $Q\beta_{T93AHA}$ coat protein (CP). The spectrum was deconvoluted using MaxEnt1. 84

Figure 2.9. Dynamic light scattering (DLS) analysis, of $Q\beta_{T93AHA}$ particles before and after lead treatment, showed capsids retained their size after lead treatment. 85

Figure 2.10. Deconvoluted ESI-MS spectrum of $Q\beta_{T93AHA}$ conjugated with hexynoic acid. The peak at 14,123 was also present in the pre-sample blank. The spectrum was deconvoluted using MAXEnt1. The number of hexynoic acid molecules conjugated to each capsid was calculated using the relative intensities of the unmodified and modified $Q\beta_{T93AHA}$ peaks. 86

Figure 2.11. Fluorescence standard curve of FSTC used to calculate **vaccine construct 1** loading..... 87

Figure 2.12. ESI-MS spectrum of Alkyne-SIINFEKL. 88

Figure 2.13. HPLC spectrum of purified Fluorescien-K(N_3)EQLESIINFEKL. Samples were detected by UV-VIS at 220 nm (black trace) and 254 nm (magenta trace). 89

Figure 2.14. ESI-MS spectrum of Fluorescien-K(N_3)EQLESIINFEKL. 90

Figure 2.15. ^{1}H NMR Spectrum of **1**. 91

Figure 2.16. ^{13}C NMR Spectrum of **1**. 92

Figure 2.17. ^{1}H NMR Spectrum of **2**. 93

Figure 2.18. ^{13}C NMR Spectrum of **2**. 94

Figure 2.19. ESI-MS spectrum of **2**. 95

Figure 2.20. ^{1}H NMR Spectrum of **3**. 96

Figure 2.21. ESI-MS Spectrum of **3**..... 97

Figure 2.22. ^{1}H NMR Spectrum of **4**. 98

Figure 2.23. ^{13}C NMR Spectrum of **4**. 99

Figure 2.24. ESI-MS Spectrum of **4**..... 100

Figure 2.25. ^{1}H NMR Spectrum of **5**. 101

Figure 2.26. ^{13}C NMR Spectrum of **5**. 102

Figure 2.27. gCOSY Spectrum of **5**. 103

Figure 2.28. gHSQC Spectrum of **5**. 104

Figure 2.29. gHMBC Spectrum of **5**. 105

Figure 2.30. ESI-MS Spectrum of **5**. 106

Figure 2.31. ^{1}H NMR Spectrum of **CDM**. 107

Figure 2.32. ^{13}C NMR Spectrum of **CDM**. 108

Figure 3.1. A) In Alzheimer's disease hyperphosphorylation of tau leads to the exposure of microtubule binding regions (MTBRs). Tau dimerizes and continues to oligomerize through interactions between MTBRs, leading to neuronal cell death. (B) Antibodies against the MTBR region should block MTBR interactions preventing dimerization/oligomerization and increase the clearance of disease associated tau resulting in healthy neurons. 116

Figure 3.2. Immunization with Qβ-GMBS-Tau produced superior titers to immunization with KLH-GMBS-Tau. The antibodies elicited were mainly of IgG subtypes and mice responded to booster injections. (A) Longitudinal titers from mice (N = 5) immunized with either Qβ-GMBS-Tau or KLH-GMBS-Tau. (B) Immunoglobulin subtyping of D35 sera from mice immunized with Qβ-GMBS-Tau. (C) Pre- and post-boost titers from mice (N = 4) immunized with Qβ-GMBS-Tau that received another booster on D365.Titers were determined as the fold of dilution that gave an absorbance value above the average + 3*S.D. of the blank. All measurements were made in quadruplicates. *p*-values were calculated by a one-tailed *t*-test. *$p < 0.05$, **$p < 0.01$, ***$p < 0.001$. 119

Figure 3.3. Western Blotting against various tau constructs. Aβ42 was used as a negative control. (A) Sera from mice immunized with Qβ alone were unable to recognize oligomeric tau (tauO) or monomeric tau. (B) Sera from mice immunized with Qβ-GMBS-Tau recognized both tauO and monomeric tau. (C & D) positive controls using a commercial pan tau antibody (Tau5). (E) Sera from mice immunized with Qβ-GMBS-Tau were capable of recognizing hyperphosphorylated tau (p-tau). All tau species were based on the 2N4R isoform. Serum was used at a 1:500 dilution. Tau5 was used at a 1:1000 dilution. Goat anti-mouse-HRP was used as the secondary antibody at a 1:1000 dilution. Gels A-C were kindly performed by the Kayed lab. 121

Figure 3.4. D35 titers against various tau constructs. Individual sera (N = 5) from D35 mice immunized with Qβ-GMBS-Tau. ELISA plates were coated with the antigen indicated on the x-axis. Titer values were calculated as the value that gave a signal greater than Ave.+3*S.D. of the blank. 122

Figure 3.5. Immunohistochemistry (IHC) of human brain tissue from a patient with Alzheimer's disease or a healthy control. Slides were stained with either pre-immunization sera, D35 pooled sera from mice immunized with Qβ-GMBS-Tau, or the pan tau monoclonal antibody Tau5. Sera showed a similar staining pattern to a commercial anti-tau antibody in diseased tissue and no staining in healthy tissue. 124

Figure 3.6. Immunofluorescence staining of brain tissue from either a patient with Alzheimer's disease or a healthy age and gender matched control. Tissue was stained with DAPI, D365 pooled sera from mice immunized with Qβ-GMBS-Tau, or polyclonal anti-tau rabbit sera. To visualize the staining, serum antibodies were stained with either goat-anti-mouse-Alexa Fluor 488 or goat-anti-rabbit-Alexa Fluor 568. Sera and a commercial anti-tau antibody tended to overlap in diseased tissue and showed minimal staining in healthy tissue. 125

Figure 3.7. p-Tau aggregation assay results. Hyperphosphorylated tau (p-tau) was incubated with thioflavin S (ThS) and purified sera from mice immunized with either KLH-GMBS-Tau, Qβ-GMBS-Tau, Qβ, or pre-immunization sera. None of the tested sera showed a difference in p-tau aggregation compared to p-tau alone. 127

Figure 3.8. Immunization with mQβ-GMBS-Tau induced superior titers compared with Qβ-GMBS-Tau and resulted in 5 timesfewer anti-carrier antibodies. (A) Longitudinal ELISA titers against BSA-GMBS-Tau from mice (N = 5) immunized with either Qβ-GMBS-Tau or mQβ-GMBS-Tau. (B) D35 ELISA titers against Qβ from pooled sera from mice (N = 5) immunized with either Qβ-GMBS-Tau or mQβ-GMBS-Tau. The titers were calculated as the dilution that gave an absorbance > ave. + 3*S.D. of a blank. *p*-values were calculated by a one-tailed *t*-test. *$p < 0.05$, **$p < 0.01$, ***$p < 0.001$. 128

Figure 3.9. (A) IgG1 ELISA data from a llama immunized with mQβ-GMBS-Tau. (B) IgG2/3 ELISA data from a llama immunized with mQβ-GMBS-Tau. 130

Figure 3.10. Deconvoluted mass spectrum from Qβ-GMBS-Tau. Analysis of the peak intensities showed an average loading of 390 antigens per capsid or 2.2 antigens per coat protein (CP). 142

Figure 3.11. SDS PAGE gel of Serum pre- or post- purification. 5 µL of pre- and post-precipitation samples were run on a non-reducing SDS-PAGE gel. Protein was visualized using Coomassie Blue stain. 142

Figure 3.12. Sera purified by ammonium sulfate cut retained their activity. ELISA plates were coated with BSA-GMBS-Tau. Purified D35 sera from mice immunized with Qβ-GMBS-Tau was incubated at different dilutions. Antibody binding was observed using a goat anti-mouse HRP conjugated secondary antibody and TMB. The absorbance was measured at 450 nm. All samples were run in quadruplicate. 143

Figure 3.13. Deconvoluted mass spectrum from mQβ-GMBS-Tau synthesized using 5 eq. GMBS and 5 eq. of peptide. Analysis of the peak intensities showed an average loading of 244 antigens per capsid or 1.4 antigens per coat protein (CP). mQβ-GMBS-Tau with this loading was using in immunization studies with C57BL/6 mice. 144

Figure 3.14. Deconvoluted mass spectrum from mQβ-GMBS-Tau synthesized using 10 eq. of GMBS and 15 eq. of peptide. Analysis of the peak intensities showed an average loading of 393 antigens per capsid or 2.2 antigens per coat protein (CP). mQβ-GMBS-Tau with this loading was used in immunization studies with rTg510 mice. 144

Figure 3.15. (A) Reaction conditions for the synthesis of BSA-GMBS-Tau. (B) MALDI TOF MS spectra showing BSA-GMBS-Tau and unmodified BSA. The peak shift shows an average loading of 17.5 antigens per BSA. 145

Figure 3.16. SDS-PAGE gel of $Tau_{151-391}$-TEV-HIS purification. 10 µL of sample from each step was retained and run on a reducing SDS-PAGE gel. Protein was visualized using Coomassie Blue stain. 145

Figure 3.17. SDS PAGE gel of Tau_{1-441} Purification. 10 µL of sample from each step was retained and run on a reducing SDS-PAGE gel. Protein was visualized using Coomassie Blue stain. 146

LIST OF SCHEMES

Scheme 2.1. An azide handle was installed on the interior of Qβ's capsid by site-directed mutagenesis of T93M, which was followed by global methionine replacement with azidohomoalanine (AHA) during expression. 54

Scheme 2.2. Functionalization of $Q\beta_{T93AHA}$ via copper-catalyzed azide alkyne cycloaddition (CuAAC) click chemistry. Cargo was either hexynoic acid (model alkyne) or alkyne-SIINFEKL (CTLe). 56

Scheme 2.3. The 3'-end of the capsid RNA can be oxidized by treatment with sodium periodate ($NaIO_4$) resulting in the dialdehyde. Incubation with fluorescein thiosemicarbazide (FSTC) results in covalent functionalization of the capsid RNA. 58

Scheme 2.4. Oxidation of 3'-end of the capsid RNA was performed by treatment with sodium periodate ($NaIO_4$) to form a dialdehyde. Hex-5-ynehydrazide was conjugated to the dialdehyde to allow for copper-catalyzed azide alkyne cycloaddition (CuAAC) click fuctionalization. Cargo was fluorescein-K(N_3)EQLESIINFEKL. 59

Scheme 2.5. Immunization schedule for *in vivo* cytotoxic T cell (CTL) experiment. Groups of 3 C57BL/6 mice were immunized 3 times bi-weekly with 0.48 μmol of CTL epitopes (CTLes) as either fluorescein-K(N_3)EQLESIINFEKL, an admix of Fluorescein-K(N_3)EQLESIINFEKL and Qβ, or **vaccine construct 1** with 20 μg of MPLA as adjuvant. On D35, animals received an injection of $CSFE^{Hi}OVA^{+}$:$CSFE^{Lo}OVA^{-}$ labeled splenocytes via tail vein injection. 24hrs later mice were sacrificed with spleens and lymph nodes collected. Flow cytometry was performed to examine the $CSFE^{Hi}OVA^{+}$:$CSFE^{Lo}OVA^{-}$ ratio. 62

Scheme 2.6. Synthesis of TO-CDM (A) initial attempts to directly incorporate a protected amine in the first step never gave more than trace product. (B) Redesigned TO-CDM synthesis. 67

Scheme 3.1. (A) Reaction scheme for synthesis of Qβ-GMBS-Tau. Average loading was determined by ESI-MS (B) Reaction scheme for synthesis of KLH-GMBS-Tau. 117

Scheme 3.2. Immunization schedule. Groups of 5 C57BL/6J mice were immunized 3 times bi-weekly with 9.6 nmol of peptide, as either Qβ-GMBS-Tau or KLH-GMBS-Tau, with 50 μL of alum as an adjuvant. Serum was collected on days 0 (pre-immunization), 21, 35, 70, and 90. 118

KEY TO ABBREVIATIONS

2-ME	2-Mercaptoethanol
7-AAD	7-Aminoactinomycin D
ACN	Acetonitrile
AHA	Azidoohomoalanine
APC	Antigen Presenting Cell
BBB	Blood-Brain Barrier
BCR	B Cell Receptors
BMDC	Bone Marrow-Derived Dendritic Cell
BSA	Bovine Serum Albumin
CDM	3-(4-Methyl-2,5-dioxo-2,5-dihydrofuran-3-yl)propanoic Acid
CDR	Complementary Determining Region
cGAMP	Cyclic GMP-AMP
CIES	Carrier Induced Epitope Suppresion
CNS	Central Nervous System
CP	Coat Protein
CpG	unmethylated Cytosine and Guanine
CPMV	Cowpea Mosaic Virus
CPRG	Chlorophenol Red-β-*D*-Galactopyranoside
CSFE	Carboxyfluorescein Succinimidyl Ester
CTL	Cytotoxic T Lymphocyte

CTLe	Cytotoxic T Lymphocyte Epitope
CuAAC	Copper Catalyzed Azide-Alkyne Cycloaddition
DAMP	Damage Associated Molecular Patterns
DAPI	4’,6-Diamino-2-phenylindole
DC	Dendritic Cell
DCM	Dichloromethane
DLS	Dynamic Light Scattering
DMF	Dimethylformamide
DMSO	Dimethylsulfoxide
DPBS	Dulbecco’s Phosphate Buffered Saline
DTT	Dithiothreitol
EDTA	Ethylenediaminetetraacetic Acid
EGRIC	Endoplasmic Reticulum-Golgi Compartment
ELISA	Enzyme-Linked Immunoassay
ER	Endoplasmic Reticulum
ESI-MS	Electrospray Ionization-Mass Spectrometry
Et_2O	Diethyl Ether
EtOAc	Ethyl Acetate
EtOH	Ethanol
FACS	Fluorescence-Activated Cell Sorting
FBS	Fetal Bovine Serum
Fmoc	9-Fluorenylmethyloxycarbonyl

FPLC	Fast Protein Liquid Chromatography
FSTC	Fluorescein Thiosemicarbazide
GM-CSF	Granulocyte-Macrophage Colony-Stimulating Factor
GMBS	4-Maleimidobutyric Acid *N*-Hydroxysuccinimide Ester
GPI	Glycosylphosphatidyl Inositol
HBcAg	Hepatitis B Core Antigen
HBsAg	Hepatitis B Surface Antigen
HEPES	4-(2-Hydroxyethyl)-1-piperazineethanesulfonic Acid
HMGB1	High Mobility Group Box 1
HPV	Human Papilloma Virus
HRP	Horse Radish Peroxidase
HSP	Heat Shock Protein
IACUC	Institutional Animal Care and Use Committee
IF	Immunofluorescence
IgG	Immunoglobulin G
IgM	Immunoglobulin M
IHC	Immunohistochemistry
KLH	Keyhole Limpet Hemocyanin
KPB	Potassium Phosphate Buffer
LCMS	Liquid Chromatography-Mass Spectrometry
LN	Lymph Node
LPS	Lipopolysaccharide

MART-1	Human Melanoma-Associated Antigen 1
MeOH	Methanol
MFI	Mean Fluorescence Intensity
MHC	Major Histocompatibility Complex
MØ	Macrophage
MoMLV	Molony Murine Leukemia Virus
MPLA	Monophosphoryl Lipid A
mQβ	$Q\beta_{A38K/A40C/D102C}$
MTBR	Microtubule Binding Regions
MWCO	Molecular Weight Cut-Off
NFT	Neurofibrillary Tangle
NIR	Near-Infrared
NLR	NOD-Like Receptor
OOM	Order of Magnitude
OVA	Ovalbumin
p-Tau	Hyperphosphorylated Tau
PAMP	Pathogen Associated Molecular Patterns
PapMV	Papaya Mosaic Virus
PBS	Phosphate Buffered Saline
pI	Isoelectric Point
PMBC	Peripheral Blood Mononuclear Cells
PMSF	Phenylmethylsulfonyl Fluoride

PPV	Porcine Parvovirus
PRR	Pattern Recognition Receptor
PVDF	Polyvinylidene Fluoride
RBC	Red Blood Cell
RHDV	Rabbit Hemorrhagic Disease Virus
ROS	Reactive Oxygen Species
RSV	Respiratory Syncytial Virus
SARS-CoV-2	Severe Acute Respiratory Syndrome Coronavirus 2
SDS-PAGE	Sodium Dodecyl Sulfate-Polyacrylamide Gel Electrophoresis
SEC	Size Exclusion Chromatography
STING	Stimulator of Interferon Genes
TAP	Transporter Associated With Antigen Processing
TauO	Oligomeric Tau
TBAI	Tetrabutylammonium Iodide
TCR	T Cell Receptor
TFA	Trifluoroacetic Acid
THF	Tetrahydrofuran
THPTA	Tris-hydroxypropyltriazolylmethylamine
ThS	Thioflavin S
TIPS	Triisopropylsilane
TLR	Toll-Like Receptor
TMB	3,3’,5,5’-tetramethylbenzidine

TMV	Tobacco Mosaic Virus
TO	Thiazole Orange
V_H Chain	Variable Heavy Chain
VHH	Single Variable Heavy Chain
V_L Chain	Variable Light Chain
VLP	Virus Like Particle
WHO	World Health Organization

CHAPTER 1 MECHANISMS OF CELLULAR AND HUMORAL IMMUNITY THROUGH THE LENS OF VLP-BASED VACCINES

This is an Accepted Manuscript of an article published by Taylor & Francis in *Expert Review of Vaccines* on January 11th, 2022, available online: https://www.tandfonline.com/doi/full/10.1080/14760584.2022.2029415. Further permissions related to the material excerpted should be directed to the Taylor & Francis Group.

1.1 Introduction

The current Severe Acute Respiratory Syndrome Coronavirus 2 (SARS-CoV-2) viral outbreak has highlighted the need for rapid vaccine development. Traditional vaccines are generally made of inactivated or live-attenuated viruses. As an example, the influenza virus is grown in chicken eggs before being purified and deactivated or killed as part of the vaccine formulation. Finally, adjuvants, stabilizers, and fillers are added before packaging. This is a labor and resource intensive process. The World Health Organization (WHO) estimates that it is a ~6-month process from identification of a new flu strain to commercial incorporation in seasonal flu vaccines.[1] This is for a well-studied virus such as influenza. If it is an entirely new viral pathogen, such as SARS-CoV-2, the process can be substantially slowed down partly because the process of attenuation is an inexact and time-consuming process to ensure safety of the vaccine. As a result, there have been attempts to reduce vaccines to just the key antigenic portions of the virus.[2] If only one or two proteins or carbohydrates are relevant to the protective immune response, recombinant expression or synthesis of these subunit antigens of interest presents a more homogenous construct, resulting in a simplified vaccine formulation.

Unfortunately, subunit vaccines are often associated with poor immunogenicity and short-lived immune responses.[3] Despite these setbacks, the appeal of a well-defined subunit

vaccine has endured. To overcome the low inherent immunogenicity or stimulate long-lived immune responses, the antigenic targets have been conjugated to immunogenic carriers that boost the immunogenicity. These conjugate vaccines come in all shapes and sizes, from single antigens covalently conjugated to small molecule adjuvants to hundreds of copies of the antigen on nanoparticle carriers.[4-8] Boosting the immunogenicity of antigens and the magnitude of the immune response have allowed the possibility of vaccines targeting non-viral diseases such as cancer, high cholesterol, Alzheimer's, and bacterial infections.[9-16] As a result, the field of conjugate vaccines is ever growing. This review will focus on a mechanistic understanding of the use of virus-like particle-based conjugate vaccines to elicit cellular and humoral immunity.

1.2 Search Strategy

Publications were identified through Searches on PubMed, Google Scholar, and SciFinder Scholar and through the bibliographies/references of relevant literature. Searches were conducted using keywords including, virus-like particles, VLP, and conjugate vaccines, alone and in combination with specific terminology related to different parts of the immune response. There was no date restriction.

1.3 Virus-Like Particles as Carriers in Conjugate Vaccines

Virus-like particles (VLPs) are protein-based nanoparticles made up of repeating copies of a coat protein(s). These structures usually include the surface proteins and another macromolecule (RNA, DNA, or protein) encapsulated to aid in the assembly of a capsid.[17, 18] Because of their viral origin, VLPs almost always contain a helper T cell epitope that can boost the immune response and bias it towards a long-lasting immunological memory.[19] Initial forays into the use of VLPs in vaccination strategies utilized human viral capsids such as Hepatitis B

surface antigen (HBsAg) or Human Papilloma Virus (HPV) L1 Major Capsid Protein.[20, 21] Commercial vaccines against HPV and hepatitis B have been approved using recombinant VLPs. These vaccines have been safe and widely effective.[22-24] Yet, there is much to learn based on clinical observations, such as the effect of age of vaccination on levels of antibodies elicited.[25]

The use of fusion proteins with these recombinantly expressed capsids sparked the wave of interest in using VLPs as conjugate vaccine platforms. The drawbacks of these VLPs are that as the natural viruses can infect humans, the human immune system may be pre-exposed to the VLP. The previous exposure to the carrier may hinder the immune response towards the vaccine.[26, 27] This underlying phenomenon is called carrier induced epitope suppression (CIES). While CIES is an observed phenomenon, it does not seem to be a major factor for every VLP in determining therapeutic efficacy.[27-30]

Concerns over CIES have led to interests in VLPs based on viruses that do not infect humans. An example is the bacteriophage Qß, which naturally infects *E. coli*. In nature, Qß is a T=3 icosahedron made of 179 copies of a 14kDa coat protein (CP), one copy of a maturation/lysis protein (required for infection and cellular escape), and an RNA-polymerase.[31, 32] A non-infectious version of the Qß VLP can be formed by recombinantly expressing just the coat protein in *E. coli*. In such a system, 180 copies of the CP make up the capsid and incorporates RNA from Qß and *E. coli.* The RNA content is consistent from batch to batch with an average of 3 strands with a length of ~800nt/strand.[33] Expression levels are also relatively high, reaching 30-50mg/L of culture media range in laboratory scale shake flasks.[34, 35] The non-infectious capsid can accommodate a wide range of modifications, either with covalent conjugates, non-covalent packaging using the RNA/REV tag, or fusion proteins.[34, 36-39] While the majority of these modifications have been

aimed at eliciting humoral immunity, there has been evidence of a cellular immune response.[40, 41]

Similar to Qß, most VLPs are aided in assembly by interactions between RNA and proteins, usually via a hairpin loop in the RNA with the interior of the CP.[18, 42] A small minority, typically double stranded DNA (dsDNA) viruses, utilize interactions between a scaffold protein and the CP. One of the most common examples is the enterobacteria phage P22. The recombinantly expressed VLP is a T=7 icosahedron made up of 420 copies of the CP and ~250 copies of the scaffolding protein.[43] The scaffold protein is amenable to a large range of modifications allowing for easy loading of the capsid interior.[44]

Besides recombinant expression in *E. coli* as used in the previous two examples, another common expression vector is plants. For example, the Tobacco Mosaic Virus (TMV), which is a 304±5 nm long rod-shaped virus made up of >2,100 repeating copies of its 17.5kDa CP, can be expressed by transfecting *N. benthamiana* plants, a close relative of tobacco, in yields of >7mg/g of infected tissue.[45, 46]

There are other VLPs that are being explored as potential carriers. Information on them can be found in **Table 1.1**. As they come up in this review, more information about them is provided as well.

VLP		Natural Targets	Recombinant Structural components	Shape and Size	Production Method	Antigens Targeted	Citations
Bacteriophage Qß		*E. coli*	180 copies of CP, RNA	Icosahedral (T=3) 24nm diameter	Recombinant Expression of the CP in *E. coli.*	MUC1, p33, D2, Tn, *Streptococcus pneumoniae,* OVA, PCSK9, ApoB, CETP, HPV, Tau, Nicotine, GD2	12, 14, 35, 40, 41, 47-55
Enterobacteria phage P22		*Salmonella typhimurium*	420 copies of CP, ~250 copies of scaffold protein, dsDNA	Icosahedral (T=7) 60nm diameter	Recombinant expression of CP and scaffold protein in *E. coli*	M/M2 proteins of RSV	56
Tobacco Mosaic Virus (TMV)		Plants related to the tobacco family	>2100 copies of CP, RNA	Rod-shaped 304±5nm in length	Transient transfection of *N. benthamiana*	OVA, GFP, p15e melanoma	46, 57
Hepatitis B	Surface Antigen (HBsAg)	*Homo sapiens*		22nm diameter	Yeast expression	HPV E7, SARS-CoV-2	20, 58
	Core Antigen (HBcAg)	*Homo sapiens*		29.4nm diameter	Cell Free Protein Synthesis	Lymphocytic Choriomeningitis virus (LCMV) p33, *Toxoplasma gondii*, FLAG, D2	48, 59-62
Papillomavirus Family		*Varies*	Varies	Varies	Varies	HPV E7, HIV gp160, Hen egg lysozyme	63-65
Pseudomonas Phage PP7		*Pseudomonas aeruginosa*	180 copies of CP, RNA	Icosahedral (T=3) 25nm diameter	Recombinant Expression of the CP in *E. coli.*	HPV, *Staph. aureus*	15, 66, 67
Molony Murine Leukemia Virus (MoMLV)		*Mus musculus*	Gag, Env, RNA, lipid bilayer	200nm diameter	Transient expression in mammalian cells	Glycoprotein epitope 33-41 of LCMV, Zika virus	68, 69
Rabbit Hemorrhagic Disease Virus (RHDV)		*Oryctolagus cuniculus*	180 copies of VP60, RNA	Icosahedral (T=3) 32-44nm diameter	Recombinant Expression of VP60 in *E. coli.* or Baculovirus	OVA, MART-1 melanoma antigen, Mel888 tumor lysate	70, 71
Mosaic Virus Family		*Varies*	Varies	Varies	Varies	p33, gp100, Influenza M1, M2	72-75
MS2		*E. Coli*	180 copies of CP, RNA	Icosahedral (T=3) 26nm diameter[76]	Recombinant expression in Yeast	Prostate Cancer, HPV	77, 78
Human Immunodeficiency Virus-1 Gag		*Homo sapiens*				HIV gag, pr55 gag,	79, 80
Parvovirus		*Varies*	Varies	Varies	Varies	OVA, LCMV	64, 81

Table 1.1. Common VLPs, their natural targets, structural features, production methods, and the antigenic targets explored.

Besides enhancing the immunogenicity of epitopes conjugated to them, VLPs' inherent stability can be an advantage over other vaccine technologies. There are a growing number of examples of VLP-based vaccines retaining their immunogenicity after drying and prolonged storage.[54, 82-84] Unlike other next generation vaccine platforms, such as mRNA vaccines which require ultra-cold temperature and the associated cold-chain, dried VLP-based vaccines would be easier to deliver and administer in low resource environment.[85] Although this discussion has focused on the VLP-based vaccine stability in terms of storage, their stability *in vivo* may also play an important role in the efficacy of VLP-based vaccines. Unfortunately, there is a paucity of evidence about the stability and half-lives of VLPs *in vivo*. More research is needed to explore VLP stability *in vivo* and its effect on the immune response.

1.4 The Innate Immune Response

1.4.1 A Primer on the Innate Immune Response

As a field, innate immunity is well-reviewed.[86-89] This section will thus be a short primer on the key events in the innate immune response and its role in kickstarting adaptive immunity. Upon injury or insult, such as an injection, local cells release chemokines that recruit antigen presenting cells (APCs) to the site. Once there, APCs, such as dendritic cells (DCs) and macrophages (MØs), sample the extracellular and intracellular (released from leaking or dying cells) environment for potential antigens. They collect information from the external environment through a mixture of phagocytosis, pinocytosis, and receptor mediated endocytosis. Unlike the receptors we will discuss in relation to cellular and humoral immunity, the receptors on innate immune cells recognize broad patterns and are not unique to each individual cell. Activation or maturation of the APCs occurs through activation of pattern

recognition receptors (PRRs), such as toll-like receptors (TLRs), stimulator of interferon genes (STING), or NOD-like receptors (NLRs).[90-93] These PRRs have evolved to recognize highly conserved pathogen associated molecular patterns (PAMPs) or molecules released by damaged cells (Damage Associated Molecular Patterns—DAMPs). PAMPs range from small molecules, like lipopolysaccharides (LPS) or cyclic GMP-AMP (cGAMP), to large repetitive protein patterns. DAMPs can include lysosomal proteases, DNA, mitochondrial DNA, adenosine triphosphate, and High Mobility Group Box 1 (HMGB1). Different PRRs are found in different regions of the cell ranging from the cell surface (TLRs 1, 2, 4, 5, 6, & 11), to sub-cellular compartments (STING, TLRs 3, 7, 8, 9), and the cytosol (NLRs).[94] Following antigen uptake, some activated APCs attempt to control the localized infection while others migrate to the lymph nodes to activate the adaptive immune response.

1.4.2 Virus-Like Particle-Based Activation of the Immune System

Canonically, the belief was that VLPs do not activate the immune system until they have entered immune cells. There is growing evidence that VLPs activate the immune system earlier than previously believed. Using Heat Shock Protein (HSP) VLPs, which do not contain any genetic material, Richert and colleagues reported that intranasal treatment of mice with the VLPs primed DCs and alveolar MØs in the lung.[95] Further studies using other VLPs including P22 revealed this priming was occurring via a TLR2 dependent mechanism (**figure 1.1A**).[96] TLR2 is located on the cell surface and recognizes repeating protein patterns regardless of sequence. This expands to repeating protein structures regardless of whether it is in a spherical or linear repeating pattern. Although both spherical and linear patterns are recognized by TLR2, they activate separate activation pathways, by coactivation of TLR6 and TLR1 respectively.[96] Following the uptake of

VLPs by APCs and activation of the APCs, the APCs migrate to the lymph nodes allowing for the interaction with the adaptive immune system (**figure 1.1B**). This includes skin-derived DCs which have been identified as the initial transporter of herpes simplex virus to lymph nodes for CTL priming.[97]

After the initial activation and recruitment of APCs, the VLPs are phagocytosed. This phagocytosis occurs through non-specific pathways including macropinocytosis, micropinocytosis, and phagocytosis.[64, 70] In addition, VLPs derived from viruses that infect humans may enter the cells through receptor mediated pathways. In the phagolysosomes, the acidic environment and proteases break down the protein shell exposing the genetic material of RNA or DNA encapsulated, which is recognized by TLRs 7/8 or 9 respectively. Comparatively, the activation signals from TLRs 7/8 or 9 appear more important for the activation of an adaptive immune response. This has been evidenced by the short protective window obtained by the innate immune activation and weaker overall immune responses when using VLPs without the genetic material.[96]

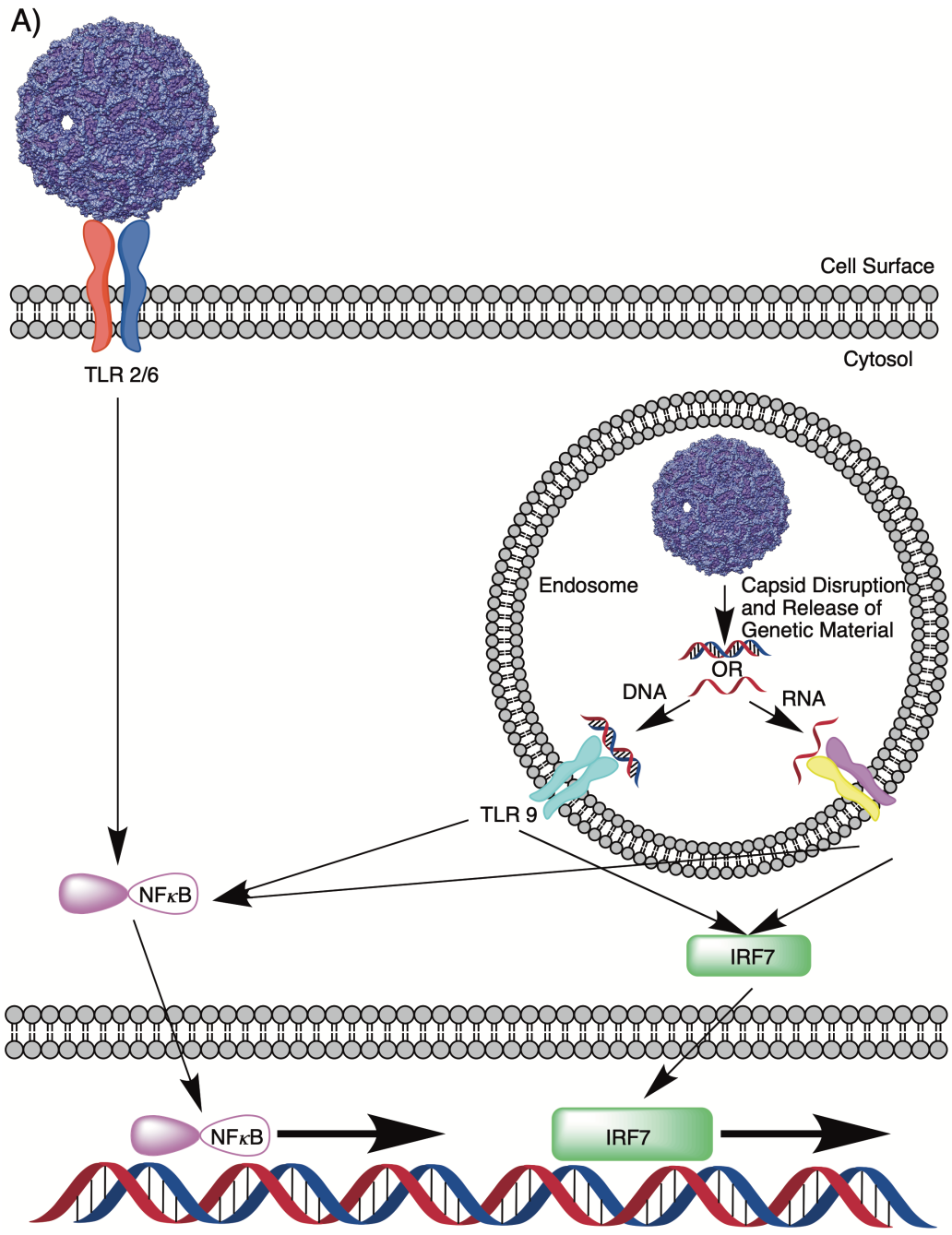

Figure 1.1. (A) The repetitive surface of virus-like particles (VLPs) first activate antigen-presenting cells (APCs) through toll-like receptor (TLR) 2/6 heterodimers located on the cell surface. This activation causes APCs to enter a temporary state of alert. Following uptake of the VLPs, into the endosome, the capsid is disrupted releasing the VLPs genetic material. The released genetic material can then activate TLR 9 homodimers (DNA) or TLR 7/8 heterodimers (RNA). Activation of APCs through TLR 9 or TLR 8/7 induces a more potent activation of the APCs. (B) Upon injection VLPs can be up taken by APCs which then migrate to the lymph nodes and present the VLPs or their conjugated antigens to the cells of adaptive immune system. VLPs can also efficiently drain from the injection site to the lymph nodes due to their size.

Figure 1.1. (cont'd)

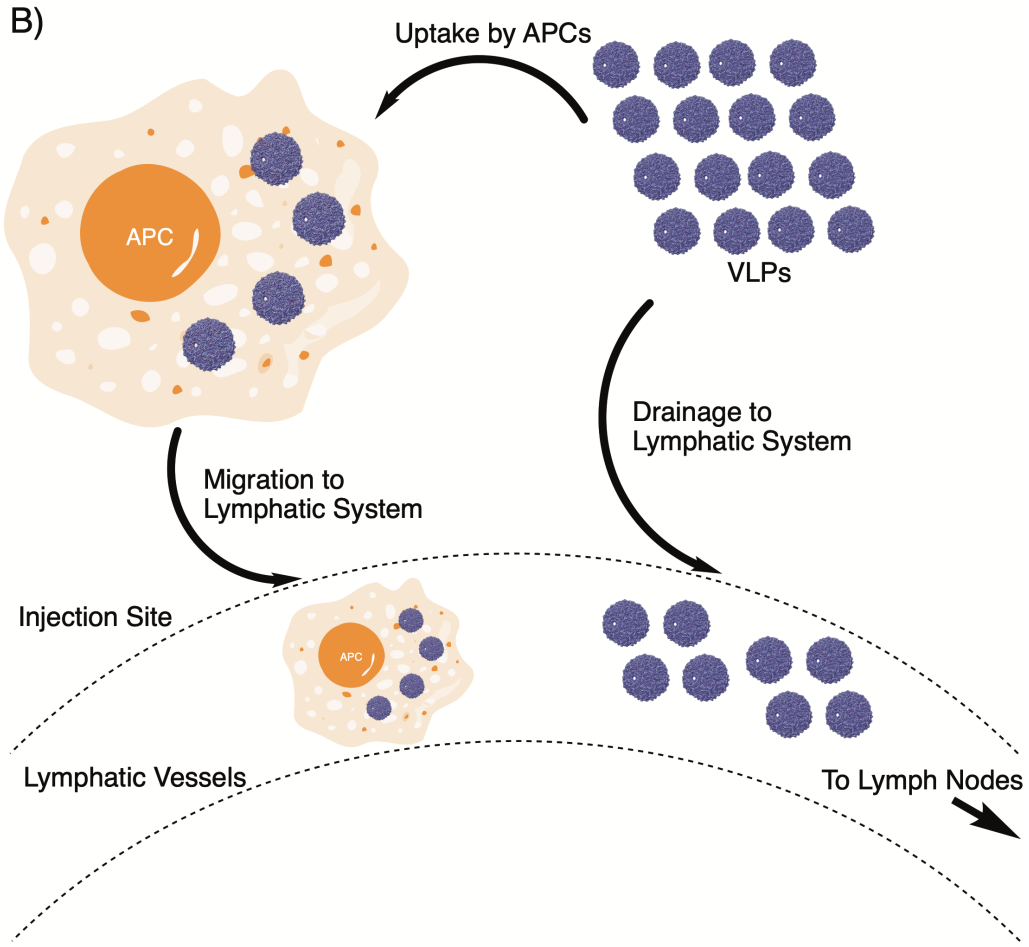

As some VLPs do not contain or can be prepared without the genetic material, there is an interest in overcoming the weak activation without TLR7/8 or 9 activation.[98-101] The simplest approach is to add an exogenous adjuvant to the vaccine formulation. To make sure the adjuvant affects the same cells that take up the VLPs, adjuvants have been covalently conjugated to or packaged in the VLPs. On the other hand, there is evidence that covalent linking of antigen and adjuvant to the same molecule may not be necessary, as the VLP is the major factor in which cells uptake the particles.[41, 102] Conjugation to the same type of VLP should result in similar uptake levels of VLPs loaded with antigen vs. VLPs loaded with adjuvant. One of the more commonly utilized adjuvants, for cytotoxic T lymphocyte (CTL) based vaccines, has been synthetic

oligodeoxynucleotides containing unmethylated cytosine and guanine (CpG). CpG activates TLR9, creating a T_H1 biased response that leads to strong B cell and T cell responses.[103] Another advantage of CpG is that, as a DNA analog, it can be used to replace the naturally occurring genetic material in VLPs.[104] This replacement can usually occur because for certain VLPs, such as Qß, assembly is dependent on interactions between the negatively charged phosphate backbone of the genetic material and the interior of the CPs. Substituting the genetic material with a well-characterized adjuvant has a further potential advantage. The genetic material packaged inside Qß may be well determined for size, length, and quantity, as compared to the host RNA encapsulated, the sequences of which are not well characterized.[33] That could pose a problem for regulatory approval for clinical applications due to batch-to-batch variability. A work around is replacing the genetic material with CpG. Although as with any solution, it has its pros and cons. CpG has a good safety profile. However, it can still lead to the overactivation of an inflammatory immune response causing immune dysregulation including cytokine storms which can be fatal.[105] Depending on the cells targeted, a potentially safer alternative is poly(I:C), a TLR-3 ligand.[106, 107]

Besides adding adjuvants that activate the entire immune response, with the concern of potential severe over-activation, there has been work on engineering VLPs to activate only one type of immune cells. Because of their large size, VLPs drain from the site of infection into the lymphatic system and end up in the draining lymph nodes.[108, 109] This is part of what makes them excellent at eliciting strong humoral responses. It also can be advantageous for cellular immunity, as naïve T cells are located in the paracortex along with DCs.[110] There, VLPs that display activation ligands for co-stimulatory receptors on T cells can bind their cognate receptors boosting activation and differentiation. Derdak *et. al.* showed that Moloney murine leukemia virus

(MoMLV) VLPs decorated with a TCR/CD3 ligand, CD80, and ICAM-1 can cause differentiation in T cells without the help of APCs.[68] Further experiments showed that the replacement of TCR/CD3 ligand with MHC class I molecules containing preprocessed antigens, can elicit antigen specific T cell responses. Although highly intriguing, this approach is specific to the VLP used.

Most VLPs reported in the literature are non-enveloped, meaning that they do not contain a lipid bilayer coating the exterior of the VLP. MoMLV VLPs have an envelope that the researchers used to anchor the ligands through glycosylphosphatidyl inositol (GPI).[111] Without the bilayer, these ligands would have to be either covalently linked or fused to the CPs. Although VLPs are known for their stability, there are limitations to VLP stability to fusion proteins, and conjugates have to be evaluated on a case-by case basis, especially if more than one ligand is to be fused to the capsid.[67, 112] This is not to exclude the possibility that injection and infiltration to lymph nodes could result in some VLPs providing co-stimulatory signals while APCs process and display the antigens. However, there is evidence that some co-stimulatory signals may be the result of size-dependent discrimination from the point of contact between the APC and the T cell.[113, 114] As such, care should be taken in ligand choice. Fusion or covalent linkers could change the spacing between the VLP's surface and cell surface effecting what ligands are excluded.

Another consideration to take is if the researcher is trying to elicit a total immune response, attaching T cell epitopes on the external surface may interfere with B cell responses, as B cell receptor signaling is highly dependent on an organized display of B cell antigens.[115] To overcome this, a general design is to use the surface of the VLP to display B cell antigens and co-stimulatory signals needed to enhance the B cell responses, while functionalizing the interior with CTL epitopes (CTLes) or adjuvants. An example of why this is important comes from the work of

Alam *et. al.*[51] Aryl mannosides conjugated to the surface of Qß altered the fate of the immune response through activation of DC-SIGN and enhanced the cellular immunity. However, the boosting of the cellular immunity came at the expense of the humoral immune response, as one would expect due to the interruption of the B cell epitope display by the aryl mannoside ligand.[51]

1.5 Cellular Immunity

1.5.1 A Primer on Cellular Immunity

There have been many excellent reviews of cellular immunity and of its individual components.[116-120] As such, this section will only be a quick primer on the major steps of the cellular immune response**.** The first step in any immune response is the activation of innate immune cells including APCs. These APCs migrate to the site of infection and sample the extracellular and intracellular (released from apoptotic cells) environment for potential antigens. Afterwards some APCs, usually a mixture of MØs and DCs, migrate to the lymph nodes. The sampled antigens are processed in order to be displayed to naïve T cells in the lymph nodes. Once in the lymph nodes, the APC's display the CTLes using major histocompatibility complex (MHC) class I molecules. If a T cell receptor (TCR) on a naïve T cell recognizes the MHC:CTLe complex, a maturation signal is received by the T cells. As a result, the activated T cells undergo clonal expansion creating a pool of effector T cells. These CTLs then migrate to the site of infection, which sample the cells in the surrounding tissue. Nearly all cells in the body produce MHC class I complexes and use them to display intracellular peptides as a signal of the cell's health status. When CTLs find cells displaying MHC:CTLe complexes that their TCRs recognize, they release granzyme and perforins to kill such cells by disrupting the cell membrane and causing apoptosis. After the initial infection is controlled, the large number of CTLs produced during clonal

expansion is no longer needed. The CTL population undergoes a contraction, leaving behind memory subpopulations in case of repeat exposure to the same pathogen.

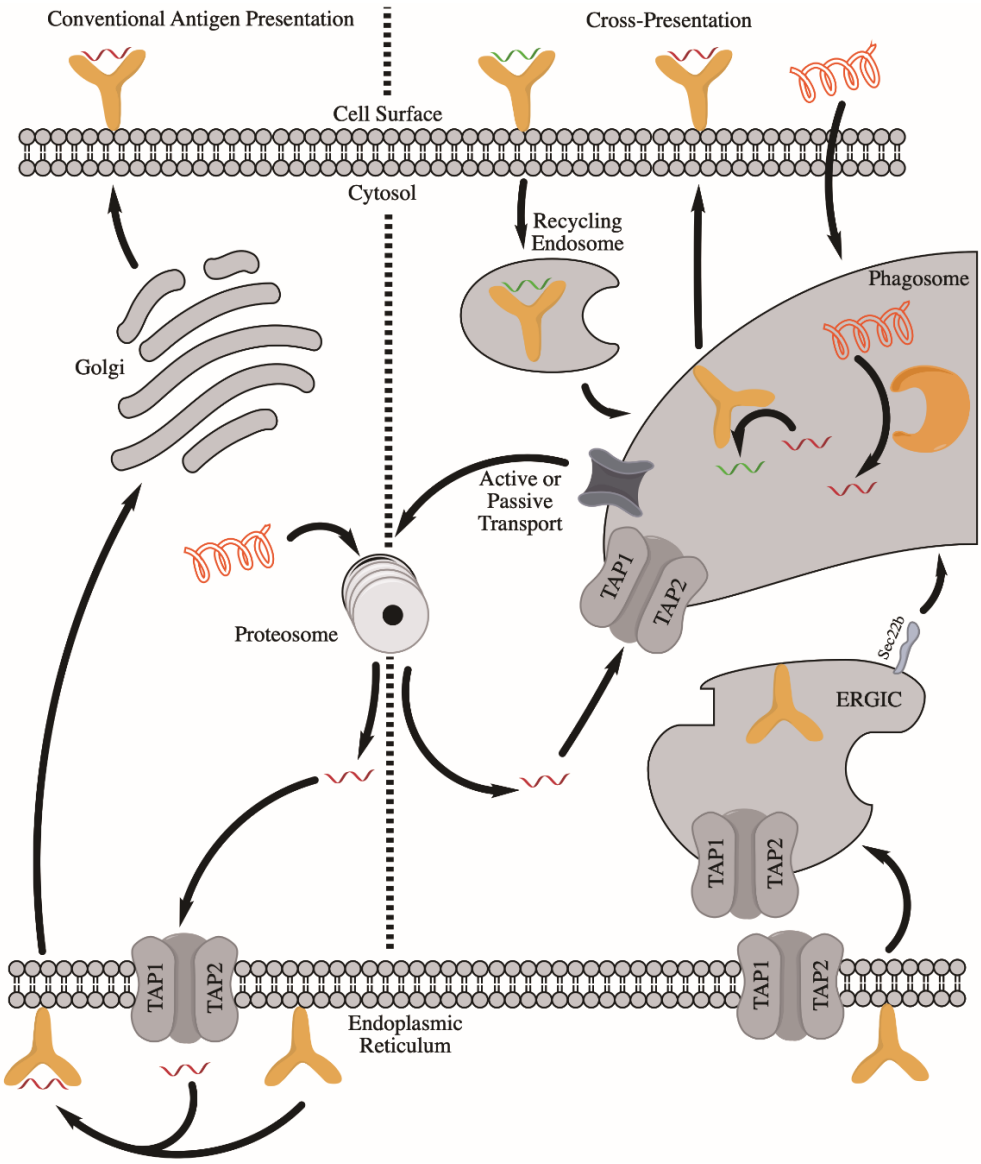

Figure 1.2. In conventional antigen presentation (left) cytosolic proteins are degraded by the proteosome. The resulting short peptides are transported to the endoplasmic reticulum (ER) by transporter associate with antigen processing (TAP) proteins. There the peptides are loaded onto new major histocompatibility complex (MHC) class I molecules and sent to the cell surface by way of the Golgi. During cross-presentation (right) extracellular proteins are phagocytosed. Inside the phagosome, enzymes can degrade the captured protein into small peptides. The peptides can then be loaded onto either recycled MHC class I molecules from the cell surface or new MHC class I molecules delivered to the phagosome by endoplasmic reticulum-Golgi compartments (ERGICs) containing Sec22b. Other pathways include the protein or peptides escaping to the cytosol where they are processed by the proteosome. Following proteasomal processing, the peptides can enter the conventional antigen presentation pathway or return to the phagosome via TAP proteins transported to the phagosome via ERGICs. Regardless of pathway once the MHC class I is loaded with the cytotoxic T lymphocyte epitope (CTLe) it is sent to the cell surface.

1.5.2 Presentation of Cytotoxic T Cell Epitopes by Antigen Presenting Cells

Because most VLP-based vaccines targeting T cell responses do not attempt to directly activate T cells, attention must be paid to the cross-presentation pathway in APCs. Cross-presentation is not as simple as the name suggests. It is not a single pathway but is a combination of multiple pathways that result in the same outcome, i.e., fragments of proteins of extracellular origin presented on MHC class I molecules. **Figure 1.2** shows the complex nature of cross-presentation. The first step regardless of pathway is phagocytosis of the VLP by the APC. The phagosome then fuses with the lysosome creating a phagolysosome. Here is where the pathways diverge. There are three main cross-presentation pathways with each having minor pathways, which are still being fiercely debated in the literature.[119, 121-123]

In the conventional antigen presentation (left side of **figure 1.2**) of MHC class I molecules, cytosolic proteins are processed into short peptides (~8-10 a.a.). Subsequently, they are transported by the transporter associated with antigen processing (TAP) proteins to the endoplasmic reticulum (ER), where the peptides are loaded onto MHC class I molecules and shipped to the cell surface.

The simplest form of cross-presentation (right side of **figure 1.2**) mimics the conventional antigen presentation process closely. After intake to the phagolysosome, proteins or peptides escape into the cytosol and are further processed by the proteasome. Then they are transported to the ER, loaded onto MHC molecules and displayed on the cell surface. While this seems straightforward, there are competing pathways out of the phagolysosome. pH changes and reactive oxygen species (ROS) can cause “leaky” endosomes allowing for passive escape. Meanwhile, active transport out of the phagolysosomes has been shown to occur through

Sec61.[124] To aid in escape, there have been attempts to increase passive escape by utilizing cell penetrating peptides fused to the antigenic peptide.[125]

Another pathway is through recycling of MHC class I molecules. As the interior membrane of the phagolysosome used to be the cell surface, proteins from the cell surface including MHC class I molecules can be trapped in the phagolysosomes. In the phagolysosomes, proteins are processed into the short antigenic peptides, which can then be loaded directly onto MHC class I molecules in phagolysosomes and presented onto the cell surface again.

The final "main" pathway involves ER-Golgi intermediate compartments (ERGICs). These ERGICs are used to transport cargo from the ER to the Golgi.[126] These compartments are believed to be directed to the phagolysosomes through Sec22b, where they can deliver new MHC class I molecules, TAP proteins, and other transporters.[121, 123, 127] This allows the phagolysosomes to act similarly to the ER in MHC loading.

Which of the three aforementioned pathways dominates is up for debate, as is which pathway is important for antigens delivered by VLP-based vaccines.[119, 128] There is very little work discussing cross-presentation of antigens delivered by VLPs. The scant information indicates the results may depend on the VLP utilized. Work from Win *et. al.* suggests it is through endosomal recycling of MHC class I molecules, by exploring cross-presentation of ovalbumin (OVA) and human melanoma-associated antigen (MART-1) delivered by rabbit hemorrhagic disease virus (RHDV)-based VLPs.[70] To study cross-presentation, inhibitors of specific pathways were utilized, which include lactacystin to inhibit proteasomal processing, US6 to prevent TAP-mediated transport, brefeldin A to inhibit vesicle secretion, bafilomycin A1 to prevent phagolysosome acidification, and primaquine to inhibit recycling of cell surface molecules. The final three

inhibitors act at different stages of endosomal recycling pathway and virtually erased cross-presentation as measured by activation of antigen-specific $CD8^+$ T cells. This was in direct contradiction to when soluble antigens were used. With soluble antigens, each inhibitor had some effects on the activation efficiency but did not completely abolish cross-presentation. This suggests that conjugation to VLPs shifted the importance of cross-presentation pathways to the endosomal recycling pathway. This was further supported by earlier work by Leclerc et. al. who used a similar lactacytsin based experiment to rule out proteasomal processing of antigens delivered by Papaya Mosaic Virus (PapMV) VLPs.[75] On the other hand, porcine parvovirus (PPV) VLPs loaded with OVA CTLes were cross-presented in a TAP and proteasome dependent, endosome-to-cytosol pathway.[64] Between the two extremes is the evidence provided by Ruedl et. al. They showed that DCs in TAP-deficient mice exhibited decreased cross-presentation efficiency compared to wild type mice when treated with Hepatitis B core antigen (HBcAg) VLPs but still retained the ability to activate potent T cell responses.[59] While each study used different sets of antigens overall, there were enough overlaps to suggest the different cross-presentation fates were likely due to the VLPs used in the studies. Taken together, these results indicate that the VLPs are biasing cross-presentation toward a certain pathway, but the exact mechanism is unknown. Size might be a determining factor as microspheres displayed size-dependent changes to cross-presentation efficiency when the proteosome was inhibited.[129] However, the smallest microspheres (d= 800nm) examined are the size of some of the largest VLPs known. This suggests that the differences described above are likely due to more than just size, as the RHDV (d= 32-44nm), PPV (d = 25-30nm), and HBcAg (d= 29.4nm) VLPs are an order of magnitude smaller than the microspheres.[130-133]

Despite these initial studies, more research is needed into the best design practices for optimizing or directing cross-presentation. This is a currently underexplored area of the literature, probably because after delivery to APCs, cross-presentation is a fairly robust process due to redundant minor pathways. A deeper understanding may lead to better designed and thus more effective vaccines. There are some studies into linker effects and epitope length (full length protein, epitope only, or extended epitopes).[134-139] For example, with RHDV VLPs loaded with gp100 CTLes, the two linkers utilized did not appear to play a role in the observed changes in immune response.[134] Instead, the differences were likely due to the decreased stability of the fusion proteins caused by the increasing number of hydrophobic CTLe repeats. Studies on non-conjugated subunit vaccines show that extended epitopes work best because they can escape lysosomes better/faster than the full protein, and yet are large enough to possibly contain sequences that aid in trafficking to the ER while the minimal peptide epitope does not.[137-139] These studies were aimed at free peptides only, so how conjugation or fusion to VLPs affects their efficacy needs to be established. Current studies are an excellent start, but deeper dives into the mechanisms of VLP-based conjugate vaccine cross-presentation would be very beneficial to guide further design.[59, 70, 75]

1.6 Humoral Immunity

1.6.1 A Primer on Humoral Immunity

Similar to the previous sections on cellular and innate immunity, this section will just be a brief primer because of the availability of numerous reviews focused solely on each sub-topic.[140, 141] The main effectors of humoral immunity are antibodies, which are produced by B cells. To activate naïve B cells, pathogens must migrate to the lymph nodes. There surface

antigens can be recognized by antigen specific B cell receptors (BCRs) on the cell surface. As BCRs are activated, they cross-link magnifying the maturation signals, which stimulate the B cell to proliferate and secrete pentameric immunoglobulin M (IgM) antibodies.[142] These antibodies are relatively low affinity and short lived, which are only the first step in the humoral response. During the activation process, the B cell engulfs the antigen and processes it, with the end product being MHC class II antigens presented on the B cell surface. If the B cell encounters a matched $CD4^+$ helper T cell with TCRs that recognizes the MHC Class II:peptide complexes on the B cell surface, it can undergo isotype switching, changing the subtype of antibodies produced from IgM to the other Ig isotypes. The specific isotype produced depends on the class of helper T cell, and the resulting cytokines they release. During isotype switching, the B cells also undergo somatic hypermutation. This is a rapid mutation of the gene encoding the variable region of the antibodies that leads to an increased binding affinity between the antibody and its cognate antigen. Following isotype switching, the B cell fully matures into a plasma cell and undergoes clonal expansion. The high affinity antibodies are then secreted into the bloodstream or mucosal barriers depending on the isotype. The effects the antibodies can have on the pathogen differ depending on their antigenic targets. They can prevent key receptor binding interactions (neutralizing), increase phagocytic clearance by MØs (opsonizing), trigger complement mediated cytotoxicity (CDC), or cause the formation of antigen-antibody plaques that are filtered from the bloodstream. Once the infection is under control, the plasma cells will undergo apoptosis. However, the memory subset of B cells will remain and can quickly reactivate and expand upon a secondary infection.

1.6.2 B Cell Activation

Naïve B cells reside mainly in the spleen and lymph nodes. In order to activate them, vaccines must be targeted to the lymphatic tissues. As discussed earlier, the sizes of VLPs are well-situated to track to lymph nodes (**figure 1.1B**). VLP's fate can be further controlled by the method of administration. Cubas et. al. utilized SHIV VLPs (SIV Gag + HIV SF162 Env) to test the immune responses following injections at various common injection sites.[109] VLPs were labeled with an IR dye and lymph nodes were harvested 24hr post injection. Intraperitoneal injection showed no VLPs in the lymph nodes and the amount of VLP in the lymph nodes increased going from subcutaneous to intramuscular and finally intradermal injection. The intradermal injection had detectable VLP levels in all four lymph nodes harvested. VLP levels in the lymph node correlated positively with the IgG titers and CTL efficacy. Therefore, caution should be taken when comparing immune responses across various studies. A relatively weak immune response could be due to the choice of the injection method and the resulting fate of VLPs tracking to lymph nodes. Additionally, the injection method can skew the class of Ig elicited. Intranasal immunization using a Qß-based vaccine against influenza was the only immunization method that elicited strong local IgA titers in the lung.[143]

Once in the lymph nodes, antigens must find naïve B cells that express BCRs capable of binding them. Binding of an antigen with a single BCR is often not sufficient for activation of naïve B cells (**figure 1.3A**). Cross-linking of multiple antigen-bound BCRs can induce a more potent response.[140, 144] VLPs, because of their repetitive surface structures, allow for both high valency and high density of antigen display (**figure 1.3B**). Use of polymers loaded with various antigens have shown that there is a minimum valency (~10-20) for effective B cell activation.[145] Most VLPs

contain >100 subunits so even at a 1:1 antigen:subunit ratio, the valency threshold can be readily reached. The issue comes from the density of the antigens on the VLP surface. There seems to be a sweet spot for antigen density, which makes sense because of the size of BCRs and their need to cross-link. At a certain point with increasing antigen density, there is a diminishing return as antigens become too clustered for BCRs to bind due to steric clashes. On the other hand, if the density is too low, the distance between antigen bound BCRs becomes too large for efficient cross-linking.

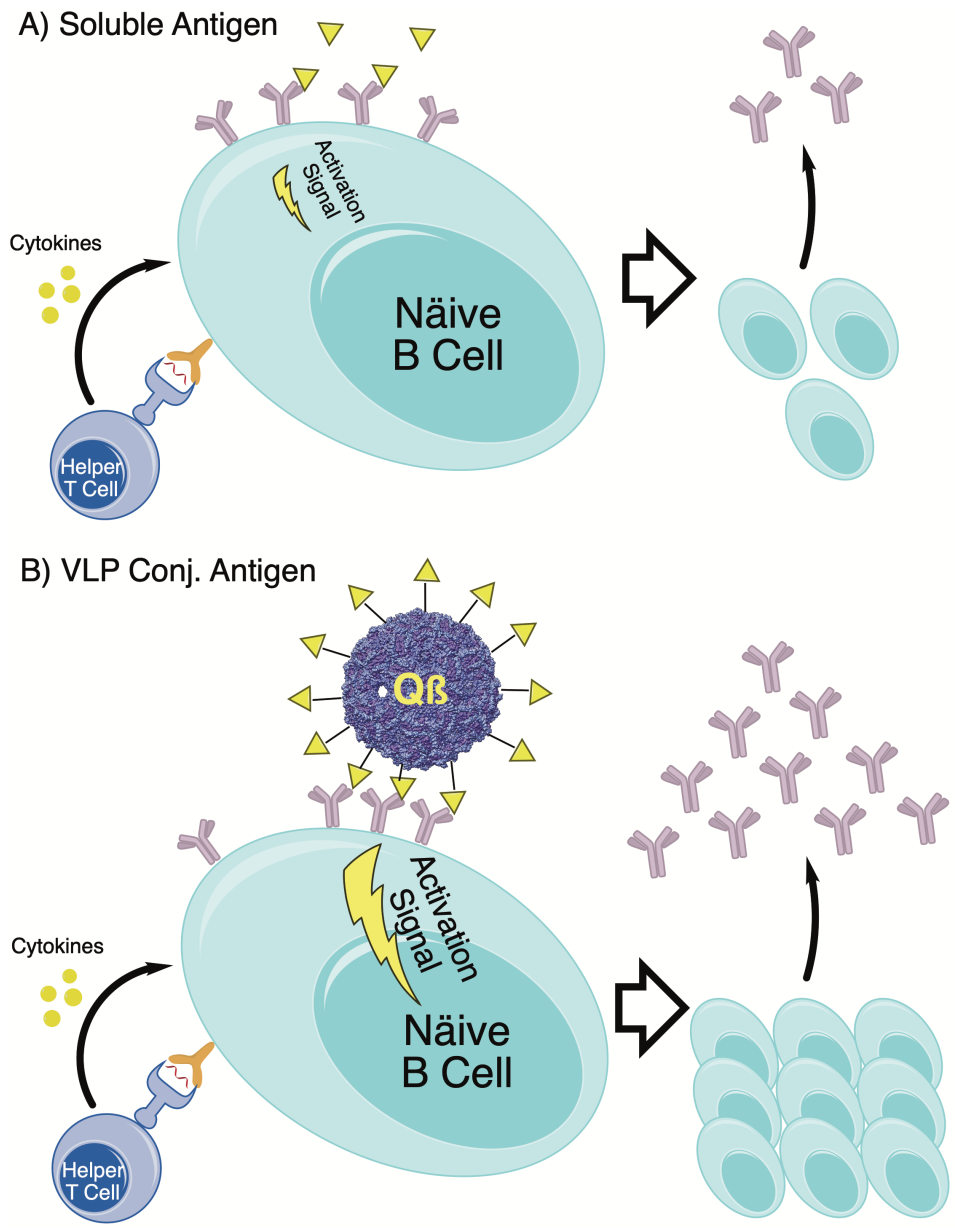

Figure 1.3. Organized antigen display is critical for B cell receptor (BCR) cross-linking. (A) Soluble antigens activate BCRs in a random fashion leading to little BCR cross-linking and thus a weak immune response. (B) Conjugation of antigens to a virus-like particle (VLP), such as Qβ, organizes the display of antigens. The organization increases the density of the activated BCRs leading to increased cross-linking and thus a stronger activation signal. This results in a more robust immune response. (C) Creation of immune synapse leading to BCR cross-linking and antigen processing. (1) Unbound BCRs do not interact with the native actin cytoskeleton; (2) BCR recognition of antigens leads to rearrangement of the actin cytoskeleton; (3) Myosin uses the remodeled actin cytoskeleton to pull antigen bound BCRs together; (4) Upon reaching a critical mass of antigen bound BCR, an intracellular vesicle containing a bud from the VLP envelope is formed; (5) The captured viral material is processed, and any captured major histocompatibility complex (MHC) Class II restricted antigens are presented on the B cell surface.

Figure 1.3. (cont'd)

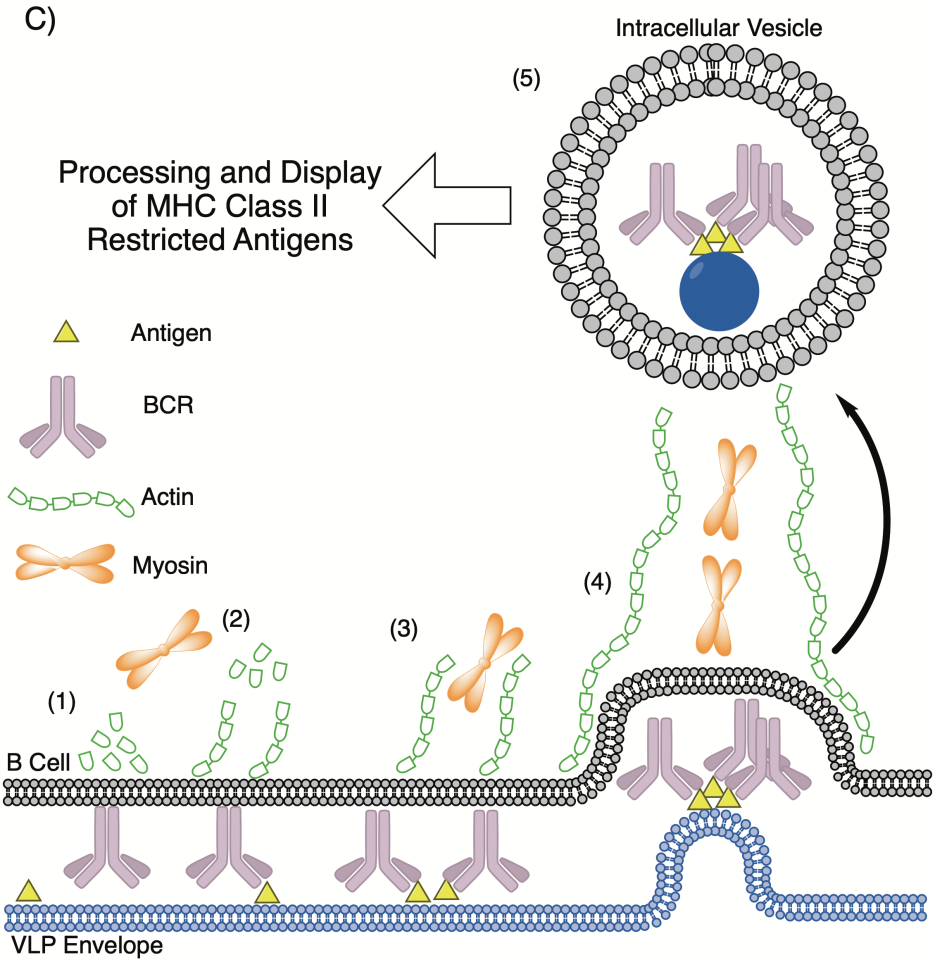

There are further biological reasons behind why antigens conjugated to VLPs can efficiently activate the immune system. Many viruses and bacteria have limited genomes, thus their structures are made up of densely repetitive structures. As a result, the immune system is sensitized toward such a PAMP, i.e., repeated patterns of epitopes spaced ~10 nm apart, or roughly the space between antigen binding sites on antibodies.[146, 147] Because this PAMP is associated with many viruses, it makes sense that most VLP coats are ideally arranged to activate B cells.[148] This pattern is so strong that it is transitive to conjugated antigens, including antigens usually selected against in B cell development.[40, 47, 62, 65]

For enveloped VLPs, density may play a less important role. Recent efforts in B cell activation research have been directed at identifying the mechanism of B cell activation by APC mediated antigen presentation. APCs and B cells form an immunological synapse mediated by monomeric BCR antigen interactions. These monomeric interactions signal for reorganization of the B cell actin cytoskeleton. The rearranged cytoskeleton and myosin pull antigen bound BCRs towards the center of the synapse causing the oligomerization required for B cell activation (**Figure 1.3C**).[149, 150] It is not hard to imagine a similar mechanism being possible with enveloped VLPs where the antigen is attached to the viral lipid bilayer, although this idea needs to be explored and validated.[68, 111]

Even more important to vaccines targeting humoral responses over cellular responses is the choice of the linker. Because they are processed prior to presentation, T cell epitopes are shown in a pristine manner. B cell epitopes on the other hand are usually presented to B cells prior to processing. This means that if the linker used is more immunogenic than the target epitope, the immune response may be redirected toward the linker instead of the target antigen. One prominent example is the triazole linker produced by the copper catalyzed azide-alkyne cycloaddition (CuAAC) reaction.[10, 151] While the CuAAC reaction is a favorite for biological conjugation, including vaccines, due to its specificity and high efficiency, the triazole ring formed competed against the antibody generation toward the target cancer antigen.[151] As a general rule of thumb, acyclic and flexible linkers are preferred to reduce the anti-linker immune responses and the resulting interference to the desired immune responses.

A recent development in conjugation techniques are non-covalent conjugation approaches, taking advantage of peptide or RNA binding sites. A commercial phage display

peptide library was used to identify a 7-mer peptide capable of binding to the surface of the cowpea mosaic virus (CPMV).[152] Another example is the use of the HIV Rev tag to load proteins on the interior of Qß via the RNA involved in capsid formation.[34, 39]

1.7 Immunological Memory and Long-Term Efficacy

1.7.1 Long-Term Cellular Immunity

Once the initial immune response eliminates the infection, there is less of a need for the large number of $CD8^+$ T cells. As a result, the pool of T cells undergoes a contraction.[153] While the pool of antigen specific T cells decreases, two main subsets of $CD8^+$ T cells remain, i.e., effector memory (T_{EM} cells) and central memory (T_{CM} cells).[154] T_{EM} cells circulate throughout the body. Upon subsequent infection, they are recruited to the site of infection and provide the initial defense through the classical contact mediated cytotoxicity, until a larger immune response can be mustered.

While the T_{EM} cells are preventing the establishment of a beachhead by the infection, APCs are sampling the infection and processing the antigens. When they reach the lymph nodes, they are able to activate T_{CM} cells. These T_{CM} cells are considered one of the more important factors in long-term cellular immunity. Upon reactivation, they undergo a process similar to clonal expansion, replicating the initial cellular immune response. The daughter cells from this population expansion are then able to differentiate into different T cell subsets. After the infection is under control again, the antigen specific T cell population undergoes another contraction leaving behind new/rejuvenated memory T cell sub-populations.

In the last decade a new subset of memory T cells, the tissue resident memory (T_{RM}), has been characterized.[155] The hallmarks of such cells are not cell surface markers but rather mainly

the fact that they are found in barrier tissues, such as the lungs, skin, reproductive tracts, etc. and do not circulate.[156, 157] In fact, T_{RM} cells can express different cell surface markers depending on the type of tissue they are in.[158] These cells are thought to play an important role in reactivation of the immune response to subsequent infections. VLP-based vaccines are able to elicit T_{RM} cells.[159] For example, intranasal immunization of mice with P22 loaded with M and M2 proteins from the Respiratory Syncytial Virus (RSV), fused to the P22 scaffold protein, was able to elicit T_{RM} cell populations in the lungs.[56] These cells were detected by flow cytometry analysis of bronchioalveolar lavage fluid up to 2 months post inoculation. Importantly while there was a small decrease in total cell counts for both M- and M2-specific T_{RM} cells, it was still protective as measured by lung viral titers, after re-challenge.

The T_{RM} mediated immune response to the secondary infection is due to a reverse of the traditional flow of information. As previously discussed, innate immune cells traditionally are the first cells to interact with pathogens through their recognition of PAMPs. Then they send signals to the adaptive immune system. Upon subsequent infection, T_{RM} cells recognize their cognate antigen. Instead of direct killing of the infected cells, they release cytokines (VCAM-1, IFN-γ, and TNF-α) to recruit innate and adaptive immune cells including DCs, T_{EM} cells, and memory B cells.[157, 160, 161] This creates a tissue-wide state of alert for infection.[162]

While T_{RM} cells seemingly play an important role in long-term cellular immunity to infectious pathogens, there is evidence that they also may play a role in immune regulation of cancers. As their main function is not direct killing of infected cells, it makes sense that they would express higher levels of inhibitory ligands/receptors including PD-1 and TIM-3. However, after the use of anti-PD-1 antibodies, they regain their cytotoxic abilities. This could explain the

outsized effectiveness of anti-PD-1 therapies in some individuals and the overall correlation between T_{RM} cell populations and cancer prognoses.[161, 163, 164] Elicitation of T_{RM} cells then should be measured post vaccination regardless of target, cancer or pathogen. As such, even though one of the draws to the use of VLPs as carriers in conjugate vaccines is the lack of a need for exogenous adjuvants, if the T_{RM} response is not strong enough for protection, adjuvants can be added to the vaccine formulation to boost the response. Of particular interest are zymosan, IL-1ß, or compounds to enable targeting certain DC subsets, most of which are being explored as adjuvants in VLP-based vaccines.[165-168] For further discussions about engineering vaccines to elicit T_{RM} cells, interested readers are referred to a recent review by Knight and Wilson.[169]

Beyond initial T cell responses, there is a paucity of evidence about the length of memory and protection from cellular immunity elicited by VLP-based vaccines, especially when compared to long-term antibody-based immunity. This makes sense due to the methodologies available for measuring immune responses between the two. For antibodies, the most commonly analyzed isotype is IgG, which can be easily measured through blood draws. Other non-circulatory isotypes can be measured through non-lethal means.[170] In comparison, the measurement of antigen-specific T cells populations, particularly the important T_{CM} cells, requires sacrifice of the subject to collect and analyze the lymphatic organs. This prevents longitudinal studies of a subject's immune response over time, and the need to collect samples from multiple time frames using multiple subjects can quickly escalate the population sizes and costs associated for the study. As such, there is a need to develop non-terminal methods of T cell analysis. Here lies an opportunity for VLPs to be utilized for such evaluations. One potential method for antigen-specific T cells could be to utilize VLPs functionalized with a tracking dye and MHC class I molecules loaded with

the relevant peptide. Because VLPs preferentially drain to the lymph node, they should be able to find and bind to antigen specific T_{CM} cells. While further development is needed to yield quantitative analysis results, as a non-lethal alternative, it is intriguing.

1.7.2 Long-Term Humoral Immunity

Initial activation of B cell leads to the expression of IgM, a pentameric isotype associated with the initial immune response and short lived-immune response. In order to generate a long-lived immune response, the B cells need to undergo isotype switching, which requires a costimulatory signal from a $CD4^+$ helper T cell. Here is the advantage of VLPs over other multivalent vaccine carriers. As immunogenic proteins themselves, VLPs contain peptide sequences identified as helper T cell epitopes.[171] After formation of the BCR micro clusters, the antigens bound to the BCRs are endocytosed and further processed to present helper T cell epitopes. Helper T cell epitopes are traditionally restricted to peptides. If the desired antibody target is not a protein, then without an additional helper T cell epitope formulated into the vaccine, the immune response will be suboptimal.[50, 141] VLPs avoid the need to include an additional factor, i.e., an exogenous helper T cell epitope, into vaccine design. Once the VLP is endocytosed and processed, the helper T cell epitope is presented on the B cell surface by MHC class II molecules. Follicular helper T cells in the lymph nodes then recognize the peptide:MHC complexes on the B cell. The resulting costimulatory signals trigger isotype switching, somatic hypermutation, and clonal expansion resulting in a large number of IgG secreting plasma and B cells.

As with T cells, once the infection is eliminated most of the antibody generating plasma cells are eliminated. This leaves behind a small population of memory B cells capable of quickly

responding to secondary infection. Even after the contraction, there is a small population of plasma cells that remain and secrete antibodies. VLP-based vaccines generate particularly high long-term titers, suggesting they are uniquely capable of eliciting long-lived plasma cells, although the exact reasoning is unknown. There is some evidence that factors beyond valency and density may be the cause.[172, 173] Upon re-infection, the memory B cell population can expand and differentiate into new plasma and memory cells. Memory B cells elicited by VLP-based vaccines are able to respond to secondary challenges as measured by IgG titers following a long-term booster.[55]

1.8 Concluding Thoughts

Overall, VLP-based conjugate vaccines pose an attractive solution to current issues in vaccine development. The variety of different VLPs, conjugation strategies, antigenic targets, and adjuvant choices present a great opportunity to fine-tune the immune response. However, there is a paucity of mechanistic understanding to guide the best practices in VLP-based vaccine design. A majority of the articles published in this field are of the proof-of-concept genre. The development of new techniques and knowledge about cellular mechanisms in the general field of immunology offer an exciting opportunity in VLP-based vaccine design. It is time to move beyond proof-of-concept to mechanistic investigations. We look forward to the availability of a powerful plug-and-play VLP-based vaccine platform, which can be rapidly deployed to address future disease outbreaks similar to SARS-CoV-2 or to personalized cancer vaccines. There is much for this field to explore but the future is bright.

1.9 Potential Future Work

While recent work has led to amazing advances in the field of virus-like particle-based vaccines, there is still more work to be done. It is time for the field to move beyond the current trend of empirical research design towards rational design based on solid theoretical and mechanistic understandings. An excellent example being the work done exploring cross-presentation of antigens delivered by VLPs.[59, 64, 70, 75] Another example being the work exploring the effect of stereochemistry on antigen stability.[52] General advances in the field of immunology have allowed for a deeper understanding of the complex interactions of immune cells. VLPs have the potential to probe the immune responses due to their ability to accommodate a wide variety of functionalization approaches. Furthermore, the use of enveloped VLPs could act as "simplified" cells for investigating specific receptor interactions, while care would have to be taken to account for multi-receptor/ligand interactions, including size discrimination-based interactions, like the need for CD45 exclusion from the binding site, for efficient opsonization of by macrophages.[114]

Due to their sizes, VLPs are well suited for imaging of the lymphatic system. Conjugation of ligands/receptors to the surface and functionalization with a wide variety of imaging probes to the interior could be utilized to monitor changes in the immune system *in vivo*. VLPs have been shown to be stable to functionalization with a wide range of biologically relevant molecules. Particularly, some VLPs are able to get large numbers of copies onto each capsid, in excess of 500 copies/VLP particle.[35] Development of carbohydrate analogues that exhibit increased specificity to one immune receptor than their natural form, such as HA, in conjunction with VLP particles could provide potent targeted imaging of the immune system.[174] The excellent safety profile of

VLPs combined with higher specificity would potentially mitigate some of the toxicity associated with current imaging dyes/procedures by lowering the required dose of the imaging agent. This would be especially beneficial for the analysis of T cell responses, enabling longitudinal monitoring for each subject. The use of radioactive PET tracers, near-infrared (NIR) dyes, RAMAN dyes, or other imaging modalities that have more tissue penetrating depth than standard fluorescent spectroscopy, could allow for semi-quantitative comparison of the magnitude of antigen specific T cell population[175]. A major hurdle to overcome would be non-specific interactions between VLPs or conjugated ligands with random cells. There is some work looking at maximizing/minimizing VLP interactions with certain cells.[176]

While the possibility of universal design rules for VLP-based vaccines are an attractive idea, looking at some of the contradicting reports in the literature and the complexity of known immunological pathways, there are likely to be design rules specific to each VLP.[27, 29, 30, 59, 70, 71, 75, 121-123, 127] Having knowledge of how different VLPs engage different immune pathways can allow for finer tailoring of the immune response. A pressing need is in the realm of personalized cancer vaccines. Some cancers downregulate MHC class I expression. Patients with such a cancer would benefit from a more robust humoral response, which could inform the decision on which VLP platform to build the vaccine on.

Previous reviews have called for the finding of a niche commercial application to drive virus-like particle-based vaccines through the rigorous process of clinical trials and regulatory approval.[177] Although three years is not a long time to see substantive change from when the review was published, the COVID-19 pandemic was a golden opportunity, seeing as it opened the door for another new type of vaccine platform (mRNA vaccines). As of January 2021 of 15 known

preclinical VLP-based vaccines against SARS-CoV-2, 2 made it to clinical trials (Trial IDs: ACTRN12620000817943, NCT04450004).[58, 178] All great journeys start with a single step. Hopefully these candidates will open the door for more VLP-based vaccines to make the jump from the lab to the clinic.

REFERENCES

REFERENCES

1. Pandemic Influenza Vaccine Manufacturing Process and Timeline. https://www.who.int/csr/disease/swineflu/notes/h1n1_vaccine_20090806/en/ (accessed May 6th, 2019).

2. Kleid, D. G.; Yansure, D.; Small, B.; Dowbenko, D.; Moore, D. M.; Grubman, M. J.; McKercher, P. D.; Morgan, D. O.; Robertson, B. H.; Bachrach, H. L., Cloned Viral Protein Vaccine for Foot-and-Mouth Disease: Responses in Cattle and Swine. *Science* **1981,** *214*, 1125-1129.

3. Vartak, A.; Sucheck, S. J., Recent Advances in Subunit Vaccine Carriers. *Vaccines* **2016,** *4*, 12.

4. Speir, M.; Authier-Hall, A.; Brooks, C. R.; Farrand, K. J.; Compton, B. J.; Anderson, R. J.; Heiser, A.; Osmond, T. L.; Tang, C. W.; Berzofsky, J. A.; Terabe, M.; Painter, G. F.; Hermans, I. F.; Weinkove, R., Glycolipid-peptide conjugate vaccines enhance $CD8^+$ T cell responses against human viral proteins. *Sci. Rep.* **2017,** *7*, 14273.

5. Compton, B. J.; Farrand, K. J.; Tang, C.-w.; Osmond, T. L.; Speir, M.; Authier-Hall, A.; Wang, J.; Ferguson, P. M.; Chan, S. T. S.; Anderson, R. J.; Cooney, T. R.; Hayman, C. R.; Yong, L.-K.; Metelitsa, L. S.; Zajonc, D. M.; Godfrey, D. I.; Gasser, O.; Weinkove, R.; Painter, G. F.; Hermans, I. F., T cell responses and tumour immunity by vaccination with peptides conjugated to a weak NKT cell agonist. *Org. Biomol. Chem.* **2019,** *17*, 1225-1237.

6. van der Put, R. M. F.; Kim, T. H.; Guerreiro, C.; Thouron, F. ç. o.; Hoogerhout, P.; Sansonetti, P. J.; Westdijk, J.; Stork, M.; Phalipon, A.; Mulard, L. A., A Synthetic Carbohydrate Conjugate Vaccine Candidate against Shigellosis: Improved Bioconjugation and Impact of Alum on Immunogenicity. *Bioconjugate Chem.* **2016,** *27*, 883-892.

7. Yin, Z.; Huang, X., Boosting Humoral Immune Responses to Tumor Associated Carbohydrate Antigens with Virus-like Particles. In *Carbohydrates in Drug Design and Discovery*, Jimenez-Barbero, J., Ed. Royal Society of Chemistry: UK, 2015; pp 132-149.

8. Yin, Z.; Delaney, S.; McKay, C. S.; Baniel, C.; Kaczanowska, K.; Ramadan, S.; Finn, M. G.; Huang, X., Chemical Synthesis of GM2 Glycan, Bioconjugation with Bacteriophage Qβ, and the Induction of Anticancer Antibodies. *ChemBioChem* **2016,** *17*, 174-180.

9. Patel, J. M.; Vartabedian, V. F.; Kim, M.-C.; He, S.; Kang, S.-M.; Selvaraj, P., Influenza Virus-Like Particles Engineered by Protein Transfer With Tumor-Associated Antigens Induces Protective Antitumor Immunity. *Biotechnol. Bioeng.* **2015,** *112*, 1102-1110.

10. Wu, X.; Yin, Z.; McKay, C.; Pett, C.; Yu, J.; Schorlemer, M.; Gohl, T.; Sungsuwan, S.; Ramadan, S.; Baniel, C.; Allmon, A.; Das, R.; Westerlind, U.; Finn, M. G.; Huang, X., Protective Epitope Discovery and Design of MUC1-based Vaccine for Effective Tumor Protections in Immunotolerant Mice. *J. Am. Chem. Soc.* **2018,** *140*, 16596-16609.

11. Lakshminarayanan, V.; Supekar, N. T.; Wei, J.; McCurry, D. B.; Dueck, A. C.; Kosiorek, H. E.; Trivedi, P. P.; Bradley, J. M.; Madsen, C. S.; Pathangey, L. B.; Hoelzinger, D. B.; Wolfert, M. A.; Boons, G.-J.; Cohen, P. A.; Gendler, S. J., MUC1 Vaccines, Comprised of Glycosylated or Non-Glycosylated Peptides or Tumor-Derived MUC1, Can Circumvent Immunoediting to Control Tumor Growth in MUC1 Transgenic Mice. *PLoS One* **2016,** *11*, e0145920.

12. Ortega-Rivera, O. A.; Pokorski, J. K.; Steinmetz, N. F., A Single-Dose, Implant-Based, Trivalent Virus-like Particle Vaccine Against "Cholesterol Checkpoint" Proteins. *Adv. Ther.* **2021,** *2100014*, https://doi.org/10.1002/adtp.202100014.

13. Crossey, E.; Amar, M. J. A.; Sampson, M.; Peabody, J.; Schiller, J. T.; Chackerian, B.; Remaley, A. T., A Cholesterol-lowering VLP Vaccine that Targets PCSK9. *Vaccine* **2015,** *33*, 5747-5755.

14. Maphis, N. M.; Peabody, J.; Crossey, E.; Jiang, S.; Ahmad, F. A. J.; Alvarez, M.; Mansoor, S. K.; Yaney, A.; Yang, Y.; Sillerud, L. O.; Wilson, C. M.; Selwyn, R.; Brigman, J. L.; Cannon, J. L.; Peabody, D. S.; Chackerian, B.; Bhaskar, K., Qß Virus-like Particle-based Vaccine Induces Robust Immunity and Protects Against Tauopathy. *npj Vaccines* **2019,** *4*, 26.

15. Daly, S. M.; Joyner, J. A.; Triplett, K. D.; Elmore, B. O.; Pokhrel, S.; Frietze, K. M.; Peabody, D. S.; Chackerian, B.; Hall, P. R., VLP-based Vaccine Induces immune Control of *Staphylococcus aureus* Virulence Regulation. *Sci. Rep.* **2016,** *7*, 637.

16. Wang, P.; Huo, C.-x.; Lang, S.; Caution, K.; Nick, S. T.; Dubey, P.; Deora, R.; Huang, X., Chemical Synthesis and Immunological Evaluation of a Potential Anti-Pertussis Vaccine. *Angew. Chem. Int. Ed.* **2020,** *59*, 6451-6458.

17. Wen, A. M.; Steinmetz, N. F., Design of Virus-Based Nanomaterials for Medicine, Biotechnology, and Energy. *Chem. Soc. Rev.* **2016,** *45*, 4074-4126.

18. Rohovie, M. J.; Nagasawa, M.; Swartz, J. R., Virus-Like Particles: Next Generation Nanoparticles for Targeted Therapeutic Delivery. *Bioeng. Transl. Med.* **2016,** *2*, 43-57.

19. Elsayed, H.; Nabi, G.; McKinstry, W. J.; Khoo, K. K.; Mak, J.; Salazar, A. M.; Tenbusch, M.; Temchura, V.; Überla, K., Intrastructural Help: Harnessing T Helper Cells Induced by Licensed Vaccines for Improvement of HIV Env Antibody Responses to Virus-Like Particle Vaccines. *J. Virol.* **2018,** *92*, e00141-18.

20. Báez-Astúa, A.; Herráez-Hernández, E.; Garbi, N.; Pasolli, H. A.; Juárez, V.; zur Hausen, H.; Cid-Arregui, A., Low-Dose Adenovirus Vaccine Encoding Chimeric Hepatitis B Virus Surface Antigen-Human Papillomavirus Type 16 E7 Proteins Induces Enhanced E7-Specific Antibody and Cytotoxic T-Cell Responses. *J. Virol.* **2005,** *79*, 12807-12817.

21. Schiller, J. T.; Lowy, D. R., Papillomavirus-Like Particle Vaccines. *JNCI Monographs* **2000,** *2000*, 50-54.

22. Harper, D. M.; Franco, E. L.; Wheeler, C. M.; Moscicki, A.-B.; Romanowski, B.; Roteli-Martins, C. M.; Jenkins, D.; Schuind, A.; Clemens, S. A. C.; Dubin, G.; Group, O. B. o. t. H. V. S., Sustained Efficacy up to 4.5 Years of a Bivalent L1 Virus-Like Particle Vaccine Against Human Papillomavirus Types 16 and 18: Follow-up from a Randomised Control Trial. *Lancet* **2006,** *367*, 1247-1255.

23. Leroux-Roels, G.; Abraham, B.; Fourneau, M.; De Clercq, N.; Safary, A., A Comparison of Two Commercial Recombinant Vaccines for Hepatitis B in Adolescents. *Vaccine* **2000,** *19*, 937-942.

24. Monie, A.; Hung, C.-F.; Roden, R.; Wu, T.-C., Cervarix: A Vaccine for the Prevention of HPV 16, 18-Associated Cervical Cancer. *Biol. Targets Ther.* **2008,** *2*, 107-113.

25. Pedersen, C.; Petaja, T.; Strauss, G.; Rumke, H. C.; Poder, A.; Richardus, J. H.; Spiessens, B.; Descamps, D.; Kardt, K.; Lehtinen, M.; Dubin, G.; Network, H. V. A. S. I., Immunization of Early Adolescent Females with Human Papillomavirus Type 16 and 18 L1 Virus-Like Particle Vaccine Containing AS04 Adjuvant. *J. Adolesc. Health.* **2007,** *40*, 564-571.

26. Day, P. M.; Kines, R. C.; Thompson, C. D.; Jagu, S.; Roden, R. B.; Lowy, D. R.; Schillller, J. T., In Vivo mechanisms of Vaccine-Induced Protection Against HPV Infection. *Cell Host Microbe* **2010,** *8*, 260-270.

27. Jegerlehner, A.; Wiesel, M.; Dietmeier, K.; Zabel, F.; Gatto, D.; Saudan, P.; Bachmann, M. F., Carrier Induced Epitopic Suppression of Antibody Responses Induced by Virus-Like Particles is a Dynamic Phenomenon Caused by Carrier-Specific Antibodies. *Vaccine* **2010,** *28*, 5503-5512.

28. Shukla, S.; Wang, C.; Beiss, V.; Steinmetz, N. F., Antibody Response against Cowpea Mosaic Viral Nanoparticles Improves *In Situ* Vaccine Efficacy in Ovarian Cancer. *ACS Nano* **2020,** *14*, 2994-3003.

29. Chuan, Y. P.; Rivera-Hernandez, T.; Wibowo, N.; Connors, N. K.; Wu, Y.; Hughes, F. K.; Lua, L. H. L.; Middelberg, A. P. J., Effects of Pre-Existing Anti-Carrier Immunity and Antigenic Element Multiplicity on Efficacy of a Modular Virus-Like Particle Vaccine. *Biotechnol. Bioeng.* **2013,** *110*, 2343-2351.

30. De Filette, M.; Martens, W.; Smet, A.; Schotsaert, M.; Birkett, A.; Londoño-Arcila, P.; Fiers, W.; Saelens, X., Universal Influenza A M2e-HBc Vaccine Protects Against Disease Even in the Presence of Pre-Existing Anti-HBc Antibodies. *Vaccine* **2008,** *26*, 6503-6507.

31. Golmohammadi, R.; Fridborg, K.; Bundule, M.; Valeg å rd, K.; Liljas, L., The Crystal Structure of Bacteriophage Qβ at 3.5 Å Resolution. *Structure* **1996,** *4*, 543-554.

32. Rumnieks, J.; Tars, K., Crystal Structure of the Maturation Protein from Bacteriophage Qβ. *J. Mol. Biol.* **2017,** *429*, 688-696.

33. Emery, J. H. A. In *Analytic Control Strategy for a VLP-Peptide Conjugate Vaccine*, 17th Symposium on the Interface of Regulatory and Analytical Sciences for Biotechnology Health Products, Washington D.C., Washington D.C., 2013.

34. Fiedler, J. D.; Brown, S. D.; Lau, J. L.; Finn, M. G., RNA-Directed Packaging of Enzymes Within Virus-Like Particles. *Angew. Chem. Int. Ed.* **2010,** *49*, 9648-9651.

35. Suttipun, S. Lipopeptide-Coated Iron Oxide Nanoparticles and Engineered Qβ Virus Like Particles as Potential Glycoconjugate-Based Synthetic Anticancer Vaccines. Michigan State University, ProQuest Dissertations Publishing, 2017.

36. Stable, E.; Prasuhn Jr., D. E.; Udit, A. K.; Brown, S.; Link, A. J.; Ngo, J. T.; Lander, G.; Quispe, J.; Potter, C. S.; Carragher, B.; Tirrell, D. A.; Finn, M. G., Unnatural Amino Acid Incorporation into Virus-Like Particles. *Bioconjugate Chem.* **2008,** *19*, 866-875.

37. Pokorski, J. K.; Breitenkamp, K.; Liepold, L. O.; Qazi, S.; Finn, M. G., Functional Virus-Based Polymer-Protein Nanoparticles by Atom Transfer Radical Polymerization. *J. Am. Chem. Soc.* **2011,** *133*, 9242-9245.

38. Pokorski, J. K.; Hovlid, M. L.; Finn, M. G., Cell Targeting with Hybrid Qβ Virus-Like Particles Displaying Epidermal Growth Factor. *ChemBioChem* **2011,** *12*, 2441-2447.

39. Fiedler, J. D.; Fishman, M. R.; Brown, S. D.; Lau, J.; Finn, M. G., Multifunctional Enzyme Packaging and Catalysis in the Qß Protein Nanoparticle. *Biomacromolecules* **2018,** *19*, 3945-3957.

40. Yin, Z.; Wu, X.; Kaczanowska, K.; Sungsuwan, S.; Aragones, M. C.; Pett, C.; Yu, J.; Baniel, C.; Westerlind, U.; Finn, M. G.; Huang, X., Antitumor Humoral and T Cell Responses by Mucin-1 Conjugates of Bacteriophage Qβ in Wild-type Mice. *ACS Chem. Biol.* **2018,** *13*, 1668-1676.

41. Mohsen, M. O.; Gomes, A. C.; Cabral-Miranda, G.; Krueger, C. C.; Leoratti, F. M. S.; Stein, J. V.; Bachmann, M. F., Delivering Adjuvants and Antigens in Separate Nanoparticles

Eliminates the Need of Physical Linkage for Effective Vaccination. *J. Control. Release* **2017,** *251*, 92-100.

42. Lim, F.; Spingola, M.; Peabody, D. S., The RNA-binding Site of Bacteriophage Qβ Coat Protein. *J. Biol. Chem.* **1996,** *271* (50), 31839-31845.

43. Yoshimura, H.; Edwards, E.; Uchida, M.; McCoy, K.; Roychoudhury, R.; Schwarz, B.; Patterson, D.; Douglas, T., Two-Dimensional Crystallization of P22 Virus-Like Particles. *J. Phys. Chem. B* **2016,** *120*, 5938-5944.

44. McCoy, K.; Douglas, T., In Vivo Packaging of Protein Cargo Inside of Virus-Like Particle P22. In *Virus-Derived Nanoparticles for Advanced Technologies*, Wege, C.; Lomonossoff, G., Eds. Humana Press: New York, NY, 2018; Vol. 1776.

45. Klug, A., The Tobacco Mosaic Virus Particle: Structure and Assembly. *Phil. Trans. R. Soc. Lond. B.* **1999,** *354*, 531-535.

46. Smith, M. L.; Lindbo, J. A.; Dillard-telm, S.; Brosio, P. M.; Lasnik, A. B.; McCormick, A. A.; Nguyen, L. V.; Palmer, K. E., Modified *Tobacco Mosaic Virus* Particles as Scaffolds for the Display of Protein Antigens for Vaccine Applications. *Virology* **2006,** *348*, 475-488.

47. Wu, X.; Mckay, C.; Pett, C.; Yu, J.; Schorlemer, M.; Ramadan, S.; Lang, S.; Behren, S.; Westerlind, U.; Finn, M. G.; Huang, X., Synthesis and Immunological Evaluation of Disaccharide Bearing MUC-1 Glycopeptide Conjugates with Virus-like Particles. *ACS Chem. Biol.* **2019,** *14* (10), 2176-2184.

48. Jegerlehner, A.; Stormi, T.; Lipowsky, G.; Schmid, M.; Pumpens, P.; Bachmann, M. F., Regulation of IgG Antibody Responses by Epitope Density and CD21-mediated Costimulation. *Eur. J. Immunol.* **2002,** *32*, 3305-3314.

49. Sungsuwan, S.; Wu, X.; Huang, X., Evaluation of Virus-Like Particle-Based Tumor-Associated Carbohydrate Immunogen in a Mouse Tumor Model. In *Methods Enzymol.*, Elsevier: New York, NY, 2017; Vol. 597, pp 359-376.

50. Polonskaya, Z.; Deng, S.; Sarkar, A.; Kain, L.; Comellas-Aragones, M.; McKay, C. S.; Kaczanowska, K.; Holt, M.; McBridge, R.; Palomo, V.; Self, K. M.; Taylor, S.; Irimia, A.; Mehta, S. R.; Dan, J. M.; Brigger, M.; Crotty, S.; Schoenberger, S. P.; Paulson, J. C.; Wilson, I. A.; Savage, P. B.; Finn, M. G.; Teyton, L., T Cells Control the Generation of Nanomolar-Affinity Anti-Glycan Antibodies. *J. Clin. Invest.* **2017,** *127*, 1491-1504.

51. Alam, M. M.; Jarvis, C. M.; Hincapie, R.; McKay, C. S.; Schimer, J.; Sanhueza, C. A.; Xu, K.; Diehl, R. C.; Finn, M. G.; Kiessling, L. L., Glycan-Modified Virus-Like Particles Evoke Helper Type 1-Like Immune Responses. *ACS Nano* **2020,** *15*, 309-321.

52. Wu, X.; McFall-Boegeman, H.; Rashidijahanabad, Z.; Liu, K.; Pett, C.; Yu, J.; Schorlemer, M.; Ramadan, S.; Behren, S.; Westerlind, U.; Huang, X., Synthesis and Immunological Evaluation of the Unnatural β-linked Mucin-1 Thomsen-Friedenreich Conjugate. *Org. Biomol. Chem.* **2021,** *19*, 2448-2455.

53. Shao, S.; Ortega-Rivera, O. A.; Ray, S.; Pokorski, J. K.; Steinmetz, N. F., A Scalable Manufacturing Approach to Single Dose Vaccination Against HPV. *Vaccines* **2021,** *9*, 66.

54. Lang, R.; Winter, G.; Vogt, L.; Zürcher, A.; Dorigo, B.; Schimmele, B., Rational Design of a Stable, Freeze-Dried Virus-Like Particle-Based Vaccine Formulation. *Drug Dev. Ind. Pharm.* **2009,** *35*, 83-97.

55. Wu, X.; Ye, J.; DeLaitsch, A. T.; Rashidijahanabad, Z.; Lang, S.; Kakeshpour, T.; Zhao, Y.; Ramadan, S.; Saavedra, P. V.; Yuzbasiyan-Gurkan, V.; Kavunja, H.; Cao, H.; Gildersleeve, J. C.; Huang, X., Chemoenzymatic Synthesis of 9NHAc-GD2 Antigen to Overcome the Hydrolytic Instability of O-Acetylated-GD2 for Anticancer Conjugate Vaccine Development. *Angew. Chem. Int. Ed.* **2021,** *60*, 24179-24188.

56. Schwarz, B.; Morabito, K. M.; Ruckwardt, T. J.; Patterson, D. P.; Avera, J.; Miettinen, H. M.; Graham, B. S.; Douglas, T., Viruslike Particles Encapsidating Respiratory Syncytial Virus M and M2 Proteins Induce Robust T Cell Responses. *ACS Biomater. Sci. Eng.* **2016,** *2*, 2324-2332.

57. McCormick, A. A.; Corbo, T. A.; Wykoff-Clary, S.; Nguyen, L. V.; Smith, M. L.; Palmer, K. E.; Pogue, G. P., TMV-Peptide Fusion Vaccines induce Cell-Mediated Immune Responses and Tumor Protection in Two Murine Models. *Vaccine* **2006,** *24*, 6414-6423.

58. Chang, A. RBD-HBsAg Conjugated Virus-Like Particle Vaccine Protects Rhesus Macaques from SARS-CoV-2 Challenge. Harvard Medical School, Boston, MA, 2021.

59. Ruedl, C.; Storni, T.; Lechner, F.; Bächi, T.; Bachmann, M. F., Cross-Presentation of Virus-Like Particles by Skin-Derived CD8- Dendritic Cells: a Dispensable Role for TAP. *Eur. J. Immunol.* **2002,** *32*, 818-825.

60. Guo, J.; Zhou, A.; Sun, X.; Sha, W.; Ai, K.; Pan, G.; Zhou, C.; Zhou, H.; Cong, H.; He, S., Immunogenicity of a Virus-Like-Particle Vaccine Containing Multiple Antigenic Epitopes of *Toxoplasma gondii* Against Acute and Chronic Toxoplasmosis in Mice. *Front. Immunol.* **2019,** *10*, 592.

61. A Jegerlehner, A molecular assembly system that renders antigens of choice highly repetitive for induction of protective B cell responses. *Vaccine* **2002,** *20* (25-26), 3104-3112.

62. Jegerlehner, A.; Tissot, A.; Lechner, F.; Sebbel, P.; Erdmann, I.; Kündig, T.; Bächi, T.; Storni, T.; Jennings, G.; Pumpens, P.; Renner, W. A.; Bachmann, M. F., A molecular assembly

system that renders antigens of choice highly repetitive for induction of protective B cell responses. *Vaccine* **2002,** *20*, 3104-3112.

63. Peng, S.; Frazer, I. H.; Fernando, G. J.; Zhou, J., Papillomavirus Virus-Like Particles Can Deliver Defined CTL Epitopes to the MHC CLass I Pathway. *Virology* **1998,** *240*, 147-157.

64. Morón, V. G.; Rueda, P.; Sedlik, C.; Leclerc, C., In Vivo, Dendritic Cells Can Cross-Present Virus-Like Particles Using an Endosome-to-Cytosol Pathway. *J. Immunol.* **2003,** *171*, 2242-2250.

65. Chackerian, B.; Durfee, M. R.; Schiller, J. T., Virus-Like Display of a Neo-Self Antigen Reverses B Cell Anergy in a B Cell Receptor Transgenic Mouse Model. *J. Immunol.* **2008,** *180* (9), 5816-5825.

66. Medford, A. The Generation and Immunogenicity of PP7 Virus-Like Particles Displaying Target Antigens. University of New Mexico, Electronic Theses and Dissertations at UNM Digital Repository, 2010.

67. Zhao, L.; Kopylov, M.; Potter, C. S.; Carragher, B.; Finn, M. G., Engineering the PP7 Virus Capsid as a Peptide Display Platform. *ACS Nano* **2019,** *13*, 4443-4454.

68. Derdak, S. V.; Kueng, H. J.; Leb, V. M.; Neunkirchner, A.; Schmetterer, K. G.; Bielek, E.; Majdic, O.; Knapp, W.; Seed, B.; Pikl, W. F., Direct Stimulation of T Lymphocytes by Immunosomes: Virus-Like Particles Decorated with T Cell Receptor/CD3 Ligands Plus Costimulatory Molecules. *Proc. Natl. Acad. Sci. USA* **2006,** *103*, 13144-13149.

69. Fluckiger, A.-C.; Bozic, J.; Diress, A.; Ontsouka, B.; Ahmed, T.; Ponce, A.; Kirchmeier, M.; Diaz-Mitoma, F.; Conlan, W.; Anderson, D. E.; Soare, C., Enveloped Virus-Like Particles (eVLPs) Expressing Modified Forms of Zika Virus Proteins E and NS1 Protect Mice from Zika Virus Infection. *bioRxiv* **2019,** *Pre-Print*, https://doi.org/10.1101/666966.

70. Win, S. J.; Ward, V. K.; Dunbar, P. R.; Young, S. L.; Baird, M. A., Cross-Presentation of Epitopes on Virus-Like Particles via the MHC I Receptor Recycling Pathway. *Immunol. Cell Biol.* **2011,** *89*, 681-688.

71. Win, S. J.; McMillan, D. G. G.; Errington-Mais, F.; Ward, V. K.; Young, S. L.; Baird, M. A.; Melcher, A. A., Enhancing tthe Immunogenicity of Tumour Lysate-Loaded Dendritic Cell Vaccines by Conjugation to Virus-Like Particles. *Br. J. Cancer* **2012,** *106*, 92-98.

72. Mohsen, M. O.; Heath, M. D.; Cabral-Miranda, G.; Lipp, C.; Zeltins, A.; Sande, M.; Stein, J. V.; Riether, C.; Roesti, E.; Zha, L.; Engeroff, P.; El-Turabi, A.; Kundig, T. M.; Vogel, M.; Skinner, M. A.; Speiser, D. E.; Knuth, A.; Kramer, M. F.; Bachmann, F. M., Vaccination with Nanoparticles Combined with Micro-Adjuvants Protects Against Cancer. *J. Immunother. Cancer* **2020,** *7*, 114.

73. Hanafi, L.-A.; Bolduc, M.; Gagné, M.-È. L.; Dufour, F.; Langelier, Y.; Boulassel, M.-R.; Routy, J.-P.; Leclerc, D.; Lapointe, R., Two Distinct Chimeric Potexviruses Share Antigenic Cross-Presentation Properties of MHC Class I Epitopes. *Vaccine* **2010,** *28*, 5617-5626.

74. Denis, J.; Acosta-Ramirez, E.; Zhao, Y.; Hamelin, M.-E.; Koukavica, I.; Baz, M.; Abed, Y.; Savard, C.; Pare, C.; Macias, C. L.; Boivin, G.; Leclerc, D., Development of a Universal Influenza A vaccine Based on the M2e Peptide Fused to the Papaya Mosaic Virus (PapMV) Vaccine Platform. *Vaccine* **2008,** *26*, 3395-3403.

75. Leclerc, D.; Beauseigle, D.; Denis, J.; Morin, H.; Paré, C.; Lamarre, A.; Lapointe, R., Proteasome-Independent Major Histocompatibility Complex Class I Cross-Presentation Mediated by Papaya Mosaic Virus-Like Particles Leads to Expansion of Specific Human T Cells. *J. Virol.* **2006,** *81*, 1319-1326.

76. Galaway, F. A.; Stockley, P. G., MS2 Viruslike Particles: A Robust, Semisynthetic Targeted Drug Delivery Platform. *Mol. Pharmaceutics* **2013,** *10*, 59-68.

77. Li, J.; Sun, Y.; Jia, T.; Zhang, R.; Zhang, K.; Wang, L., Messenger RNA Vaccine Based on Recombinant MS2 Virus-Like Particles Against Prostate Cancer. *Int. J. Cancer* **2014,** *134*, 1683-1694.

78. Zhai, L.; Peabody, J.; Pang, Y.-Y. S.; Schiller, J.; Chackerian, B.; Tumban, E., A Novel Candidate HPV Vaccine: MS2 Phage VLP Displaying a tandem HPV L2 Peptide Offers Similar Protection in Mice to Gardasil-9. *Antiviral Res.* **2017,** *147*, 116-123.

79. Lynch, A. G.; Tanzer, F.; Fraser, M. J.; Shephard, E. G.; Williamson, A.-L.; Rybicki, E. P., Use of the *piggyBac* Transposon to Create HIV-1 *gag* Transgenic Insect Cell Lines for Continuous VLP Production. *BMC Biotechnol.* **2010,** *10*, 30.

80. Chang, M. O.; Suzuki, T.; Yamamoto, N.; Watanabe, M.; Takaku, H., HIV-1 Gag-Virus-Like Particles Inhibit HIV-1 Replication in Dendritic Cells and T Cells Through IFN-α-Dependent Upregulation of APOBEC3G and 3F. *J. Innate Immun.* **2012,** *4*, 579-590.

81. Seldlik, C.; Dridi, A.; Deriaud, E.; Saron, M. F.; Rueda, P.; Sarraseca, J.; Casal, J. I.; Leclerc, C., Intranasal Delivery of Recombinant Parvovirus-Like Particles Elicits Cytotoxic T-Cell and Neutralizing Antibody Responses. *J. Virol.* **1999,** *73*, 2739-2744

82. Peabody, J.; Muttil, P.; Chackerian, B.; Tumban, E., Characterization of a Spray-Dried Candidate HPV L2-VLP Vaccine Stored for Multiple Years at Room Temperature. *Papillomavirus Res.* **2017,** *3*, 116-120.

83. Lan, N. T.; Kim, H. J.; Han, H.-J.; Lee, D.-C.; Kang, B. K.; Han, S. Y.; Moon, H.; Kim, H.-J., Stability of Virus-Like Particles of Red-Spotted Grouper Nervous Necrosis Virus in the Aqueous State, and the Vaccine Potential of Lyophilized Particles. *Biologicals* **2018,** *51*, 25-31.

84. Czyż, M.; Dembczyński, R.; Marecik, R.; Wojas-Turek, J.; Milczarek, M.; Pajtasz-Piasecka, E.; Wietrzyk, J.; Pniewski, T., Freeze-Drying of Plant Tissue Containing HBV Surface Antigen for the Oral Vaccine Against Hepatitis B. *Biomed Res. Int.* **2014,** *2014*, 485689.

85. Warzecha, H.; Mason, H. S.; Lane, C.; Tryggvesson, A.; Rybicki, E.; Williamson, A.-L.; Clements, J. D.; Rose, R. C., Oral Immunogenicity of Human Papillomavirus-Like Particles Expressed in Potato. *J. Virol.* **2003,** *77*, 8702-8711.

86. Janeway Jr, C. A.; Medzhitov, R., Innate Immune Recognition. *Annu. Rev. Immunol.* **2002,** *20*, 197-216.

87. Sonnenberg, G. F.; Hepworth, M. R., Functional Interactions Between Innate Lymphoid Cells and Adaptive Immunity. *Nat. Rev. Immunol.* **2019,** *19*, 599-613.

88. Wculek, S. K.; Cueto, F. J.; Mujal, A. M.; Melero, I.; Krummel, M. F.; Sancho, D., Dendritic Cells in Cancer Immunology and Immunotherapy. *Nat. Rev. Immunol.* **2020,** *20*, 7-24.

89. Cui, J.; Chen, Y.; Wang, H. Y.; Wang, R.-F., Mechanisms and Pathways of Innate Immune Activation and Regulation in Health and Cancer. *Hum. Vaccines Immunother.* **2014,** *10*, 3270-3285.

90. Gordon, S., Pattern Recognition Receptors: Doubling Up for the Innate Immune Response. *Cell* **2002,** *111*, 927-930.

91. Kawasaki, T.; Kawai, T., Toll-like Receptor Signaling Pathways. *Front. Immunol.* **2014,** *5*, 461.

92. Zhu, Y.; An, X.; Zhang, X.; Qiao, Y.; Zheng, T.; Li, X., STING: A Master Regulator in the Cancer-Immunity Cycle. *Mol. Cancer* **2019,** *18*, 152.

93. Saxena, M.; Yeretssian, G., NOD-like Receptors: Master Regulators of Inflammation and Cancer. *Front. Immunol.* **2014,** *5*, 327.

94. Yamamoto, M.; Takeda, K., Current Views of Toll-Like Receptor Signaling Pathways. *Gasteroenterol. Res. Pract.* **2010,** *1*, 240365.

95. Richert, L. E.; Rynda-Apple, A.; Harmsen, A. L.; Han, S.; Wiley, J. A.; Douglas, T.; Larson, K.; Morton, R. V.; Harmsen, A. G., $CD11c^{+}$ Cells Primed with Unrelated Antigens Facilitate an Accelerated Immune Response to Influenza Virus in Mice. *Eur. J. Immunol.* **2014,** *44*, 397-408.

96. Shepardson, K. M.; Schwarz, B.; Larson, K.; Morton, R. V.; Avera, J.; McCoy, K.; Caffrey, A.; Harmsen, A.; Douglas, T.; Rynda-Apple, A., Induction of Antiviral Immune Response

Through Recognition of the Repeating Subunit Pattern of Viral Capsids Is Toll-Like Receptor 2 Dependent. *MBio* **2017,** *8*, e01356-17.

97. Allan, R. S.; Waithman, J.; Bedoui, S.; Jones, C. M.; Villadangos, J. A.; Zhan, Y.; Lew, A. M.; Shortman, K.; Heath, W. R.; Carbone, F. R., Migratory Dendritic Cells Transfer Antigen to a Lymph Node-Resident Dendritic Cell Population for Efficient CTL Priming. *Immunity* **2006,** *25*, 153-162.

98. Douglas, T.; Young, M., Host-Guest Encapsulation of Materials by Assembled Virus Protein Cages. *Nature* **1998,** *393*, 152-155.

99. Strods, A.; Ose, V.; Bogans, J.; Cielens, I.; Kalnins, G.; Radovica, I.; Kazaks, A.; Pumpens, P.; Renhofa, R., Preparation by Alkaline Treatment and Detailed Characterisation of Empty Hepatitis B Virus Core Particles for Vaccine and Gene Therapy Applications. *Sci. Rep.* **2015,** *5*, 11639.

100. Li, T.-C.; Takeda, N.; Miyamura, T.; Matsuura, Y.; Wang, J. C. Y.; Engvall, H.; Hammar, L.; Xing, L.; Cheng, R. H., Essential Elements of the Capsid Protein for Self-Assembly into Empty Virus-Like Particles of Hepatitis E Virus. *J. Virol.* **2005,** *79*, 12999-13006.

101. Hovlid, M. L.; Lau, J. L.; Breitenkamp, K.; Higginson, C. J.; Lauder, B.; Manchester, M.; Finn, M. G., Encapsidated Atom-Transfer Radical Polymerization in Qβ Virus-Like Nanoparticles. *ACS Nano* **2014,** *8*, 8003-8014.

102. Lang, S.; Tan, Z.; Wu, X.; Huang, X., Synthesis of Carboxy-Dimethylmaleic Amide Linked Polymer Conjugate Based Ultra-pH-Sensitive Nanoparticles for Enhanced Antitumor Immunotherapy. *ACS Macro Lett.* **2020,** *9*, 1693-1699.

103. Klinman, D. M., Immunotherapeutic Uses of CpG Oligodeoxynucleotides. *Nat. Rev. Immunol.* **2004,** *4*, 249-259.

104. Storni, T.; Ruedl, C.; Schwarz, K.; Schwendener, R. A.; Renner, W. A.; Bachmann, M. F., Nonmethylated CG Motifs Packaged into Virus-Like Particles Induce Protective Cytotoxic T Cell Responses in the Absence of Systemic Side Effects. *J. Immunol.* **2004,** *172*, 1777-1785.

105. Mirsoian, A.; Bouchlaka, M. N.; sckisel, G. D.; Chen, M.; Pai, C.-C. S.; Maverakis, E.; Spencer, R. G.; Fishbein, K. W.; Siddiqui, S.; Monjazeb, A. M.; Martin, B.; Maudsley, S.; Hesdorffer, C.; Ferrucci, L.; Longo, D. L.; Blazar, B. R.; Wiltrout, R. H.; Taub, D. D.; Murphy, W. J., Adiposity Induces Lethal Cytokine Storm After Systemic Administration of Stimulatory Immunotherapy Regimens in Aged Mice. *J. Exp. Med.* **2014,** *211*, 2373-2383.

106. Bardel, E.; Doucet-Ladeveze, R.; Mathieu, C.; Harandi, A. M.; Dubois, B.; Kaiserlian, D., Intradermal Immunisation Using the TLR3-Ligand Poly (I:C) as Adjuvant induces Mucosal Antibody Responses and Protects Against Genital HSV-2 Infection. *NPJ Vaccines* **2016,** *1*, 16010.

107. Kadowaki, N.; Antonenko, S.; Liu, Y.-J., Distinct CpG DNA and Polyinosic-Polycytidylic Acid Double-Stranded RNA, Respectively, Stimulate $CD11c^-$ Type 2 Dendritic Cell Precursors and $CD11c^+$ Dendritic Cells to Produce Type I IFN. *J. Immunol.* **2001,** *166*, 2291-2295.

108. Mohsen, M. O.; Gomes, A. C.; Vogel, M.; Bachmann, M. F., Interaction of Ciral Capsid-Derived Virus-Like Particles (VLPs) with the Innate Immune System. *Vaccines* **2018,** *6*, 37.

109. Cubas, R.; Zhang, S.; Kwon, S.; Sevick-Muraca, E. M.; Li, M.; Chen, C.; Yao, Q., Virus-Like Particle (VLP) Lymphatic Trafficking and Immune Response Generation After Immunization by Different Routes. *J. Immunother.* **2009,** *32*, 118-128.

110. Bousso, P., T-cell Activation by Dendritic Cells in the Lymph Node: Lessons from the Movies. *Nat. Rev. Immunol.* **2008,** *8*, 675-684.

111. Heider, S.; Dangerfield, J. A.; Metzner, C., Biomedical Applications of Glycosylphosphatidylinositol-Anchored Proteins. *J. Lipid Res.* **2016,** *57*, 1778-1788.

112. Fiedler, J. D.; Higginson, C.; Hovlid, M. L.; Kislukhin, A. A.; Castillejos, A.; Manzenrieder, F.; Campbell, M. G.; Voss, N. R.; Potter, C. S.; Carragher, B.; Finn, M. G., Engineered Mutations Change the Structure and Stability of a Virus-Like Particle. *Biomacromolecules* **2012,** *13*, 2339-2348.

113. Davis, S. J.; van der Merwe, P. A., The Kinetic-Segregation Model: TCR Triggering and Beyond. *Nat. Immunol.* **2006,** *7*, 803-809.

114. Bakalar, M. H.; Joffe, A. M.; Schmid, E. M.; Son, S.; Podolski, M.; Fletcher, D. A., Size-Dependent Segregation Controls Macrophage Phagocytosis of Antibody-Opsonized Targets. *Cell* **2018,** *174*, 131-142.

115. Qin, Q.; Yin, Z.; Wu, X.; Haas, K. M.; Huang, X., Valency and Density Matter: Deciphering Impacts of Immunogen Structures on Immune Responses Against a Tumor Associated Carbohydrate Antigen Using Synthetic Glycopolymers. *Biomaterials* **2016,** *101*, 189-198.

116. Harty, J. T.; Badovinac, V. P., Shaping and Reshaping CD8+ T-Cell Memory. *Nat. Rev. Immunol.* **2008,** *8*, 107-119.

117. Kaech, S. M.; Wherry, E. J.; Ahmed, R., Effector and Memory T-Cell Differentiation: Implications for Vaccine Development. *Nat. Rev. Immunol.* **2002,** *2*, 251-262.

118. Kaech, S. M.; Cui, W., Transcriptional Control of Effector and Memory CD8+ T Cell Differentiation. *Nat. Rev. Immunol.* **2012,** *12*, 749-761.

119. Grotzke, J. E.; Sengupta, D.; Lu, Q.; Cresswell, P., The ongoing saga of the mechanism(s) of MHC class I-restricted cross-presentation. *Curr. Opin. Immunol.* **2017,** *46*, 89-96.

120. Sede, R. A.; Darrah, P. A.; Roederer, M., T-Cell Quality in Memory and Protection: Implications for Vaccine Design. *Nat. Rev. Immunol.* **2008,** *8*, 247-258.

121. Alloatti, A.; Rookhuizen, D. C.; Joannas, L.; Cartier, J.-M.; Iborra, S.; Magalhaes, J. G.; Yatim, N.; Kozik, P.; Sancho, D.; Albert, M. L.; Amigorena, S., Critical role for Sec22b-dependent cross-presentation in antitumor immunity. *J. Exp. Med.* **2017,** *214*, 2231-2241.

122. van Endert, P.; Montealegre, S., MHC Class I Cross-Presentation: Stage Lights on Sec22b. *Trends Immunol.* **2017,** *38*, 618-621.

123. Wu, S. J.; Niknafs, Y. S.; Kim, S. H.; Oravecz-Wilson, K.; Zajac, C.; Tuba, T.; Sun, Y.; Prasad, J.; Peltier, D.; Fujiwara, H.; Hedig, I.; Mathewson, N. D.; Khoriaty, R.; Ginsburg, D.; Reddy, P., A Critical Analysis of the Role of SNARE Protein SEC22B in Antigen Cross-Presentation. *Cell Rep.* **2017,** *19*, 2645-2656.

124. Houde, M.; Bertholet, S.; Gagnon, E.; Brunet, S.; Goyette, G.; Laplante, A.; Princiotta, M. F.; Thibault, P.; Sacks, D.; Desjardins, M., Phagosomes are Competent Organelles for Antigen Cross-Presentation. *Nature* **2003,** *425*, 402-406.

125. Yang, J.; Luo, Y.; Shibu, M. A.; Toth, I.; Skwarczynskia, M., Cell-Penetrating Peptides: Efficient Vectors for Vaccine Delivery. *Curr. Drug. Deliv.* **2019,** *16*, 430-443.

126. Appenzeller-Herzog, C.; Hauri, H.-P., The ER-Golgi Intermediate Compartment (ERGIC): in Search of its Identity and Function. *J. Cell. Sci.* **2006,** *119*, 2173-2183.

127. Serbian, I.; Visentin, G.; Blanchard, N.; Jove, M.; Bobard, A.; Moita, C.; Inning, J.; Moita, L. F.; Amigorena, S.; Savina, A., Sec22b Regulates Phagosomal Maturation and Antigen Crosspresentation by Dendritic Cells. *Cell* **2011,** *147*, 1355-1368.

128. Gutiérrez-Martínez, E.; Planès, R.; Anselmi, G.; Reynolds, M.; Menezes, S.; Adiko, A. C.; Saveanu, L.; Guermonprez, P., Cross-Presentation of Cell-Associated Antigens by MHC Class I in dendritic Cell Subsets. *Front. Immunol.* **2015,** *6*, 363.

129. Mant, A.; Chinnery, F.; Elliott, T.; Williams, A. P., The pathway of Cross-Presentation is Influenced by the Particle Size of Phagocytosed Antigen. *Immunology* **2012,** *136*, 163-175.

130. Ohlinger, V. F.; Haas, B.; Meyers, G.; Weiland, F.; Thiel, H.-J., Identification and Characterization of the Virus Causing Rabbit Hemorrhagic Disease. *J. Virol.* **1990,** *64*, 3331-3336.

131. Parra, F.; Prieto, M., Purification and Characterization of a Calicivirus as the Causative Agent of a Lethal Hemorrhagic Disease in Rabbits. *J. Virol.* **1990,** *64*, 4013-4015.

132. Tamošiūnas, P. L.; Petraitytė-Burneikienė, R.; Lasickienė, R.; Akatov, A.; Kundrotas, G.; Sereika, V.; Lelešius, R.; Žvirblienė, A.; Sasnauskas, K., Generation of Recombinant Porcine Parvovirus Virus-Like Particles in Saccharomyces cerevisiae and Development of Virus-Specific Monoclonal Antibodies. *J. Immunol.* **2014,** *2014*, 573531.

133. Spice, A. J.; Aw, R.; bracewell, D. G.; Polizzi, K. M., Synthesis and Assembly of Hepatitis B Virus-Like Particles in a Pichia pastoris Cell-Free System. *Front. Bioeng. Biotechnol.* **2020,** *8*, 72.

134. Kramer, K.; Al-Barwani, F.; Baird, M. A.; Young, V. L.; Larsen, D. S.; Ward, V. K.; Young, S. L., Functionalisation of Virus-Like Particles Enhances Antitumour Immune Responses. *J. Immunol. Res.* **2019,** *2019*, 5364632.

135. Gonciarz-Swiatek, M.; Rechsteiner, M., Proteasomes and Antigen Presentation: Evidence that a KEKE Motif Does Not Promote Presentation fo the Class I Epitope SIINFEKL. *Mol. Immunol.* **2006,** *43*, 1993-2001.

136. Kapadia, C. H.; Tian, S.; Perry, J. L.; Luft, C.; DeSimone, J. M., Role of Linker Length and Antigen Density in Nanoparticle Peptide Vaccine. *ACS Omega* **2019,** *4*, 5547-5555.

137. Bijker, M. S.; van den Eeden, S. J. F.; franken, K. L.; Melief, C. J. M.; van der Burg, S. H.; Offringa, R., Superior Induction of Anti-Tumor CTL Immunity by Extended Peptide Vaccines Involves prolonged, DC-Focused Antigen Presentation. *Eur. J. Immunol.* **2008,** *38*, 1033-1042.

138. Craiu, A.; Akopian, T.; Goldberg, A.; Rock, K. L., Two Distinct Proteolytic processes in the Generation of a Major Histocompatibility Complex Class I-Presented Peptide. *Proc. Natl. Acad. Sci. USA* **1997,** *94*, 10850-10855.

139. Rosalia, R. A.; Quakkelaar, E. D.; Redeker, A.; Khan, S.; Camps, M.; Drijfhout, J. W.; Silva, A. L.; Jiskoot, W.; van Hall, T.; van Veelen, P. A.; Janssen, G.; Franken, K.; Cruz, L. J.; Tromp, A.; Oostendorp, J.; van der Burg, S. H.; Ossendorp, F.; Melief, C. J. M., Dendritic Cells Process Synthetic Long Peptides Better than Whole Protein, Improving Antigen Presentation and T-Cell Activation. *Eur. J. Immunol.* **2013,** *43*, 2554-2565.

140. Pierce, S. K.; Liu, W., The Tipping points in the Initiation of B Cell Signalling; How Small Changes Make Big Differences. *Nat. Rev. Immunol.* **2010,** *10*, 767-777.

141. Mond, J. J.; Lees, A.; Snapper, C. M., T Cell-Independent Antigens Type 2. *Annu. Rev. Immunol.* **1995,** *13*, 655-692.

142. Metzger, H., Transmembrane Signaling: The Joy of Aggregation. *J. Immunol.* **1992,** *149*, 1477-1487.

143. Bessa, J.; Schmitz, N.; Hinton, H. J.; Schwarz, K.; Jegerlehner, A.; Bachmann, M. F., Efficient Induction of Mucosal and Systemic Immune Responses by Virus-Like Particles Administered Intranasally: Implications for Vaccine Design. *Eur. J. Immunol.* **2008,** *38*, 114-126.

144. S. Minguet; E.-P. Dopfer; A. Schamel, W. W., Low-valency, but not monovalent, antigens trigger the B-cell antigen receptor (BCR). *Int. Immunol.* **2010,** *22* (3), 205-212.

145. M. Dintzis, H.; Z. Dintzis, R.; B. Vogelstein, Molecular determinants of immunogenicity: the immunon model of immune response. *Proc. Natl. Acad. Sci. USA* **1976,** *73*, 3671-3675.

146. Sosnick, T. R.; Benjamin, D. C.; Novotny, J.; Seeger, P. A.; Trewhella, J., Distances Between the Antigen-Binding Sites of Three Murine Antibody Subclasses Measured Using Neutron and X-Ray Scattering. *Biochemistry* **1992,** *31*, 1779-1786.

147. Dintzis, R. Z.; Vogelstein, B.; Dintzis, H. M., Specific Cellular Stimulation in the Primary Immune Response: Experimental Test of a Quantized Model. *Proc. Natl. Acad. Sci. USA* **1982,** *79*, 884-888.

148. Bachmann, M. F.; Hengartner, H.; Zinkernagel, R. M., T helper cell-independent neutralizing B cell response against vesicular stomatitis virus: Role of antigen patterns in B cell induction? *Eur. J. Immunol.* **1995,** *25*, 3445-3451.

149. Tolar, P.; Spillane, K. M., Force Generation in B-Cell Synapsis: Mechanisms Coupling B-Cell Receptor Binding to Antigen Internalization and Affinity Discrimination. *Adv. Immunol.* **2014,** *123*, 69-100.

150. Fleire, S. J.; Goldman, J. P.; Carrasco, Y. R.; Weber, M.; Bray, D.; Batista, F. D., B Cell Ligand Discrimination Through a Spreading and Contraction Response. *Science* **2006,** *312*, 738-741.

151. Yin, Z.; Chowdhury, S.; McKay, C.; Baniel, C.; Wright, W. S.; Bentley, P.; Kaczanowska, K.; Gildersleeve, J. C.; Finn, M. G.; BenMohamed, L.; Huang, X., Significant Impact of Immunogen Design on the Diversity of Antibodies Generated by Carbohydrate-Based Anticancer Vaccine. *ACS Chem. Biol.* **2015,** *10* (10), 2364-2372.

152. Chan, S. K.; Steinmetz, N. F., Isolation of Cowpea Mosaic Virus-Binding Peptides. *Biomacromolecules* **2021,** *22*, 3613-3623.

153. Garrod, K. R.; Moreau, H. D.; Garcia, Z.; Lemaître, F.; Bouvier, I.; Albert, M. L.; Bousso, P., Dissecting T Cell Contraction *In Vivo* Using a Genetically Encoded Reporter of Apoptosis. *Cell Rep.* **2012,** *2*, 1438-1447.

154. Mahnke, Y. D.; Brodie, T. M.; Sallusto, F.; Roederer, M.; Lugli, E., The Who's Who of T-Cell Differentiation: Human Memory T-Cell Subsets. *Eur. J. Immunol* **2013,** *43*, 2797-2809.

155. Mami-Chouaib, F.; Tartour, E., Editorial: Tissue Resident Memory T Cells. *Front. Immunol.* **2019,** *10*, 1018.

156. Jiang, X.; Clark, R. A.; Liu, L.; Wagers, A. J.; Fuhlbrigge, R. C.; Kupper, T. S., Skin Infection Generates Non-Migratory Memory $CD8^+$ T_{RM} Cells Providing Global Skin Immunity. *Nature* **2012,** *483*, 227-231.

157. Schenkel, J. M.; Fraser, K. A.; Vezys, V.; Masopust, D., Sensing and Alarm Function of Resident Memory $CD8^+$ T Cells. *Nat. Immunol.* **2013,** *14*, 509-513.

158. Szabo, P. A.; Miron, M.; Farber, D. L., Location, Location, Location: Tissue Resident Memory T Cells in Mice and Humans. *Sci. Immunol.* **2019,** *4*, eaas9673.

159. Lee, Y.-N.; Lee, Y.-T.; Kim, M.-C.; Gewirtz, A. T.; Kang, S.-M., A Novel Vaccination Strategy Mediating the Induction of Lung-Resident Memory CD8 T Cells Confers Heterosubtypic Immunity Against Future Pandemic Influenza Virus. *J. Immunol.* **2016,** *196*, 2637-2645.

160. Schenkel, J. M.; Fraser, K. A.; Beura, L. K.; Pauken, K. E.; Vezys, V.; Masopust, D., Resident Memory CD8 T Cells Trigger Protective Innate and Adaptive Immune Responses. *Science* **2014,** *346*, 98-101.

161. Menares, E.; Gálvez-Cancino, F.; Cáceres-Morgado, P.; Ghorani, E.; López, E.; Díaz, X.; Saavedra-Almarza, J.; Figueroa, D. A.; Roa, E.; Quezada, S. A.; Lladser, A., Tissue-Resident Memory CD8+ T Cells Amplify Anti-Tumor Immunity by Triggering Antigen Spreading Through Dendritic Cells. *Nat. Commun.* **2019,** *10*, 4401.

162. Ariotti, S.; Hogenbirk, M. A.; Dijkgraaf, F. E.; Visser, L. L.; Hoekstra, M. E.; Song, J.-Y.; Jacobs, H.; Haanen, J. B.; Schumacher, T. N., Skin-Resident Memory $CD8^+$ T Cells Trigger a State of Tissue-Wide Pathogen Alert. *Science* **2014,** *346*, 101-105.

163. Djenidi, F.; Adam, J.; Goubar, A.; Durgeau, A.; Meurice, G.; de Montpréville, V.; Validire, P.; Besse, B.; Mami-Chouaib, F., $CD8^+CD103^+$ Tumor-Infiltrating Lymphocytes are Tumor-Specific Tissue-Resident Memory T Cells and a Prognostic Factor for Survival in Lung Cancer Patients. *J. Immunol.* **2015,** *194*, 3475-3486.

164. Edwards, J.; Wilmott, J. S.; Madore, J.; Gide, T. N.; Quek, C.; Tasker, A.; Ferguson, A.; Chen, J.; Hewavisenti, R.; Hersey, P.; Gebhardt, T.; Wenigner, W.; Britton, W. J.; Saw, R. P. M.; Thompson, J. F.; Menzies, A. M.; Long, G. V.; Scolyer, R. A.; Palendira, U., $CD103^+$ Tumor-Resident $CD8^+$ T Cells are Associated with Improved Survival in Immunotherapy-Naïve Melanoma Patients and Expanded Significantly During Anti-PD-1 Treatment. *Clin. Cancer Res.* **2018,** *24*, 3036-3045.

165. Caminschi, I.; Lahoud, M. H.; Pizzola, A.; Wakim, L. M., Zymosan By-Passes the Requirement for Pulmonary Antigen Encounter in Lung Tissue-Resident Memory $CD8^+$ T Cell Development. *Mucosal Immunol.* **2019,** *12*, 403-412.

166. Lapuent, D.; Storcksdieck genannt Bonsmann, M.; Maaske, A.; Stab, V.; Heinecke, V.; Watzstedt, K.; Heß, R.; Westendorf, A. M.; Bayer, W.; Ehrhardt, C.; Tenbusch, M., IL-1ß as Mucosal Vaccine Adjuvant: The Specific Induction of Tissue-Resident Memory T Cells Improves the Heterosubtypic Immunity Against Influenza A Viruses. *Mucosal Immunol.* **2018,** *11*, 1265-1278.

167. Wakim, L. M.; Smith, J.; Caminschi, I.; Lahoud, M. H.; Villadangos, J. A., Antibody-Targeted Vaccination to Lung Dendritic Cells Generates Tissue-Resident Memory CD8 T Cells That are Highly Protective Against Influenza Virus Infection. *Mucosal Immunol.* **2015,** *8*, 1060-1071.

168. Zepeda-Cervantes, J.; Ramírez-Jar-quín, J.; Vaca, L., Interaction Between Virus-Like Particles (VLPs) and Pattern Recognition Receptors (PRRs) From Dendritic Cells (DCs): Towards Better Engineering of VLPs. *Front. Immunol.* **2020,** *11*, 1100.

169. Knight, F. C.; Wilson, J. T., Engineering Vaccines for Tissue-Resident Memory T Cells. *Adv. Ther.* **2021,** *4*, 2000230.

170. Grewal, H. M.; Karlsen, T. H.; Vetvik, H.; Ahrén, C.; Gjessing, H. K.; Sommerfelt, H.; Haneberg, B., Measurement of Specific IgA in Faecal Extracts and Intestinal Lavage Fluid for Monitoring of Mucosal Immune Responses. *J. Immunol. Methods* **2000,** *239*, 53-62.

171. Braun, M.; Jandus, C.; Maurer, P.; Hammann-Haenni, A.; Schwarz, K.; Bachmann, M. F.; Speiser, D. E.; Romero, P., Virus-Like Particles Induce Robust Human T-Helper Cell Responses. *Eur. J. Immunol.* **2012,** *42*, 330-340.

172. Slifka, M. K.; Amanna, I. J., Role of Multivalency and Antigenic Threshold in Generating Protective Antibody Responses. *Front. Immunol.* **2019,** *10*, 956.

173. Chackerian, B.; Peabody, D. S., Factors That Govern the Induction of Long-Lived Antibody Responses. *Viruses* **2020,** *12*, 74.

174. Dicker, K. T.; Gurski, L. A.; Pradhan-Bhatt, S.; Witt, R. L.; Farach-Carson, M. C.; Jia, X., Hyaluronan: A Simple Polysaccharide with Diverse Biological Functions. *Acta Biomater.* **2014,** *10*, 1558-1570.

175. Lauber, D. T.; Fülöp, A.; Kovács, T.; Szigeti, K.; Máthé, D.; Szijártó, A., State of the Art *In Vivo* Imaging Techniques for Laboratory Animals. *Lab. Anim.* **2017,** *51*, 465-478.

176. Martino, M. L.; Crooke, S. N.; Manchester, M.; Finn, M. G., Single-Point Mutations in Qβ Virus-Like particles Change Binding to Cells. *Biomacromolecules* **2021,** *22*, 3332-3341.

177. Braeden, D.; Lateef, Z.; Walker, G. F.; Young, S. L.; Ward, V. K., Virus-Like Particle Vaccines: Immunology and Formulation for Clinical Translation. *Expert Rev. Vaccines* **2018,** *17*, 833-849.

178. Karpiński, T. M.; Ozarowski, M.; Seremak-Mrozikiewicz, A.; Wolski, H.; Wlodkowic, D., The 2020 Race Towards SARS-CoV-2 Specific Vaccines. *Theranostics* **2021,** *11*, 1690-1702.

CHAPTER 2 FUNCTIONALIZATION OF THE INTERIOR OF BACTERIOPHAGE Qβ WITH T CELL EPITOPES

2.1 Introduction

The general appeal of virus-like particle (VLP)-based conjugate vaccines is their ability to generate long-lived antibody responses towards antigens conjugated to their surface.[1, 2] It is believed that the repetitive structure and spacing makes them excellent candidates as carriers in conjugate vaccines targeting humoral responses.[3-5] Additionally, the presence of helper T cell epitopes in the capsid proteins allows for efficient isotype switching of B cells leading to long lasting immunological memory against immunogenic targets including non-protein antigens.[6-8]

This focus on the efficient activation of humoral immunity ignores the other half of the adaptive immune response, cellular immunity, although there is evidence that VLP-based conjugate vaccines can also induce potent cellular immune responses.[9-11] Unlike humoral immunity, organized antigen presentation on the surface of the VLP for T cell activation is not as important. Whereas B cell receptors recognize intact antigens, cytotoxic T cells (CTLs) require CTL epitopes (CTLes) to be processed and presented on major histocompatibility complex (MHC) class I by antigen presenting cells first (APCs).[12, 13] This opens up the opportunity to functionalize the interior of the VLP with CTLes leaving the surface available for B cell epitope conjugation.

A variety of strategies for functionalizing VLPs to induce CTLes have been reported in the literature. The VLP surface has been functionalized through fusion proteins and lysine functionalization.[9, 14] Specific functionalization of VLP interiors, however, has been reported less frequently. Interior functionalization has been performed by taking advantage of VLPs that contain a scaffold protein like P22.[10, 15]

The bacteriophage Qβ is an icosahedral VLP formed from 180 copies of a 14 kDa coat protein and RNA on the interior. Conjugation of B cell antigens to the surface of Qβ has elicited protective humoral responses against a number of potential diseases.[2, 9, 16, 17] There are also pores along the 3-fold symmetry axis on the surface of Qβ. These pores have been previously used to access the interior of the capsid to grow polymers, suggesting that funtionalization of the intact interior of the Qβ capsid with CTLes is theoretically possible.[18]

Herein we report the lessons learned from three attempts at functionalizing the interior of the VLP bacteriophage Qβ with CTLes, covalent functionalization of the capsid interior, covalent functionalization of encapsulated RNA, and non-covalent binding interaction with the encapsulated RNA.

2.2 Results and Discussions

2.2.1 Covalent Functionalization of the Capsid Interior

2.2.1.1 Expression of a Qβ Mutant Containing the Unnatural Amino Acid Azidohomoalanine

Our first approach was to selectively conjugate a CTLe to the interior face of the Qβ capsid. To selectively functionalize the interior, we chose to introduce an azide moiety through the incorporation of an unnatural amino acid, azidohomoalanine (AHA) (**scheme 2.1**). Site directed mutagenesis was performed to introduce a methionine residue at the 93rd position (T93M). AHA was incorporated by expressing $Q\beta_{T93M}$ in methionine auxotrophic *e. coli* fed media supplemented with AHA. $Q\beta_{T93AHA}$ formed similar sized capsids as wt Qβ (11.3 mL vs 11.6 mL retention volume on SEC, **figure 2.7**). ESI-MS showed complete incorporation of AHA at amino acid residue 93 (**figure 2.8**).

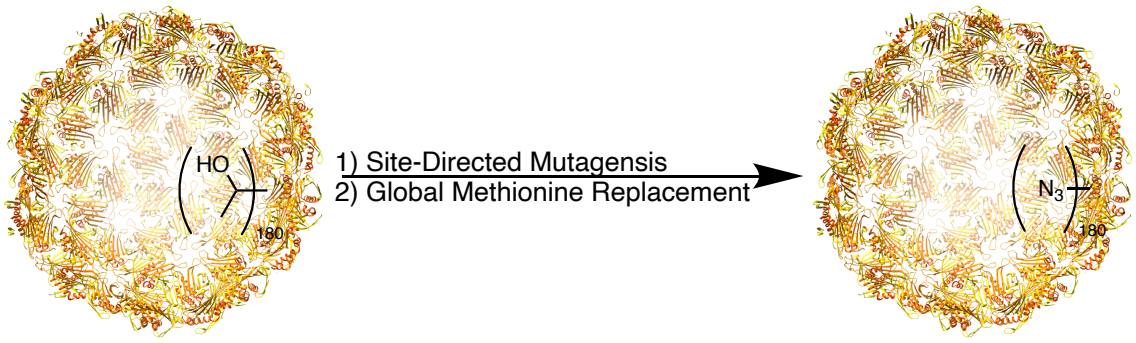

Scheme 2.1. An azide handle was installed on the interior of Qβ's capsid by site-directed mutagenesis of T93M, which was followed by global methionine replacement with azidohomoalanine (AHA) during expression.

2.2.1.2 Removal of Packaged RNA from Qβ

Co-crystal structures of the RNA and Qβ CP indicate that a RNA hairpin loop lies across the AHA at residue 93.[19] To ensure that the azide was available for conjugation we needed to remove the RNA from the interior of the capsid. The interactions between the RNA and the CP are dependent on the presence of the hairpin loop.[20] To disrupt the hairpin loop we used lead(II)acetate to cleave the phosphate backbone (**figure 2.1A**). Lead salt has been shown to cleave the phosphate backbone at well-defined tertiary structures in RNA, including hairpin loops.[21-23] Following cleavage, the RNA dissociates from the capsid and can diffuse through the pores in the capsid. The free RNA was then removed by centrifuge filtration. RNA removal was confirmed by comparison of the UV-vis spectra pre- and post-lead treatment. The 260nm:280nm optical density ratio went from 1.76 to 1.18 (**figure 2.1B**). Removal of RNA from the Qβ capsid was confirmed by analysis of native page gels looking for colocalization of protein and RNA stains (**figure 2.1C**). Samples treated with lead stained only with Coomassie blue, suggesting a lack of capsid RNA, while samples without lead treatment stained both with Coomassie blue and ethidium bromide, suggesting the capsids still contained RNA. Although the

migration pattern in the native gels shifted pre- vs post- lead treatment, DLS analysis showed almost no change in the size of the capsids (r = 14.68 nm vs 15.95 nm, **figure 2.1D**).

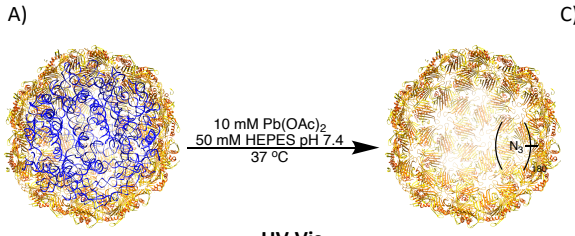

B)

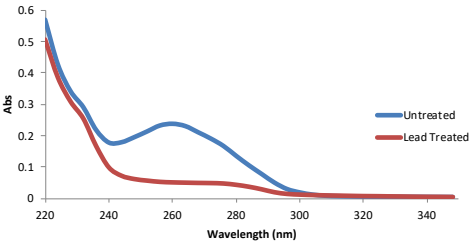

Sample	A260	A280	260:280
Untreated	0.236	0.134	1.76
Lead Treated	0.052	0.045	1.18

C)

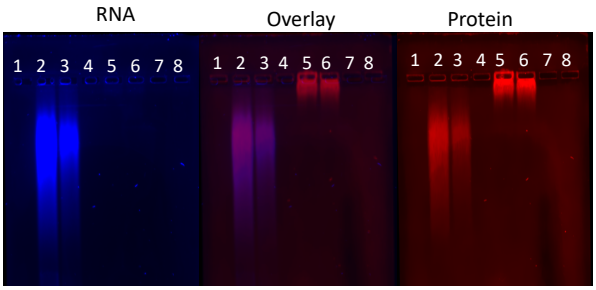

Lane	1	2	3	4	5	6	7	8
Qβ	-	+	+	-	+	+	-	-
Lead Treatment	-	-	-	-	+	+	-	-

D)

Sample	Average Radius (nm)	PDI
Pre-Lead Treatment	14.68	0.051
Post-Lead Treatment	15.95	0.137

Figure 2.1. (A) RNA (blue ribbon) inside the $Q\beta_{T93AHA}$ capsid (red-to-yellow ribbon) can be removed from the capsid, via lead-mediated hydrolysis, exposing the azide functionality. (B) Removal of the RNA from the capsid results in a change in the 260:280 abs ratio. (C) Native gel electrophoresis of intact $Q\beta_{T93AHA}$ capsids with or without lead treatment. RNA was visualized by ethidium bromide and protein was visualized by Coomassie blue staining. (D) DLS analysis of particle size before and after lead treatment.

2.2.1.3 Conjugation with Small Molecule Cargo

To confirm the availability of the azide for functionalization, a model alkyne was conjugated to the interior of the capsid through copper(I)-catalyzed alkyne-azide cycloaddition (CuAAC) click chemistry (**scheme 2.2**). Mass spectrometry analysis showed ~73% functionalization of the capsid azides with the model alkyne (**figure 2.10**).

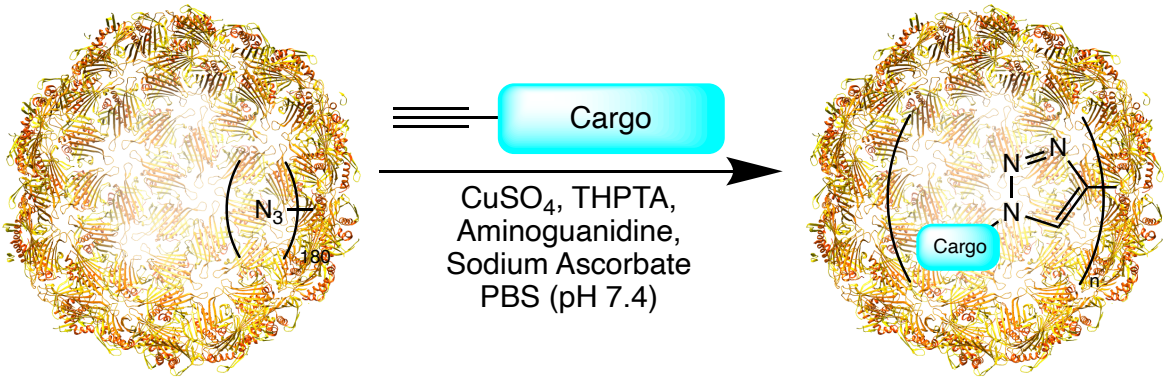

Scheme 2.2. Functionalization of $Q\beta_{T93AHA}$ via copper-catalyzed azide alkyne cycloaddition (CuAAC) click chemistry. Cargo was either hexynoic acid (model alkyne) or alkyne-SIINFEKL (CTLe).

2.2.1.4 Hydrophobic Epitopes Destabilize the Capsid

Following the successful conjugation of the model fluorophore to the interior of Qβ, we attempted to conjugate a model CTLe (alkyne-SIINFEKL) using the same reaction conditions. Within half an hour the reaction solution turned cloudy. Centrifugation to remove the precipitate and Bradford assay of the reaction solution confirmed that the precipitate was Qβ crashing out of the reaction. T cell epitopes bind to MHC molecules through hydrophobic interactions. They tend to contain hydrophobic amino acids and as such are only sparingly soluble in water if at all.[24] To rule out unforeseen interactions between alkyne-SIINFEKL and the Qβ capsid, we co-incubated the two together in the reaction buffer with or without the reagents for the CuAAC reaction. Precipitation only appeared in the solution with the complete reaction conditions. This suggests that the conjugation of Qβ and alkyne-SIINFEKL was key for the destabilizing effects. Our hypothesis is that once the hydrophobic peptides were confined to the interior of the capsid, they tended to aggregate and destabilize the capsid resulting in the

precipitation. Tuning of the reaction conditions failed to find a loading level that did not result in precipitation.

2.2.2 Covalent Functionalization of the Packaged RNA

2.2.2.1 Conjugation to RNA Through Thiosemicarbazides

Following failed functionalization of the capsid interior, we looked for a way to overcome the solubility issues introduced by the hydrophobic CTLe peptides. One solution is to conjugate the peptide to a highly hydrophilic species, such as the encapsulated RNA. The negatively charged phosphate backbone in RNA would increase the solubility of any hydrophobic moieties conjugated to the RNA. We selectively functionalized the RNA through oxidation of the furanose ring on the 3' end. Treatment with sodium periodate ($NaIO_4$) resulted in opening the furanose ring and the formation of aldehydes at the 2' and 3' positions, as shown in **scheme 2.3**. The dialdehydes could then react with a thiosemicarbazide-labeled cargo. As a proof-of-concept we treated Qβ as described and the RNA was functionalized with fluorescein-5-thiosemicarbazide. After washing, Qβ samples retained fluorescence indicating successful conjugation.

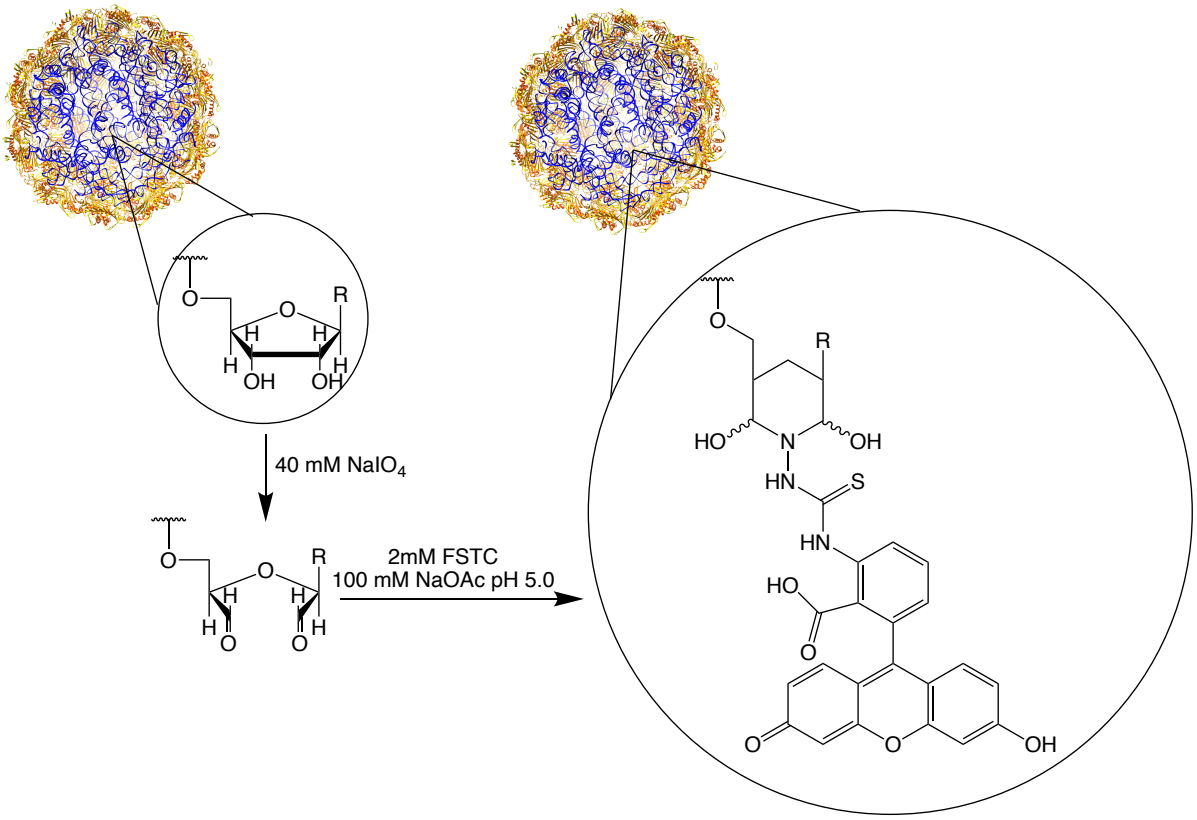

Scheme 2.3. The 3'-end of the capsid RNA can be oxidized by treatment with sodium periodate ($NaIO_4$) resulting in the dialdehyde. Incubation with fluorescein thiosemicarbazide (FSTC) results in covalent functionalization of the capsid RNA.

2.2.2.2 Loading Efficiency

Qβ expressed from *e. coli* generally contains three strands of RNA.[25] With a max potential loading of ~3 cargo/capsid the length of the oxidation step was optimized. To quantify loading, a standard curve of fluorescein-5-thiosemicarbazide was made (**figure 2.11**). Loading with FSTC was able to approach 3 cargo molecules/capsid. Under the same conditions (**scheme 2.4**), hex-5-ynehyrazide functionalization of the capsid, followed by CuAAC click chemistry to conjugate the CTLe, gave only a slight decrease in loading level (2.4 cargo molecules/capsid)

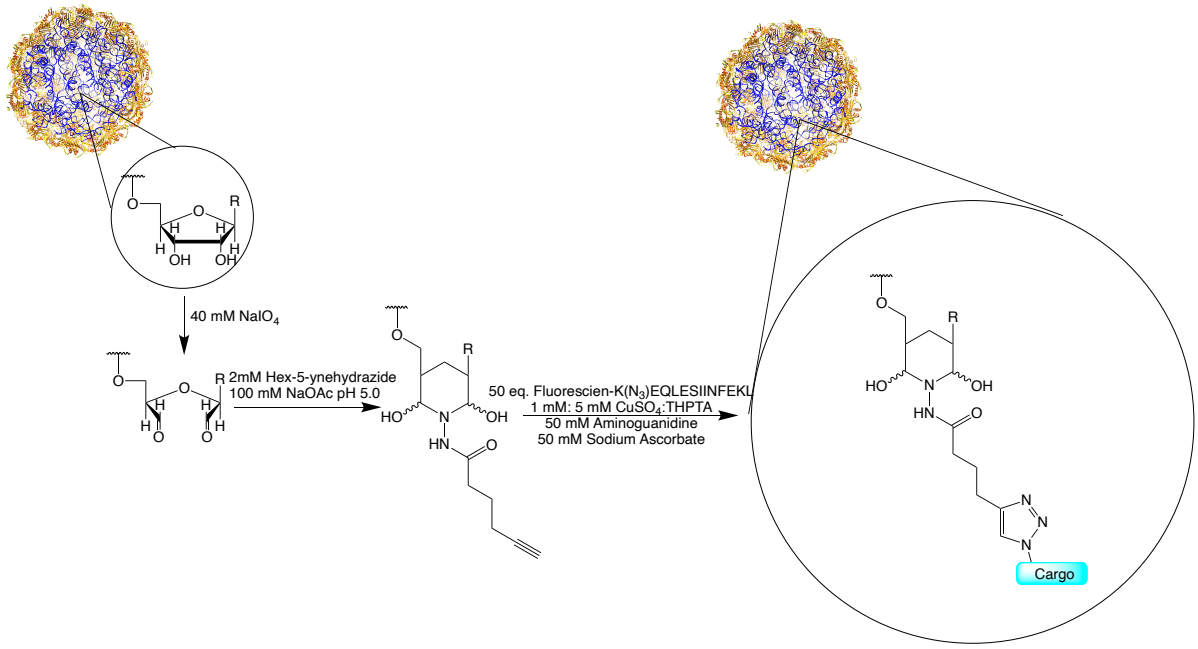

Scheme 2.4. Oxidation of 3'-end of the capsid RNA was performed by treatment with sodium periodate ($NaIO_4$) to form a dialdehyde. Hex-5-ynehydrazide was conjugated to the dialdehyde to allow for copper-catalyzed azide alkyne cycloaddition (CuAAC) click fuctionalization. Cargo was flourescien-K(N_3)EQLESIINFEKL.

2.2.2.3 *In Vitro* Testing

The first step in activation of a cellular immune response is that foreign antigens need to be processed by antigen presenting cells (APCs). Bone marrow dendritic cells (BMDCs) were co-incubated with **vaccine construct 1** at varying concentrations of antigen. Flow cytometry analysis of SIINFEKL-loaded MHC molecules on the BMDC cell surface showed a dose dependent response (**figure 2.2**)

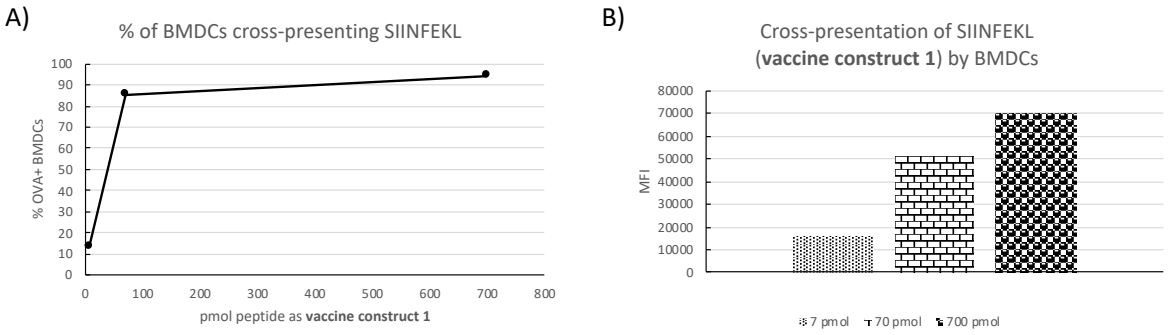

Figure 2.2. Bone marrow-derived dendritic cells (BMDCs) can cross present SIINFEKL delivered by **vaccine construct 1**. BMDCs were pulsed with **vaccine construct 1** at different amounts. BMDCs were stained with anti-mouse H-2K^b bound to SIINFEKL (Clone 25-D1.16). (A) Percentage of BMDCs that stained positive. Mean fluorescence intensity (MFI) gate for OVA$^+$ cells was set as the minimal MFI that would exclude 99% of cells from an unlabeled BMDC sample. (B) MFI of samples pulsed with different amounts of **vaccine construct 1**.

With evidence that BMDCs could cross-present the model epitope delivered by **vaccine construct 1**, the next step was to confirm that the cross-presented antigens could activate antigen-specific CTLs. B3Z cells are an engineered CD8 T cell, whose T cell receptor (TCR) is specific for SIINFEKL-MHC constructs.[26, 27] Upon TCR activation they express an enzyme that can catalyze a colorimetric reaction. BMDCs were first cultured with either SIINFEKL, Fluorescien-K(N_3)EQLESIINFEKL or **vaccine construct 1** then the BMDCs were co-cultured with B3Z cells. Unfortunately, only mild activation of B3Z cells was observed when co-cultured with BMDCs pre-treated with **vaccine construct 1** especially compared to B3Z cells co-cultured with BMDCs pre-treated with SIINFEKL peptides (**figure 2.3**). Although there appeared to be little to no advantage from delivering the CTLe through **vaccine construct 1**, the decision to move into *in vivo* models was made. The reasoning being that cross-presentation is a fairly robust system so the benefit of conjugation to a VLP platform may be in more specific tracking to the immune system upon vaccination.[28, 29] If that would be the advantage to our construct, animal models are more likely to show positive effects.

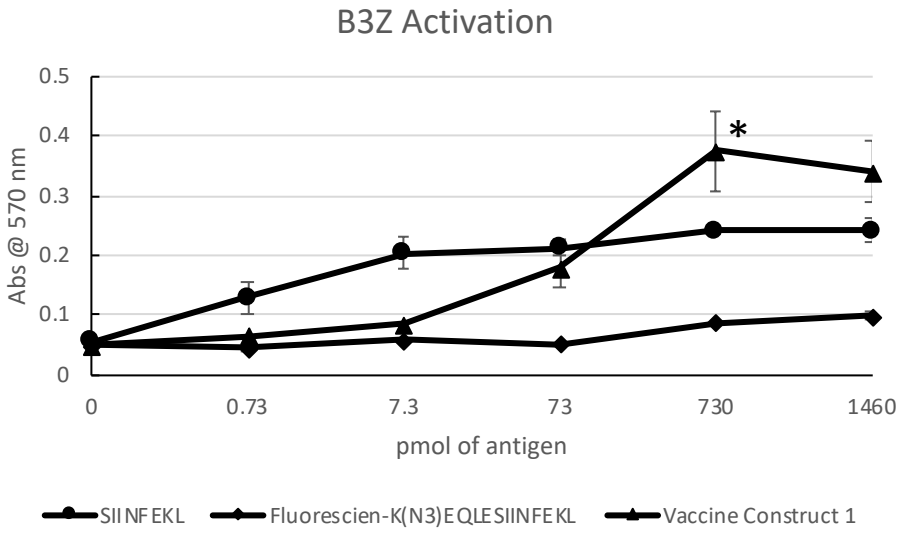

Figure 2.3. B3Z T cell activation assay. Bone marrow-derived dendritic cells (BMDCs) were co-incubated with varying concentrations of antigen in different forms. Following incubation, antigen loaded BMDCs were co-cultured with B3Z T cells. T cell activation was measured by the development of color from chlorophenol red-β-*D*-galactopyranoside with the absorbance measured at 570nm. All samples were measured in triplicate. *p*-values were calculated by a one-tailed *t*-test. *$p < 0.05$.

2.2.2.4 *In Vivo* Testing

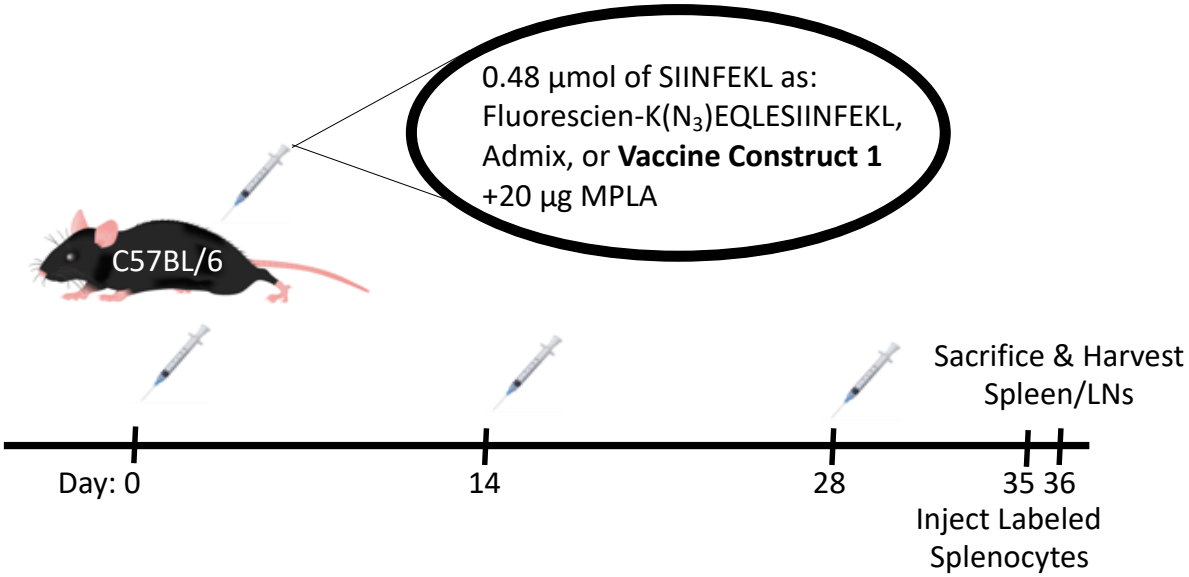

Scheme 2.5. Immunization schedule for *in vivo* cytotoxic T cell (CTL) experiment. Groups of 3 C57BL/6 mice were immunized 3 times bi-weekly with 0.48 µmol of CTL epitopes (CTLes) as either Fluorescein-K(N_3)EQLESIINFEKL, an admix of Fluorescein-K(N_3)EQLESIINFEKL and Qβ, or **vaccine construct 1** with 20 µg of MPLA as adjuvant. On D35, animals received an injection of $CSFE^{Hi}OVA^{+}$:$CSFE^{Lo}OVA^{-}$ labeled splenocytes via tail vein injection. 24hrs later mice were sacrificed with spleens and lymph nodes collected. Flow cytometry was performed to examine the $CSFE^{Hi}OVA^{+}$:$CSFE^{Lo}OVA^{-}$ ratio.

To test if our **vaccine construct 1** could activate CTLs *in vivo*, mice were immunized three times with **vaccine construct 1** (0.48 µmol CTLe) and monophosphoryl lipid A (MPLA) as adjuvant (**scheme 2.5.**). On D35, a 1:1 mixture of murine splenocytes labeled carboxyfluorescein succinimidyl ester $(CSFE)^{Hi}OVA^{+}$:$CSFE^{Lo}OVA^{-}$ was injected into immunized mice via tail vein injection. 24 hrs later mice were sacrificed and their spleens and lymph nodes (LNs) were harvested. Flow cytometry analysis was performed to look for a change in the ratio of $CSFE^{Hi}OVA^{+}$:$CSFE^{Lo}OVA^{-}$ labeled cells. If vaccination induced OVA specific CTLs, they should selectively kill the $CSFE^{Hi}OVA^{+}$ labeled splenocytes while having minimal effect on the

$CSFE^{Lo}OVA^{-}$ cells. Unfortunately there were no significant changes between mice, in different immunization groups (**figure 2.4**).

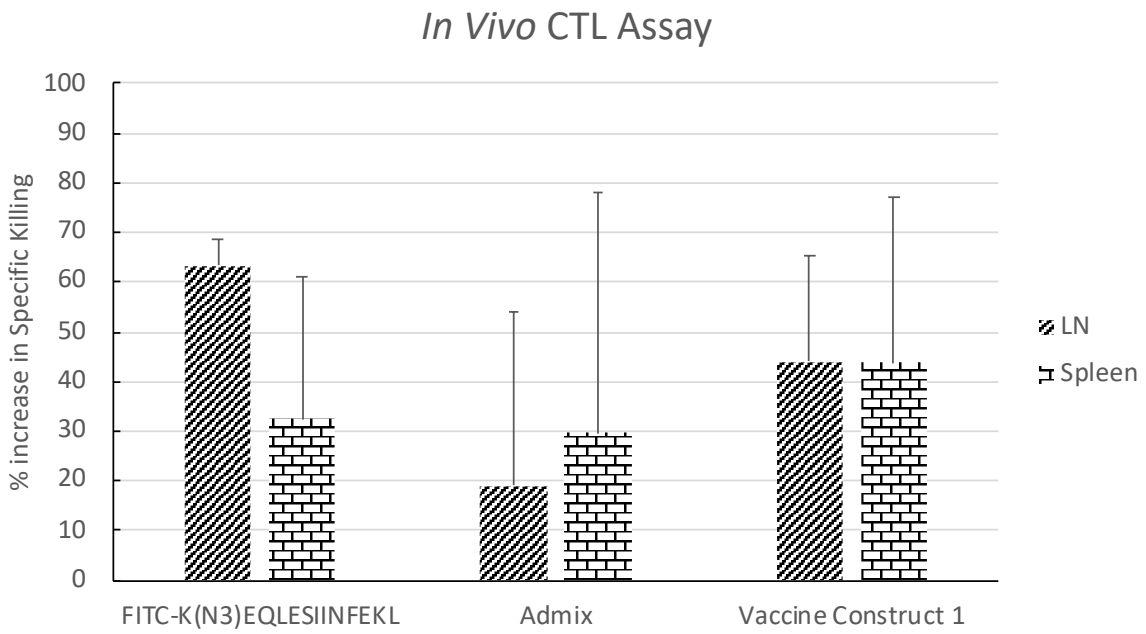

Figure 2.4. Percent increase in specific killing of $CSFE^{Hi}OVA^{+}$ splenocytes by mice (N = 3/group) immunized with either FITC-K(N_3)EQLESIINFEKL, an admix of FITC-K(N_3)EQLESIINFEKL and Qβ, or **vaccine construct 1**, compared to naïve mice. No difference was observed between immunization groups.

Since OVA specific CTL activity was not detected the T cell population, further immunological analysis was performed. On D35, immunized mice were sacrificed and their spleens and LNs were harvested (**figure 2.5A**). Splenocytes and lymphocytes were analyzed by flow cytometry. Although distinct $CD8^{+}$ and $CD4^{+}$ T cell populations were identified, no cells stained positive for SIINFEKL-MHC specific TCRs, suggesting that vaccination with **vaccine construct 1** failed to elicit large significant amounts of OVA specific CTLs (**figure 2.5B**).

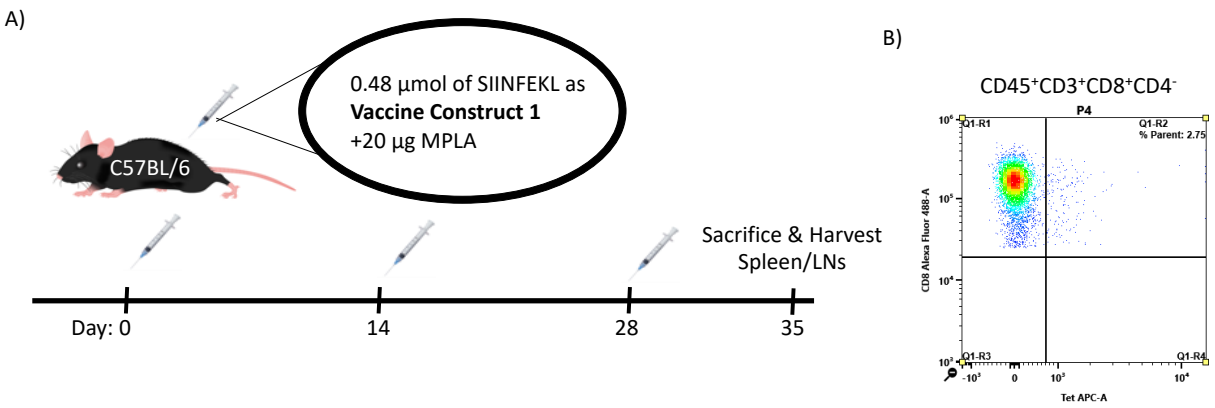

Figure 2.5. Analysis of CTL populations in immunized mice. (A) Immunization timeline. A group of 3 C57BL/6 mice were immunized 3 times bi-weekly with 0.48 µmol of cytotoxic T cell epitope (CTLe) as **vaccine construct 1** with 20 µg of MPLA as adjuvant. On D35, mice were sacrificed, and their spleens and lymph nodes were harvested. (B) Flow cytometry analysis was performed on the harvested cells. Cells were stained for CD45 (lymphocyte marker), CD3 (T cell marker), CD4 (helper T cell marker), CD8 (CTL marker) and tetramers against CTLe specific T cell receptors. Cells were gated for CTLs ($CD45^+CD3^+CD4^-CD8^+$) and the percentage of antigen specific CTLs was examined. Representative result shown.

This lack of CTL induction may be due to the relatively low loading of CTLes/capsid. Analysis of the Qβ capsid has shown that each capsid has on average three strands of RNA and our strategy can only put one CTLe per RNA strand. To efficently load enough MHC class I molecules to activate CTLs, each APC would have to uptake lots of VLPs. VLP-based conjugate vaccines that have successfully elicited CTL responses have significantly higher antigen loading than we can obtain with our conjugation strategy.[9, 10] Upon solving the solubility problem through covalent conjugation to RNA, another problem was discovered, i.e., loading efficiency.

2.2.3 Non-Covalent Functionalization of the Packaged RNA

2.2.3.1 Synthesis of Thiazole Orange-CDM

Since covalent conjugation to the capsid RNA solved the solubility issue, a more efficient method of loading through interactions with RNA was desired. One potential solution is to use a small molecule tag that could non-covalently bind the capsid RNA. To that end, thiazole orange

(TO) was selected, which is a small molecule dye that intercalates RNA (**figure 2.6**). The molecule is permissive to substitution on the amines and such derivatives retain RNA binding activity.[30-32]

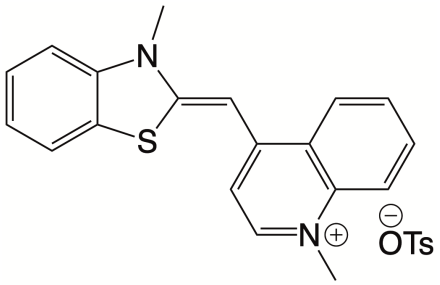

Thiazole Orange

Figure 2.6. The structure of thiazole orange. A small molecule dye capable of binding to RNA.

A TO derivative containing an azide functionalization (TO-N_3) was recently reported to be capable of loading the interior of Qβ with poly(ethylenglycol) (PEG) chains or short peptides.[32] Das and coworkers first conjugated PEG chains of various length to the TO-N_3 through CuAAC click chemistry and were capable of loading over 100 cargo molecules/capsid even with the largest PEG chains used. This also held for hydrophobic peptides with loading >100 peptides/capsid. This suggests that this approach may solve the two problems presented by the covalent conjugation approaches previously discussed.

Although CuAAC click chemistry is well known and widely used in conjugate vaccines, it does have some drawbacks. One being that the resulting triazole moiety is immunogenic in and of itself.[33] The other being that it adds additional processing steps for APCs before the CTLe could be presented on MHC molecules. To overcome those drawbacks, we developed a synthesis that replaced the azide with an acid sensitive linker, 3-(4-Methyl-2,5-dioxo-2,5-dihydrofuran-3-yl)propanoic acid (**CDM**) (**Scheme 2.6**). **CDM** was chosen because under basic conditions it can

react with amines, like those found on the *N*-terminus of CTLes to form a covalent bond. Then when the pH drops, such as in the lysosome, the reaction reverses regenerating the unmodified antigen.

The first-generation synthetic scheme attempted to introduce a 9-fluorenylmethyloxycarbonyl (Fmoc)- protected amine as part of the first step (**scheme 2.6A**). At room temperature no reaction was observed after even a week. The reaction had previously been reported using 1,3-diiodopropane.[32] To speed up the diiodo reaction, the original published synthesis of TO-N_3 heated the reaction. When the reaction was heated to reflux, the linker was consumed but no product was obtained. The likely cause was thermal decomposition of the Fmoc protecting group, resulting in peralkylation of the now unprotected amine. Lowering the temperature below the thermal decomposition temperature and adding a tetrabutylammonium iodide (TBAI) failed to produce more than trace amounts of the desired product after extended reaction times.

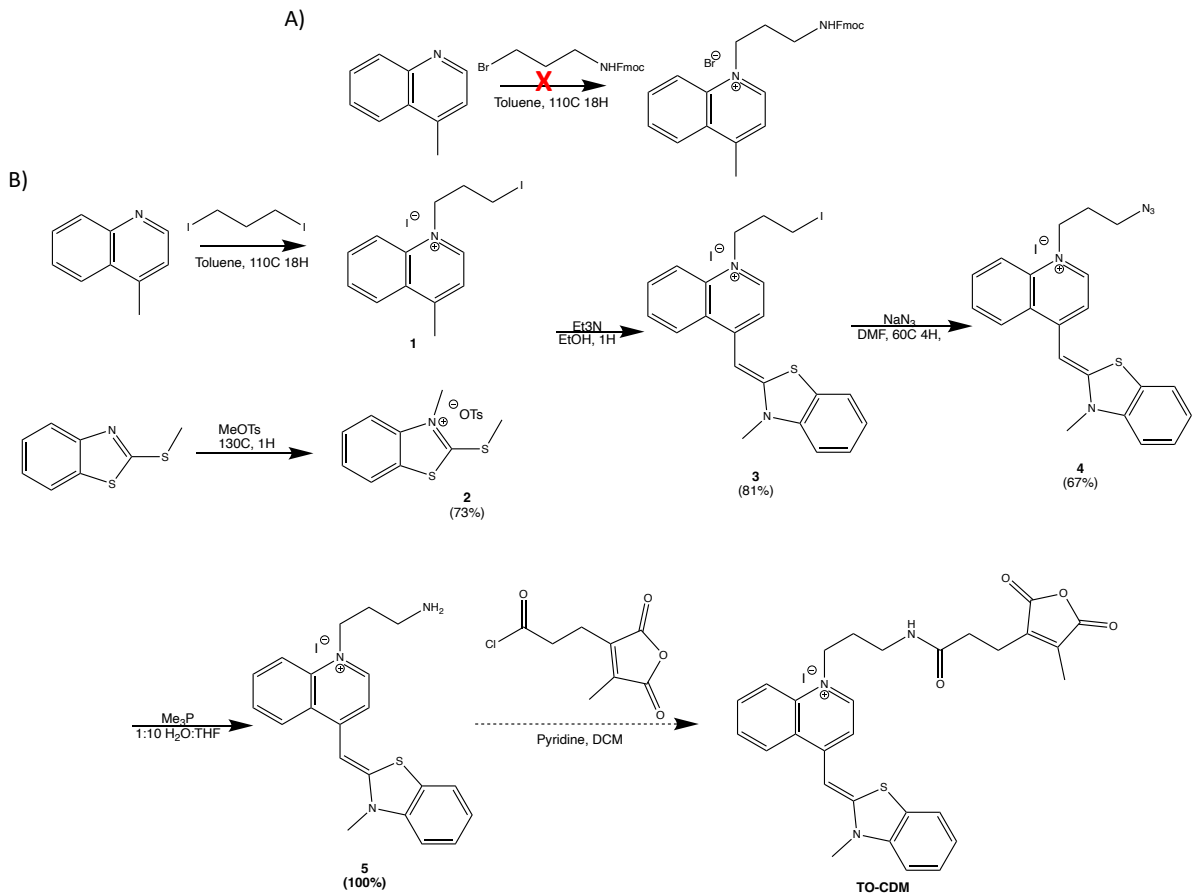

Scheme 2.6 Synthesis of TO-CDM (A) initial attempts to directly incorporate a protected amine in the first step never gave more than trace product. (B) Redesigned TO-CDM synthesis.

With the failure to directly add the Fmoc-amine in the first step, the synthesis was redesigned. The synthesis was reverted to the previously published synthesis of TO-N_3. From TO-N_3 the azide was reduced via a Staudinger reduction to generate the free amine (5) (**Scheme 2.6B**). In the final step, the free acid form of **CDM** will be converted to the acyl chloride *in situ* and reacted with **5** to form **TO-CDM**.

2.3 Conclusions

A variety of methods were explored to load CTLes into the interior of the Qβ capsid. Direct covalent conjugation to the interior of the capsid failed due to the inherent hydrophobicity of CTLes. Covalent functionalization of the encapsulated RNA overcame the

solubility issues but failed in biological testing, likely because of the low loading capacity. Use of an RNA binding small molecule (TO) appears promising to overcome the issues reported in the previous trials.

2.4 Future Work

Upon the successful synthesis of the TO-CDM and confirmation that it can be used to load CTLes in Qβ, the investigation of the immunological properties of the Qβ@TO-CDM-CTLe particles will be performed. Initial studies will follow a similar experimental design as work done on the covalent funtionalization of RNA strategy. If the treatment with Qβ@TO-CDM-CTLe leads to SIINFEKL cross-presentation in BMDCs and they are able to activate OVA specific T cells, the plan is to move into animal studies using OVA expressing tumor cell lines. If successful, there are two other planned lines of investigation.

One goal is to explore the effect of peptide length on cross-presentation efficiency. There is evidence that vaccines based on extended CTLes perform better than vaccines based on either the minimal CTLe or full proteins.[34-36] Those studies focus on free soluble peptides so it is important to explore if conjugation of VLP to the epitope effects the cross-presentation process.

The other goal is to explore the incorporation of disease-associated helper T cell epitopes into the vaccine. Although Qβ contains its own helper T cell epitopes and the helper T cells elicited through vaccination are cappable of inducing isotype switching and eliciting memory B cells against antigens conjugated to Qβ, they are anti-Qβ helper T cells. During an infection challenge there would be no Qβ to reactivate the anti-Qβ helper T cells. Without the helper T cell reactivation, the memory B cell response may be delayed or otherwise hampered.

Therefore there are interests in loading VLP-based cooonjugate vaccines with B cell antigens and disease specific helper T cell epitopes.

2.5 Material and Methods

2.5.1 General Experimental Procedures and Methods for Synthesis

All chemicals were reagent grade and were used as received from the manufacturer, unless otherwise noted. Solvents were dried using a solvent purification system. Reactions were visualized by UV light (254 nm) and by staining with either $Ce(NH_4)_2(NO_3)_6$ (0.5 g) and $(NH_4)_6MO_7O_{24}*4H_2O$ (24.0 g) in 6% H_2SO_4 (500 mL) or 5% H_2SO_4 in EtOH. Flash chromatography was performed on silica gel 601 (230-400 Mesh).

Centrifugal filter units of 10,000 and 100,000 molecular weight cut-off (MWCO) were purchased from EMD Millipore. Fast protein liquid chromatography (FPLC) was performed on a GE ÄKTA Explorer (Amersham Pharmacia) instrument equipped with a Superose-6 column. For characterization of Qβ mutants, liquid chromatography-mass spectrometry (LCMS) analysis was performed. The samples for LCMS were prepared as follows: 1:1 v/v of 40 μg mL^{-1} of Qβ-MUC1 stock solution and 100 mM DTT was mixed and incubated in a water bath at 37 °C for 30 min. One drop of 50% formic acid was added to the mixture. LCMS was performed on Waters Xevo G2-XS quadrupole/time-of-flight UPLC/MS/MS. The liquid chromatography was done on ACUITY UPLC® Peptide BEH C18 column, 130Å, 1.7 μm, 2.1 mm x 150 mm, using gradient eluent from 95% 0.1% formic acid in CH_3CN (0.3 mL min^{-1} flowrate) at a column temperature of 40 °C. The spectra were deconvoluted using MaxEnt1. Protein concentration was measured using the Coomassie Plus Protein Reagent (Bradford Assay, Pierce) with BSA as the standard.

All animal experiments were performed in accordance with the guidelines of the Institutional Animal Care and Use Committee (IACUC) of Michigan State University. The animal usage protocol number is PROTO201900423.

2.5.2 Expression of wt Qβ

Wild-type Qβ was expressed as previously reported.[1]

2.5.3 Expresion of $Q\beta_{T93AHA}$ Mutants by Global Methionine Replacement

B834(DE3) *E. Coli* cells containing the p75M plasmid were used to inoculate 10 mL of SelenoMet media, containing 100 μg/mL carbenicillin and 40 mg/L of L-methionine. The starter culture was incubated overnight at 37°C. The starter culture was then added to 1 L of SelenoMet media containing 100 μg/mL carbenicillin and 40 mg/L of L-methionine. The cells were cultured at 37°C until the OD_{600} reached 0.6-1.0. The media was removed by pelleting the cells using a Fiberlite F20-4x1000 LEX rotor at 6000 rpm for 20 min. The cells were washed with 1 L of SelenoMet media via centrifugation using a Fiberlite F20-4x1000 LEX rotor at 6000 rpm for 20 min. The pelleted cells were resuspended in 1 L of pre-warmed SelenoMet media, containing 100 μg/mL of carbenicillin and 100 mg/L of azidohomoalanine (AHA). The cells were allowed to recover for an hour at 37°C. Following the recovery period, expression was induced by the addition of IPTG to a final concentration of 1 mM. The culture was incubated for 6 hrs at 37°C before cells were collected by centrifugation using a Fiberlite F20-4x1000 LEX rotor at 6000 rpm for 20 min. The pelleted cells were resuspended in 30 mL of 0.1M KPB, pH 7.4, and stored at -20°C until purification.

2.5.4 Purification of Qβ or $Qβ_{T93AHA}$

Cells were lysed using a sonicator set to 30% power for 10 minutes with 5 seconds on and 5 seconds off (20 min total). The lysis was centrifuged for 20 min at 14,000 rpm using a Fiberlite F21-8x50y rotor to remove cellular debris. The supernatant was transferred to a 50 mL centrifuge tube with 5 g of PEG8000 and diluted to 50 mL. The resulting protein and 10% (w/v) PEG8000 solution was mixed on a nutating mixer overnight. The PEG:protein complexes were pelleted by centrifugation at 14,000rpm for 20 min using a Fiberlite F21-8x50y rotor. The pellet was resuspended in 10 mL of milliQH_2O. The solution was diluted to 1:1 (v/v) with 1:1 (v/v) chloroform:n-butanol to form a colloidal mixture in glass centrifuge tubes. The PEG was extracted by centrifuging the mixture at 7000 rpm for an hour using a Fiberlite F21-8x50y rotor. The aqueous layer was extracted and washed with milliQH_2O to remove any trace organic solvent using centrifuge filtration (MWCO 100 kDa). The protein solution was concentrated and applied to a 10-40% sucrose gradient. The sucrose gradient was then centrifuged at 28000 rpm for 3-5 hrs using a TH-641 rotor. Bands containing Qβ or $Qβ_{T93AHA}$ were visualized via UV light scattering and were collected in fractions. Fractions were analyzed for purity using SEC. Fractions containing pure Qβ were combined and concentrated to ~1mL and the protein concentration quantified via a Bradford assay.

2.5.5 Lead Mediated Hydrolysis of Capsid RNA

This protocol was adapted from a previous publication.[18] The following were added in order with the final conditions shown: 1mg Qβ, 50 mM HEPES, and 5mM lead(II)acetate, total volume 1 mL. The solution was incubated for 7 days at 37°C with shaking. Following incubation, the lead salt was removed by exchanging the solvent with a 5 mM solution of EDTA 5 times

followed by 5 times with milliQH_2O using centrifuge filtration (MWCO 30 kDa). The entire process was repeated a second time. The empty capsids were analyzed via UV-Vis and native gel electrophoresis.

2.5.6 Synthesis of OVA Peptides Used in the Study

p-Benzyloxybenzyl alcohol resin (100-200 mesh) (Wang Resin) loaded with Fmoc-protected lysine at 0.32 meq/g was used as the solid phase support. The *N*-terminal Fmoc was deprotected using 20% piperidine in DMF. The amino acid coupling was carried out with Fmoc-amino acids/hexynoic acid/5(6)-carboxyfluorescein (5 equiv.) using (2-(1H-benzotriazol-1-yl)-1,1,3,3-tetramethyluronium hexafluorophosphate (HBTU)/hydroxybenzotriazole (HOBt) (4.9 equiv.) and DIPEA (10 equiv.). The amino acid side chains were deprotected and the peptide was cleaved from the resin using a solution of 18:1:1 TFA:triisopropylsilane (TIPS):H_2O. After 4hrs, the peptide was precipitated by diethyl ether (Et_2O) and pelleted by centrifugation. The crude peptide was purified by HPLC using a Shimadzu HPLC (LC-8A Liquid Chromatograph Pump, DGU-14A Degasser, and SPD-10A UV-Vis Detector), using a reverse phase SUPERCOSIL LC18, 25 cm × 10 mm 5 µm with an acetonitrile (ACN):H_2O (0.1% TFA) gradient. The gradient was 5% ACN for 5 min, 5-50% ACN in 5-20 min, 50-100% ACN in 20-50 min, 100% ACN for 50-55min, 100-5% ACN in 55-57 min, and 5% ACN from 57-60 min. The flow rate was 5 ml/min. Peptides were characterized by ESI-TOF MS and obtained in a yield of 40-50% (alkyne-SIINFEKL **figure 2.12**, FITC-K(N_3)EQLESIINFEKL, **figures 2.13-2.14**)

2.5.7 General CuAAC Click Reaction Conditions

This procedure was adapted from a previous publication.[37] Qβ (1 mg, 1 mg/mL final conc.) containing either an azide or alkyne functionality in PBS (pH 7.4) was mixed with between 5-50

equiv. of the corresponding azide or alkyne containing peptide dissolved in DMSO so that the final amount of DMSO was 10%. To the mixture the following were added in order; premixed Cu:tris-hydroxypropyltriazolylmethylamine (THPTA) to a final concentration of 1mM:5mM, aminoguanidine HCl to a final concentration of 50mM, and sodium ascorbate to a final concentration of 50mM. The reaction was capped and mixed on a nutating mixer in the dark overnight at RT. Precipitation was removed by centrifugation. Unreacted peptides were removed by centrifuge filtration (MWCO 30 kDa) against PBS (pH 7.4).

2.5.8 Covalent Functionalization of Capsid RNA

The procedure was adapted from a previous publication.[38] A solution of Qβ (final conc. 30 mg/mL) in 40 mM sodium periodate ($NaIO_4$) was prepared. The solution was mixed on a nutating mixer in the dark at RT for 48 hr. $NaIO_4$ was removed by centrifuge filtration (MWCO 30 kDa) against 100 mM sodium acetate (NaOAc) twice. The concentration of Qβ was adjusted to 30 mg/mL. Either fluorescein-5-thiosemicarbazide (FSTC) or hex-5-ynehydrazide in DMSO was added to a final concentration of 2mM. The resulting solution was mixed on a nutating mixer in the dark at RT overnight. Following the incubation with hex-5-ynehydrazide, the sample was washed twice by centrifuge filtration (MWCO 30 kDa) against PBS (7.4) and CuAAC click chemistry was performed as described above. After the click reaction in the case of hex-5-ynehydrazide or after FSTC conjugation, samples were washed to remove unconjugated dye or peptides by centrifuge filtration (MWCO 30 kDa) against PBS (pH 7.4). Samples were washed until the flow through appeared colorless (~3-5 washes). Loading was determined by fluorescence spectroscopy (ex. 490 em. 512) through comparison to a standard curve of FSTC at similar concentrations.

2.5.9 Bone Marrow-Derived Dendritic Cell (BMDC) Isolation and Culture

The procedure was adapted from previous publications.[39, 40] Femurs of C57BL/6 mice were collected with flesh removed, and sterilized. Both ends of the bones were removed and the marrow was removed from the femurs by flushing the bones with Dulbecco's phosphate buffered saline (DPBS). Cells were collected by centrifugation at 300 x g for 5 min at 4 ^{o}C. Cells were resuspended in red blood cell (RBC) lysis buffer (5 mL). The solution was shaken at RT for 5 min. To halt the lysis reaction, 20 mL of DPBS was added. Cells were collected by centrifugation at 300 x g for 5 min at 4 ^{o}C. The harvested cells were washed twice with BMDC media (RPMI 1640 supplemented with 10% fetal bovine serum (FBS), 1 mM sodium pyruvate, 55 µM 2-mercaptoethanol (2-ME), 10 mM 4-(2-hydroxyethyl)-1-piperazineethanesulfonic acid (HEPES), 1x MEM non-essential amino acids solution, 100 µg/mL penicillin G, 100 U/mL streptomycin) and centrifugation (300 x g for 5 min at 4 ^{o}C). Cells were resuspended in BMDC media supplemented with 20 ng/mL murine GM-CSF and plated at a density of 1 x 10^4 cells/mL in 100 mm petri dishes (10 mL/dish). Cells were cultured in a humidified CO_2 incubator at 37 ^{o}C with 5% CO_2. On day 3, 10 mL of BMDC media supplemented with 20 ng/mL murine GM-CSF was added to each plate. On days 6, 8, and 10, 50% of the culture media was replaced with fresh BMDC media supplemented with 20 ng/mL. For the media changes, cells in the conditioned media were collected by centrifugation (300 x g for 5 min at 4 ^{o}C) resuspended in the fresh media and returned to the plate. On day 11, 75% of the media was replaced in the same manor. On days 12 and 13, 100% of the media was replaced as described above. Cells were harvested and used on day 14.

2.5.10 General Flow Cytometry Protocol

Cells of interest were washed three times with fluorescence-activated cell sorting (FACS) buffer (1% FBS, 0.5% sodium azide (NaN_3) in PBS (pH 7.4)) and centrifugation (300 x g for 5 min at 4 ^oC). Cells were stained with fluorophore-conjugated antibodies/MHC tetramers for 30 min on ice in the dark with vortexing every 15 min. Unbound antibodies/tetramers were removed by washing three times with FACS buffer and centrifugation (300 x g for 5 min at 4 ^oC). If cells needed to be fixed, samples were treated with 100 µL fixation/permeabilization buffer for 30 min at RT in the dark with vortexing every 15 min. Following fixation, cells were washed three times with FACS buffer and centrifugation (300 x g for 5 min at 4 ^oC). After the final wash, the cells were resuspended in 300 µL of FACS buffer. Samples were run on either an Accuri C6 or Cytek Aurora flow cytometer.

2.5.11 Cross-Presentation Assay

This procedure was adapted from a previous publication.[41] BMDCs were pulsed with varying concentrations of either the peptide or **vaccine construct 1** for 1 hr in a humidified CO_2 incubator at 37 ^oC with 5% CO_2. Cells were washed by pelleting (300 x g, 5 min, 4 ^oC) and resuspended in fresh BMDC buffer. Flow cytometry was performed as described above, using anti-mouse H-2K^b bound to SIINFEKL (Clone 25-D1.16) conjugated to PE.

2.5.12 B3Z T Cell Activation Assay

This procedure was adapted from a previous publication.[41] 2 x 10^4 BMDCs were cultured in a 96-well plate overnight in a humidified CO_2 incubator at 37 ^oC with 5% CO_2. The BMDCs were pulsed with varying concentrations of either the peptide or **vaccine constructs 1** for 6 hrs. The cells were washed by pelleting (300 x g, 5 min, 4 ^oC) with fresh BMDC buffer. 1 x 10^5 B3Z cells

were added to the BMDC cells. The cells were co-cultured for 16 hrs in a humidified CO_2 incubator at 37 ^oC with 5% CO_2. The cells were pelleted (300 x g, 5 min, 4 ^oC) and the media replaced with 100 µL of chlorophenol red-β-*D*-galactopyranoside (CPRG) buffer (9.1 mg CPRG, 0.125 mg triton-X, 90 mg magnesium chloride ($MgCl_2$) in 100 mL of PBS (pH 7.4)) was added to each well. The cells were incubated for 6 hrs, in a humidified CO_2 incubator at 37 ^oC with 5% CO_2. The abs was measured at 595 nm. Samples were run in quadruplicate.

2.5.13 Harvesting of Cells from Spleens and Lymph Nodes (LNs)

Mice were euthanized and the spleens and LNs were harvested. Spleens or LNs were put in a culture dish containing 10 mL of splenocyte washing media (RPMI 1640, 2% FBS, 10 mM HEPES, 55 uM 2-ME, 2 mM L-glutamine, and 100 µg/mL penicillin G, 100 U/mL streptomycin). The tissue was macerated using the end of a syringe and transferred to a centrifuge tube. The plate was washed with an additional 2 mL of washing media and added to the centrifuge tube. The solution was centrifuged (300 x g, 5 min, 4 ^oC) and the supernatant was removed by aspiration. The pellet was resuspended in 3 mL RBC lysis buffer. The solution was mixed on a nutating mixer at RT for 5 min. The lysis reaction was halted by the addition of 9 mL of cold washing medium and centrifuged (300 x g, 5 min, 4 ^oC). The supernatant was aspirated and replaced with 10 mL of culture medium and filtered through a 70 µm nylon mesh filter. Cells were immediately used in the necessary experiments.

2.5.14 *In Vivo* CTL Activity Assay

This procedure was adapted from a previous publication.[9] 6-week old C57BL/6 mice were injected subcutaneously with either the peptide, **vaccine construct** 1, or an admix of Qβ and fluorescien-K(N_3)EQLESIINFEKL at 0.48 µmol peptide with 20 µg monophosphoryl-lipid A (MPLA)

as adjuvant on days 0, 14, and 28. On day 35, mice were injected via the tail vein with a 1:1 mixture of peptide$^-$carboxyfluorescein succinimidyl ester (CFSE)^{lo}:peptide$^+$CFSE^{hi} splenocytes (0.2 mL, 2 x 10^6 cells), harvested from a naïve C57BL/6 mouse. The excess cell mixture was stored in splenocyte culture media, in a humidified CO_2 incubator at 37 ^oC with 5% CO_2, as a pre-injection sample. After 24 hrs, mice were euthanized and the spleens and LNs were harvested. The collected cells were analyzed by flow cytometry as described above. 5 µL of 7-AAD was added to the final sample 10 min before analysis.

2.5.15 Flow Cytometry Analysis of T Cell Populations.

6-week old C57BL/6 mice were injected subcutaneously with either the peptide, **vaccine construct 1**, or admix at 0.48 µmol peptide with 20 µg MPLA as adjuvant on days 0, 14, and 28. On day 35, mice were sacrificed and their spleens and LNs were harvested. The harvested cells were analyzed by flow cytometry using mouse anti-CD45 Alexa Fluor 532 conjugate, mouse anti-CD8 Alexa Fluor 488 conjugate, mouse anti-CD4 Qdot800 conjugate, mouse anti-CD3 BV510 conjugate, and live/dead blue.

2.5.16 Synthesis of TO-CDM

1-(3-Iodopropyl)-4-methylquinolin-1-ium iodide (**1**)

The synthetic procedure was adapted from the literature.[32] 4-Methylquinoline (1.0 g, 7.0 mmol) was dissolved in dry toluene (27.8 mL), followed by the addition of 1,3-diiodopropane (5 equiv., 4.0 mL, 34.9 mmol). The reaction was heated to reflux (110 ^oC). Upon completion, the yellow-orange precipitate was collected by vacuum filtration and washed with diethyl ether (Et_2O). The crude product was used without further purification. ^{1}H NMR (500MHz, $CDCl_3$) δ 10.31 (d, *J* = 5.9 Hz, 1H), 8.46 (d, *J* = 9.2 Hz, 1H), 8.41 (d, *J* = 9.2 Hz, 1H), 8.26 (t, *J* = 8.2 Hz, 1H), 8.05-7.99

(m, 2H), 5.47 (t, *J* = 7.9 Hz, 2H), 3.50 (t, *J* = 6.3 Hz, 2H), 3.07 (s, 3H), 2.72 (p, *J* = 6.3 Hz, 2H). ^{13}C NMR (126 MHz, DMSO-d_6) δ 161.79, 146.13, 142.96, 138.10, 129.62, 128.51, 127.45, 125.93, 124.42, 116.16, 36.86, 21.25, 18.47 (**figures 2.15-2.16**)

3-Methyl-2-(methylthio)benzo[d]thiazol-3-ium 4-methylbenzenesulfonate (**2**)

The synthetic procedure was adapted from a prior publication.[32] 2-(Methylthio)benzo[d]thiazole (2.04g, 11.3 mmol) and methyl-*p*-toluenesulfonate (1.2 equiv., 2.10 mL, 13.5 mmol) were heated to 130 °C under N_2 gas. After 1 hr, the reaction turned yellow and the temperature was reduced to 40 °C. Acetone was added until the solid dissolved and the reaction refluxed (60 °C) for 30 min. The reaction was cooled to room temperature (RT). The resulting crystals were vacuum filtered and washed with acetone to afford 3-methyl-2-(methylthio)benzo[d]thiazol-3-ium 4-methylbenzenesulfonate (**2**) as a white solid (3.03 g) in 73% yield. ^{1}H NMR (500MHz, DMSO-d_6) δ 8.37 (d, *J* = 8.2 Hz, 1H), 8.18 (d, *J* = 8.4Hz, 1H), 7.83 (dd, *J* = 7.3, 1.2 Hz, 1H), 7.71 (dd, *J* = 7.3, 1.1 Hz, 1H), 7.46 (d, *J* = 7.9 Hz, 2H), 7.09 (d, *J* = 7.5 Hz, 1H), 4.09 (s, 3H), 3.10 (s, 3H), 2.27 (s, 3H). ^{13}C NMR (126 MHz, DMSO-d_6) δ 181.79, 146.16, 142.99, 138.07, 129.65, 128.75, 128.51, 127.48, 125.94, 124.43, 116.18, 36.87, 21.24, 18.46. HRMS (ESI) m/z calcd for $C_9H_{10}NS_2^+$ $[M]^+$ 196.0255, found 196.0255. (**figures 2.17-2.19**)

(Z)-1-(3-Iodopropyl)-4-((3-methylbenzo[*d*]thiazol-2(3*H*)-ylidene)methyl)quinoline-1-ium iodide (**3**)

The synthetic procedure was adapted from a published procedure.[32] A mixture of **1** (1.2 equiv, 0.72 g, 1.6 mmol) and **2** (0.50 g, 1.4 mmol) were dissolved in ethanol (EtOH) (20.5 mL). Triethylamine (1.1 equiv., 0.21 mL, 1.5 mmol) was added to the solution dropwise. The reaction was stirred for 1 hr at RT. Et_2O was added to precipitate the product. The product was collected

by centrifugation and washed with Et_2O. (Z)-1-(3-Iodopropyl)-4-((3-methylbenzo[*d*]thiazol-2(3*H*)-ylidene)methyl)quinoline-1-ium iodide (**3**) was collected as a reddish-brown solid (0.65 g) in 81% yield. ^{1}H NMR (500MHz, DMSO-d_6) δ 8.80 (d, J = 8.8 Hz, 1H), 8.59 (d, *J* = 7.2 Hz, 1H), 8.13 (d, *J* = 8.8 Hz, 1H), 8.06 (d , *J* = 8.0 Hz, 1H), 8.00 (t , *J* = 7.2 Hz, 1H), 7.81 (d , *J* = 8.0 Hz, 1H), 7.75 (t, *J* = 7.7 Hz, 1H) 7.64-7.60 (m , 1H), 7.43 (t , *J* = 7.5 Hz, 1H), 7.37 (d , *J* = 7.2 Hz, 1H), 6.94 (s, 1H) 4.61 (t , *J* = 7.1 Hz, 2H), 4.03 (s, 3H), 3.36-3.34 (m, 2H), 2.42-2.30 (m, 2H). HRMS (ESI) m/c calcd for $C_{21}H_{20}IN_2S^+$ $[M]^+$ 459.0392, found 459.0402. (**figures 2.20-2.21**)

(Z)-1-(3-Azidopropyl)-4-((3-methylbenzo[*d*]thiazol-2(3H)-ylidene)methyl)quinoline-1-ium iodide (**4**)

The synthetic procedure was adapted from a previous publication.[32] **3** (0.80 g, 1.4 mmol) was dissolved in dry dimethylformamide (DMF) (10 mL). To the solution, sodium azide (3.3 equiv., 0.30 g, 4.6 mmol) and TBAI (1.1 equiv., 0.57 g, 1.5 mmol) were added sequentially. The reaction was stirred for 4 hrs at 60 °C. The solvent was removed by rotovap and the crude product was redissolved in EtOH (10 mL). The crude product was precipitated using Et_2O (25 mL) and collected by centrifugation. The crude product was purified by silica gel flash chromatography using 10% methanol (MeOH) in dichloromethane (DCM). (Z)-1-(3-Azidopropyl)-4-((3-methylbenzo[*d*]thiazol-2(3H)-ylidene)methyl)quinoline-1-ium iodide (**4**) was obtained as a dark red powder (0.47 g) in 67% yield. ^{1}H NMR (500MHz, DMSO-d_6) δ 8.81 (d, *J* = 8.4 Hz, 1H), 8.61 (d, *J* = 7.26 Hz, 1H), 8.14 (d, *J* = 8.9 Hz, 1H), 8.07 (d, *J* = 8.0Hz, 1H), 8.00 (dd, *J* = 1.5Hz, 7.0Hz, 1H), 7.81 (d, *J* = 8.0 Hz, 1H), 7.76 (dd, *J* =1.0 Hz, 7.0 Hz, 1H), 7.62 (dd, *J* = 1.3 Hz, 7.3 Hz, 1H), 7.43 (dd, *J* = 1.0 Hz, 7.3 Hz, 1H), 7.38 (d, *J* = 7.3 Hz, 1H), 6.95 (s, 1H), 4.65 (t, *J* = 7.0 Hz, 2H), 4.03 (s, 3H), 3.53 (t, *J* = 7.21Hz, 2H), 2.15-2.07 (m, 2H) ^{13}C NMR (126 MHz, DMSO-d_6) δ 160.68, 149.07, 144.93,

140.95, 187.50, 133.78, 128.67, 127.23, 126.36, 125.03, 124.70, 124.38, 123.40, 118.44, 113.56, 108.34, 88.72, 48.36, 34.35, 28.35, 13.96. HRMS (ESI) m/z calcd for $C_{21}H_{20}N_5S^+$ $[M]^+$ 374.1439, found 374.1462. (**figures 2.22-2.24**)

(Z)-1-(3-Aminopropyl)-4-((3-methylbenzo[*d*]thiazol-2(3H)-ylidene)methyl)quinoline-1-ium iodide (**5**)

4 (0.5 g, 1.0 mmol) was dissolved in 1:10 H_2O:tetrahydrofuran (THF) (10 mL) under an N_2 atmosphere. 1M Trimethylphosphine in THF (3 equiv., 3.0 mL, 3.0 mmol) was added dropwise to the solution. The reaction was stirred at RT overnight. The solvent was removed by rotovap and the crude product was purified by silica gel flash chromatography using 10% MeOH in CH_2Cl_2. (Z)-1-(3-Aminopropyl)-4-((3-methylbenzo[*d*]thiazol-2(3H)-ylidene)methyl)quinoline-1-ium iodide (**5**) was obtained as a dark red powder (0.47 g) quantitatively. ^{1}H NMR (500MHz, DMSO-d_6) δ 8.81 (dd, *J* = 1.48, 8.87 Hz, 1H), 8.63 (d, *J* = 7.34 Hz, 1H), 8.14 (d, *J* = 8.87 Hz, 1H), 8.06 (dd, *J* = 1.35, 7.96 Hz, 1H), 7.99 (ddd, *J* = 1.36, 7.09, 8.77 Hz, 1H), 7.80 (d, *J* = 8.07 Hz, 1H), 7.76 (ddd, *J* = 1.12, 7.05, 7.96 Hz, 1H), 7.62 (ddd, *J* = 1.22, 7.21, 7.42 Hz, 1H), 7.42 (dt, *J* = 1.09, 7.65 Hz, 1H), 7.36 (d, *J* = 7.22 Hz, 1H), 6.94 (s, 1H), 4.65 (t, *J* = 7.23 Hz, 2H), 4.03 (s, 3H), 3.54 (t, *J* = 6.60 Hz, 2H), 2.21 (p, *J* = 6.92 Hz, 2H), 1.37 (d, *J* = 13.22 Hz, 1H), 1.22 (s, 1H). ^{13}C NMR (126 MHz, DMSO-d_6) δ 160.69, 149.08, 144.97, 140.96, 137.51, 133.78, 128.68, 127.24, 126.38, 125.03, 124.72, 124.39, 123.41, 118.46, 113.56, 108.35, 88.73, 48.38, 40.06, 34.35, 28.37. HRMS (ESI) m/z calcd for $C_{21}H_{22}N_3S^+$ $[M]^+$ 348.1534, found 348.1537. (**figures 2.25-2.30**)

3-(4-Methyl-2,5-dioxo-2,5-dihydrofuran-3-yl)propanoic acid (**CDM**)

The synthetic procedure was adapted from a previous publication.[42] Triethyl 2-phosphonopropionate (1.5 equiv., 1.8g, 7.5 mmol) was dissolved in THF (5 mL) and added to a

suspension of sodium hydride (NaH) (60% dispersion in mineral oil, 1.3 equiv., 250 mg, 6.25 mmol) in THF (30 mL) on ice. The mixture was stirred for 30 min. on ice, followed by addition of a solution of diethyl ketoglutarate (1 g, 5 mmol) in THF (5 mL). The stirring was continued for 30 min. The reaction was quenched by pouring the solution into sat. aq. ammonium chloride (NH_4Cl) (100 mL) and then extracted with Et_2O. The organic phase was dried over sodium sulfate (Na_2SO_4) and concentrated. The crude product was then purified by silica gel flash column chromatography using 2:1 Et_2O:hexanes as the eluent. The resulting clear oil-like product was then dissolved in a mixture of 2 N aq. Potassium hydroxide (KOH) (12.5 mL) and EtOH (50 mL) and heated to reflux for 1 hr. The solution was diluted with water and EtOH was removed by a rotavapor. The resulting aqueous solution was acidified by HCl to pH 2 and extracted with ethyl acetate (EtOAc). The organic phase was dried and concentrated to give 3-(4-methyl-2,5-dioxo-2,5-dihydrofuran-3-yl)propanoic acid (**CDM**) (460 mg) as a yellow-white solid in 50% yield. ^{1}H NMR (500MHz, $CDCl_3$) δ 2.78 (s, 4H), 2.13 (s, 3H). ^{13}C NMR (126 MHz, $CDCl_3$) δ 177.14, 165.75, 165.53, 142.47, 141.78, 30.70, 19.59, 9.75. (**figures 2.31-2.32**)

APPENDIX

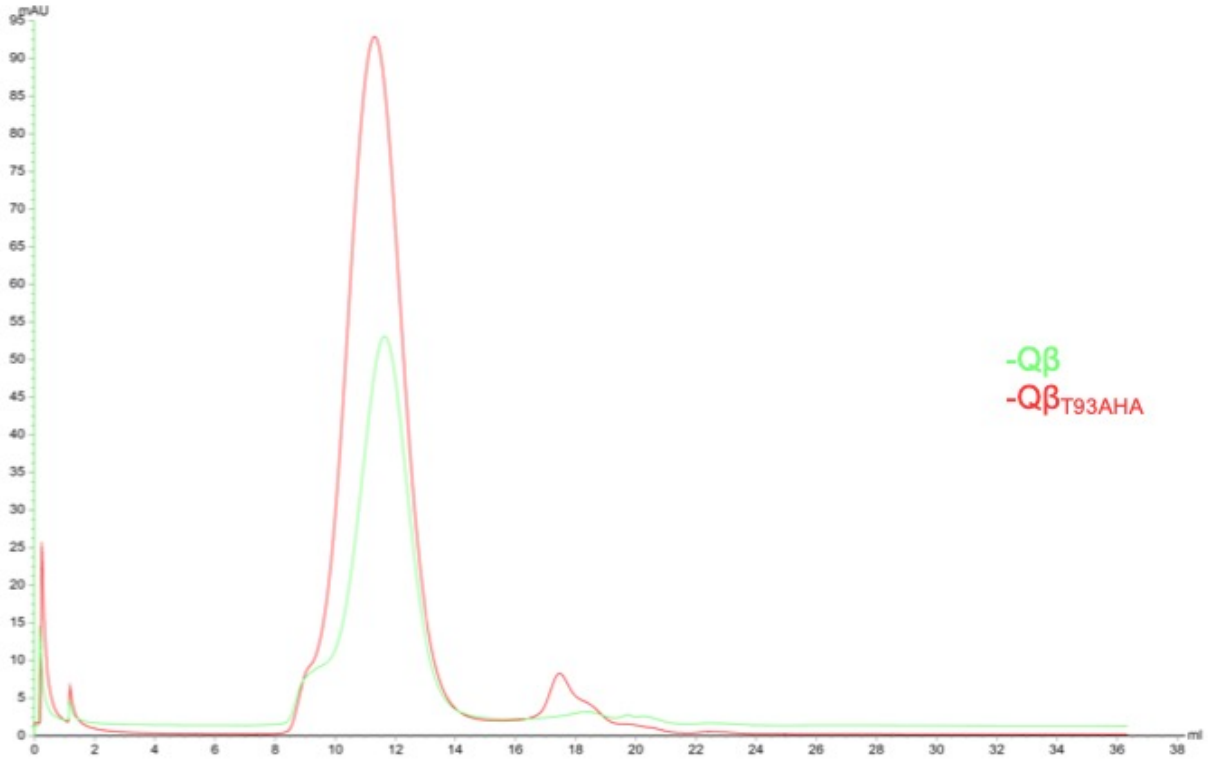

Figure 2.7. Size exclusion chromatography (SEC) traces of wt Qβ (green) and $Q\beta_{T93AHA}$ (Red), showed minimal size change in assembled capsids due to the engineered mutation.

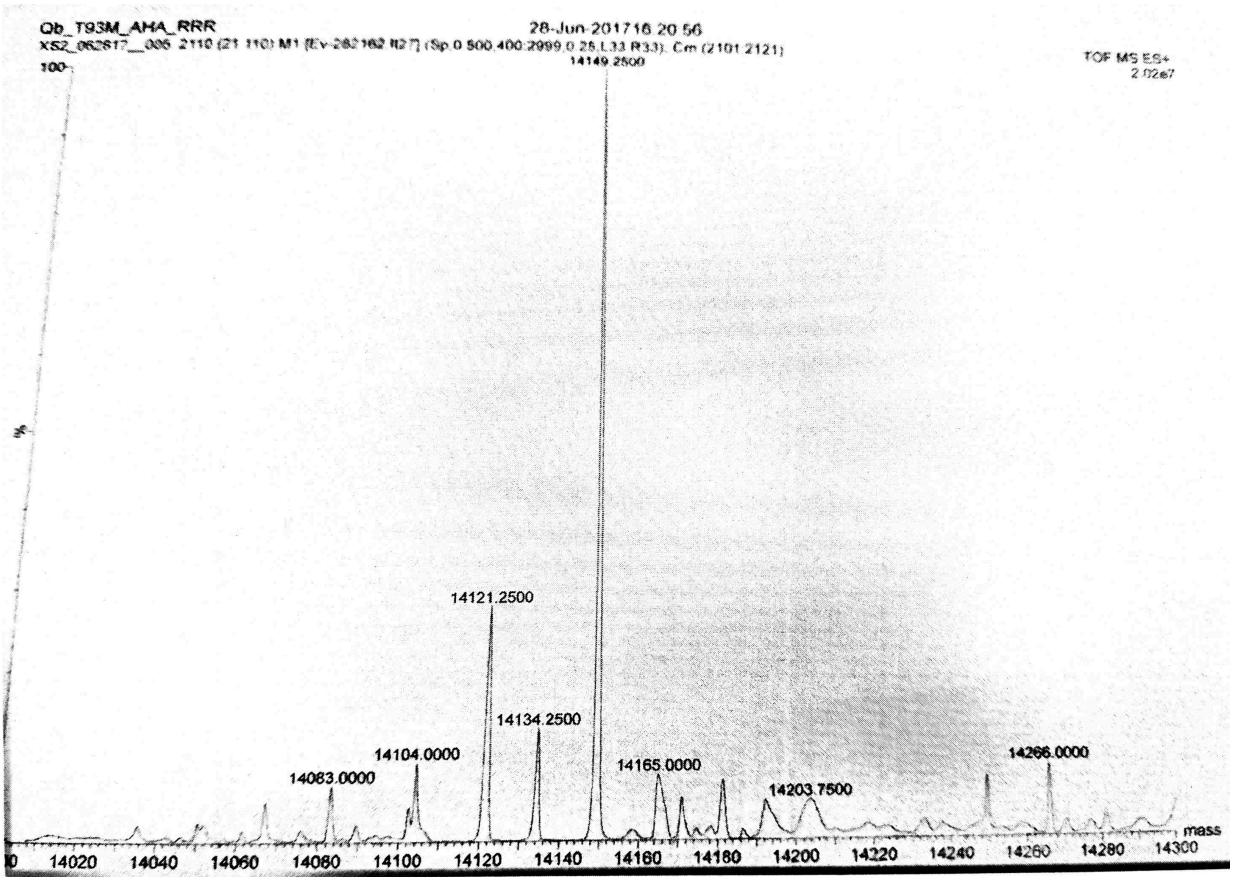

Figure 2.8. Deconvoluted ESI-MS Spectrum of $Q\beta_{T93AHA}$ coat protein (CP). The spectrum was deconvoluted using MaxEnt1.

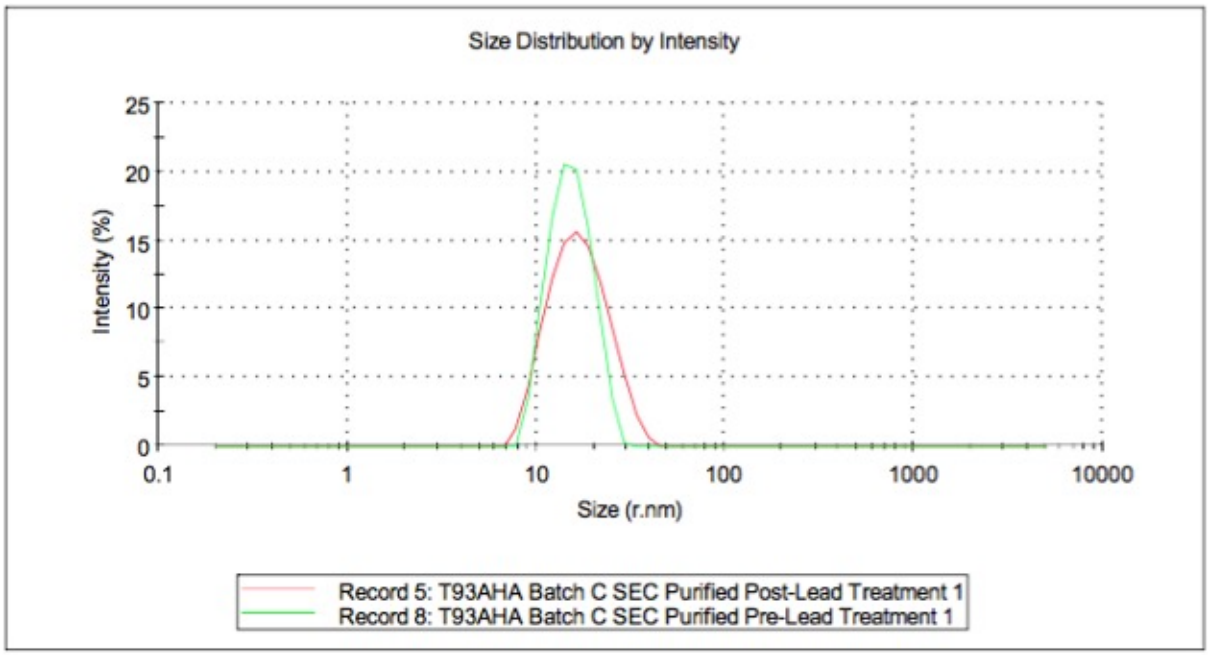

Sample	Average Radius (nm)	PDI
Pre-Lead Treatment	14.68	0.051
Post-Lead Treatment	15.95	0.137

Figure 2.9. Dynamic light scattering (DLS) analysis, of $Q\beta_{T93AHA}$ particles before and after lead treatment, showed capsids retained their size after lead treatment.

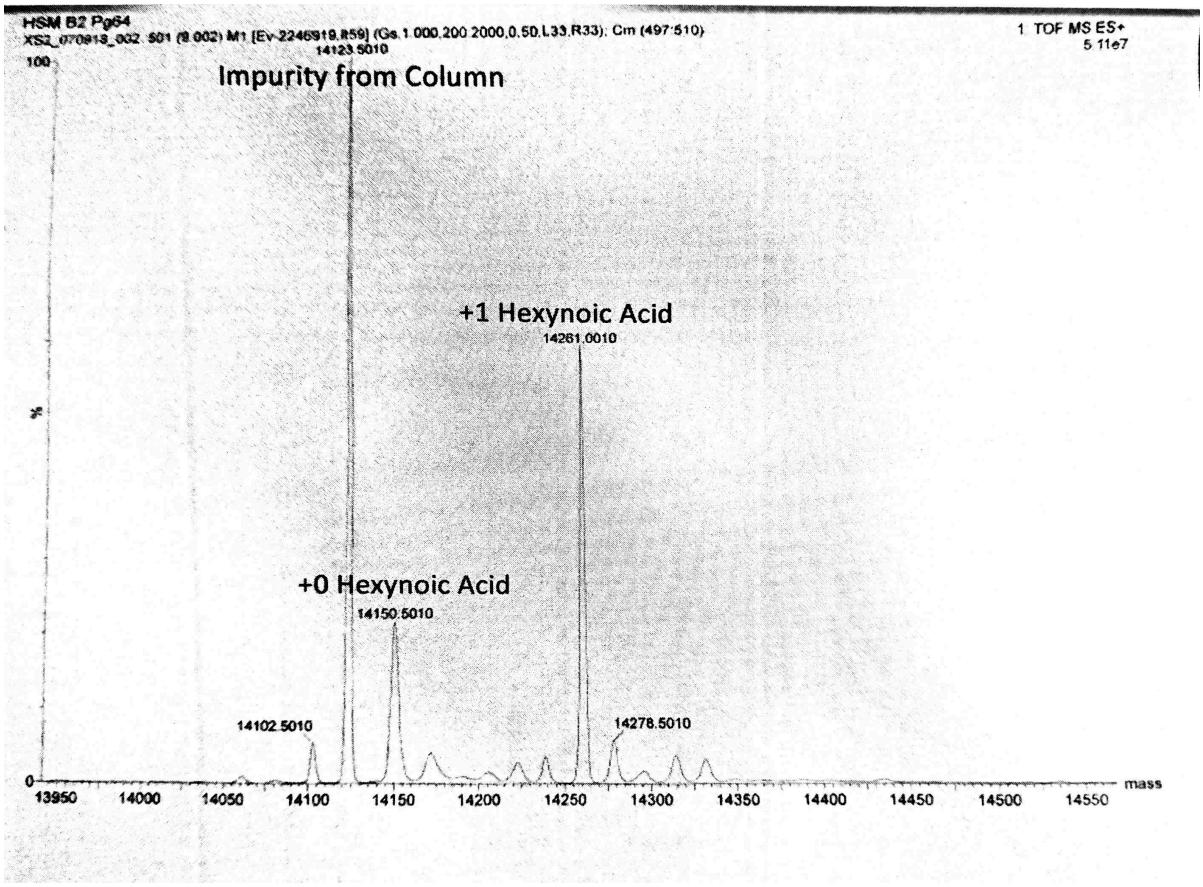

Figure 2.10. Deconvoluted ESI-MS spectrum of $Q\beta_{T93AHA}$ conjugated with hexynoic acid. The peak at 14,123 was also present in the pre-sample blank. The spectrum was deconvoluted using MAXEnt1. The number of hexynoic acid molecules conjugated to each capsid was calculated using the relative intensities of the unmodified and modified $Q\beta_{T93AHA}$ peaks.

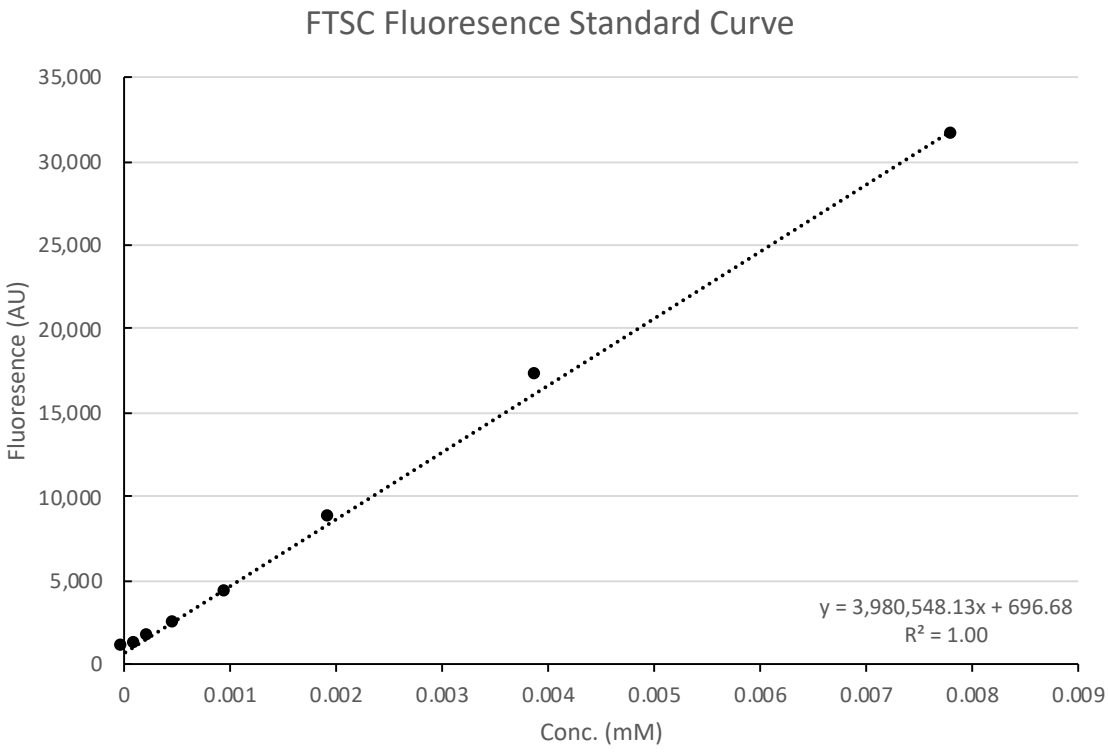

Figure 2.11. Fluorescence standard curve of FSTC used to calculate **vaccine construct 1** loading.

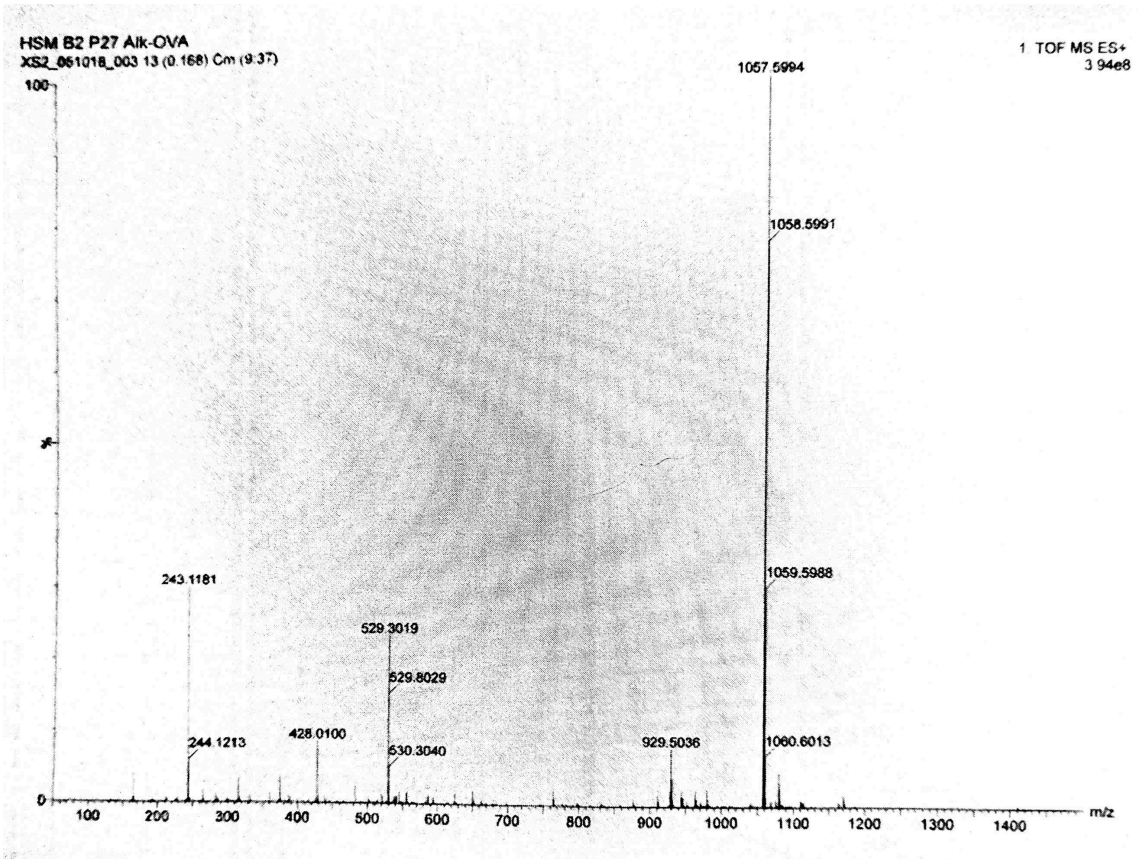

Figure 2.12. ESI-MS spectrum of Alkyne-SIINFEKL.

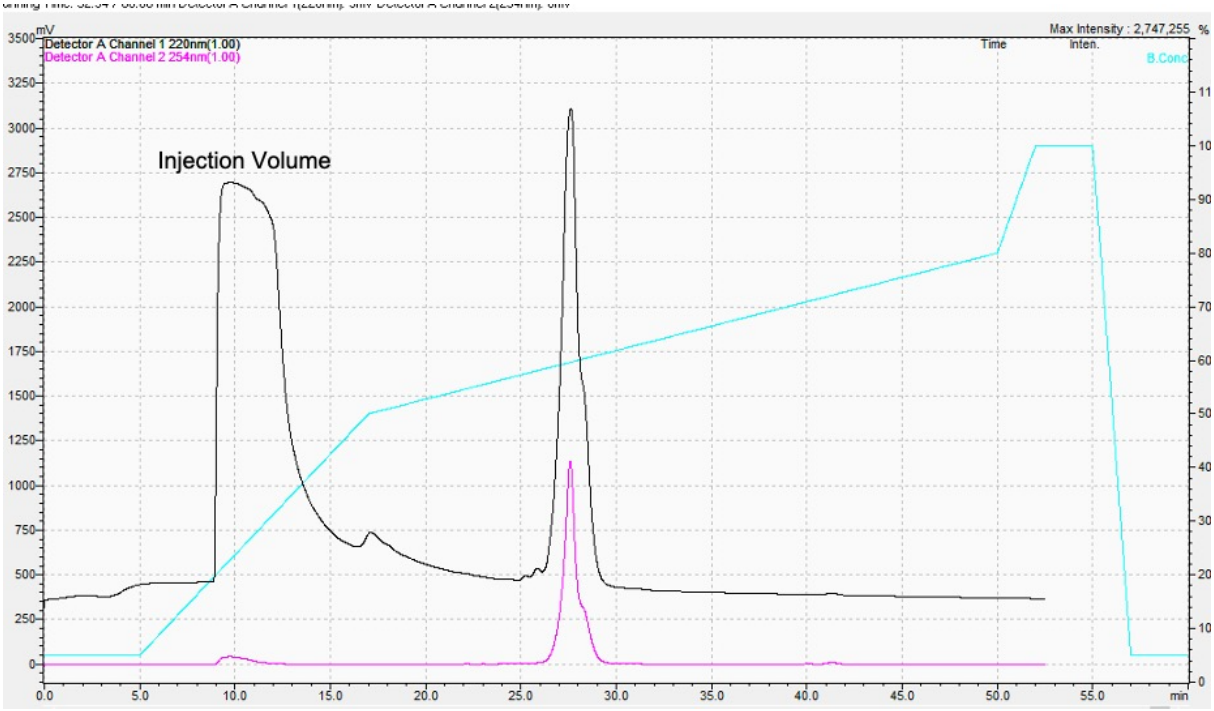

Figure 2.13. HPLC spectrum of purified Fluorescien-K(N_3)EQLESIINFEKL. Samples were detected by UV-VIS at 220 nm (black trace) and 254 nm (magenta trace).

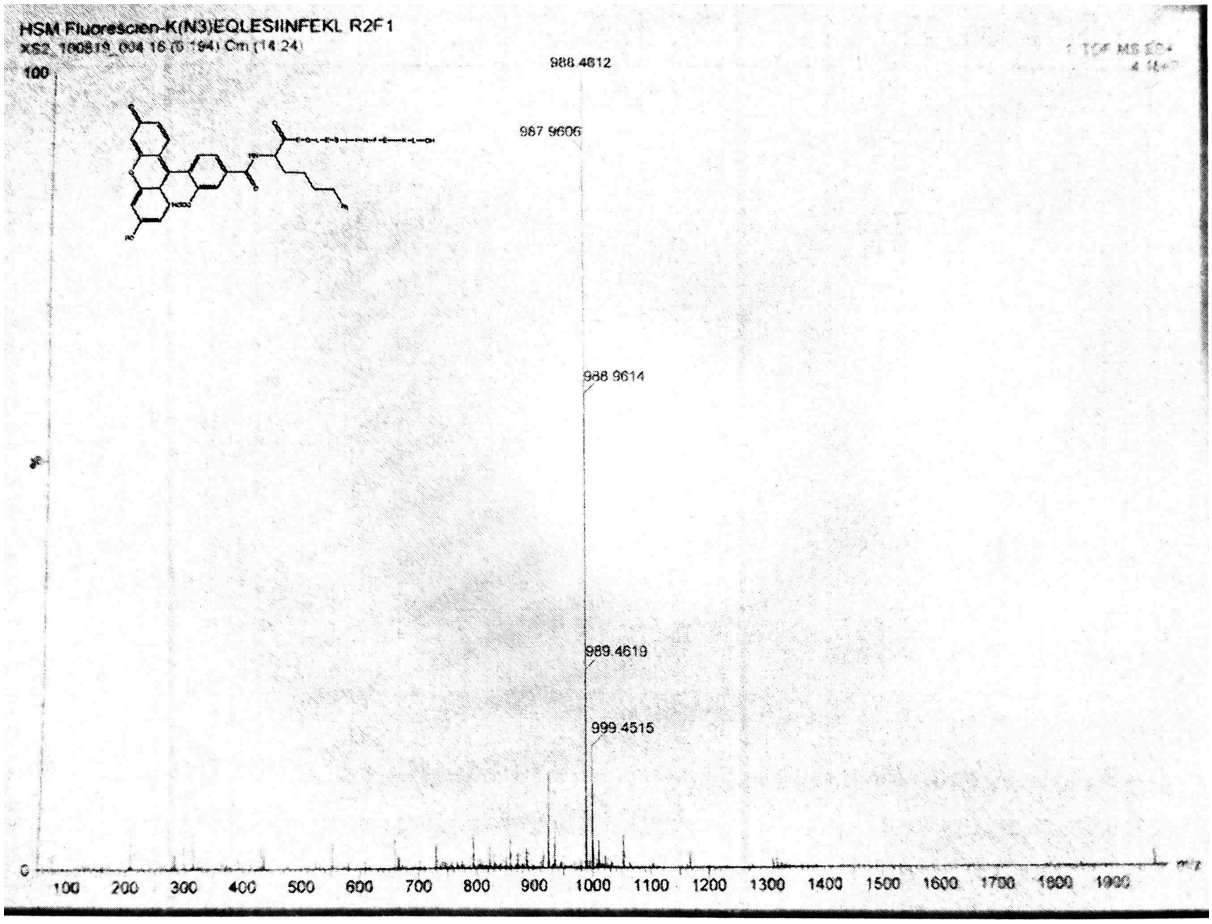

Figure 2.14. ESI-MS spectrum of Fluorescien-K(N_3)EQLESIINFEKL.

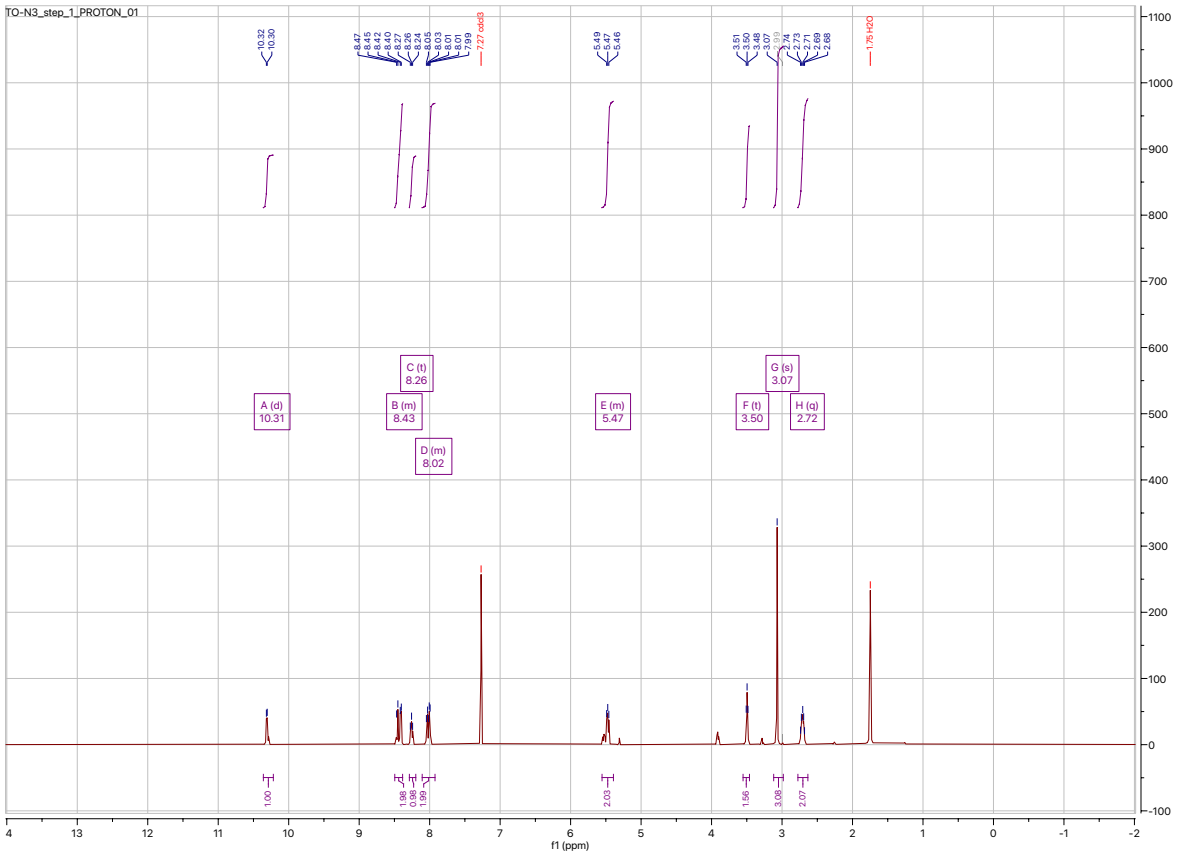

Figure 2.15. ^{1}H NMR Spectrum of **1**.

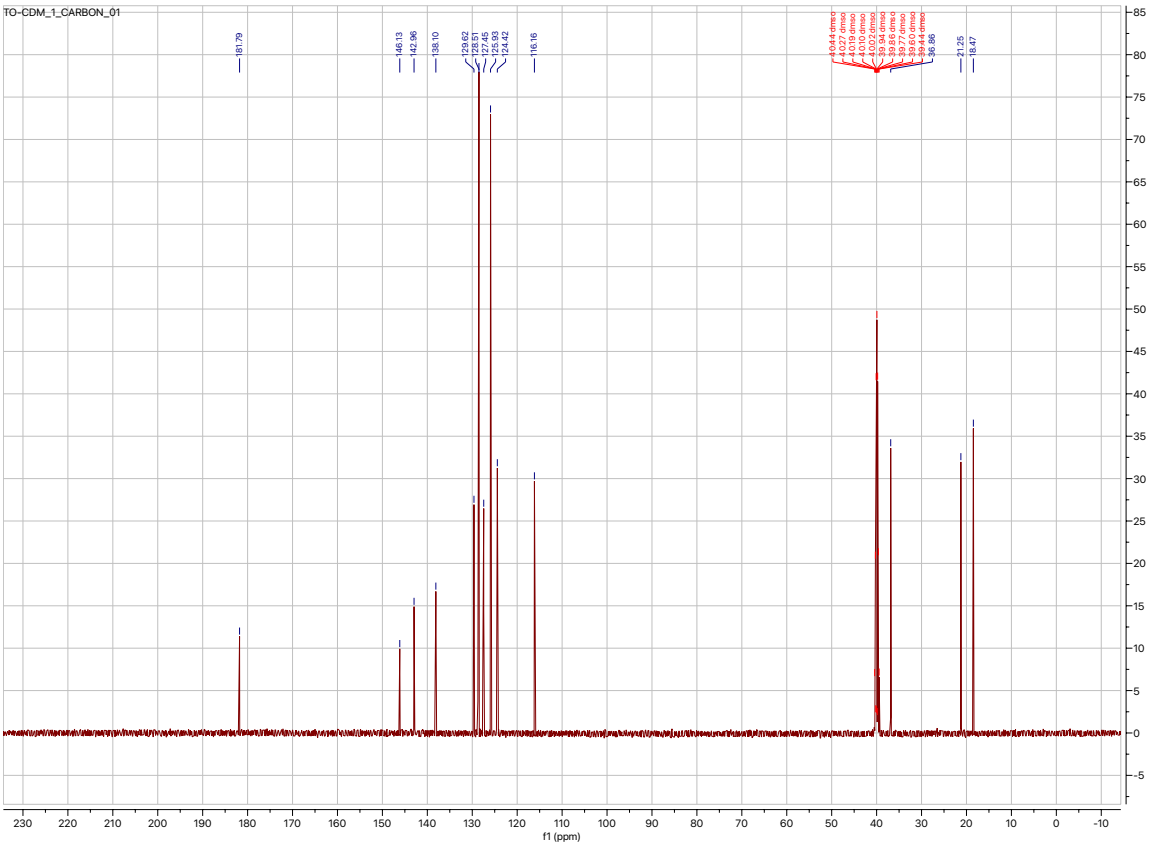

Figure 2.16. ^{13}C NMR Spectrum of **1**.

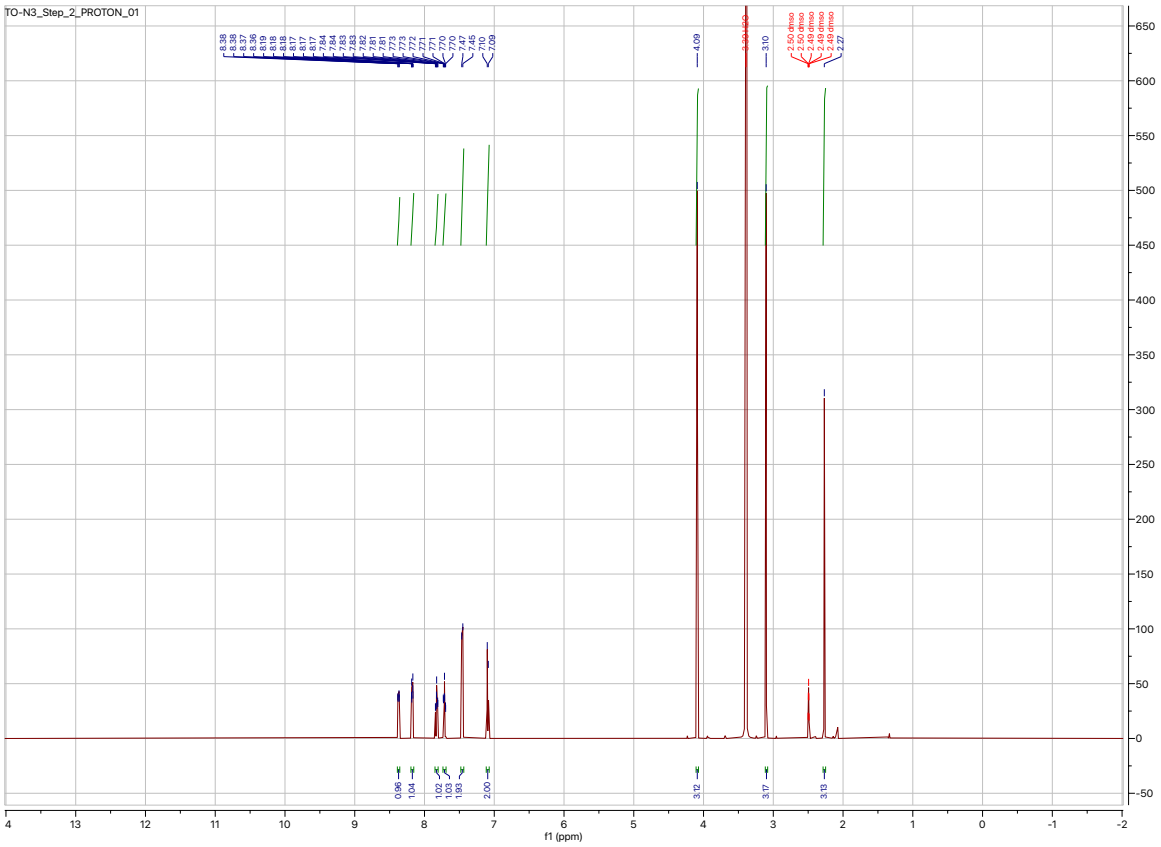

Figure 2.17. ^{1}H NMR Spectrum of **2**.

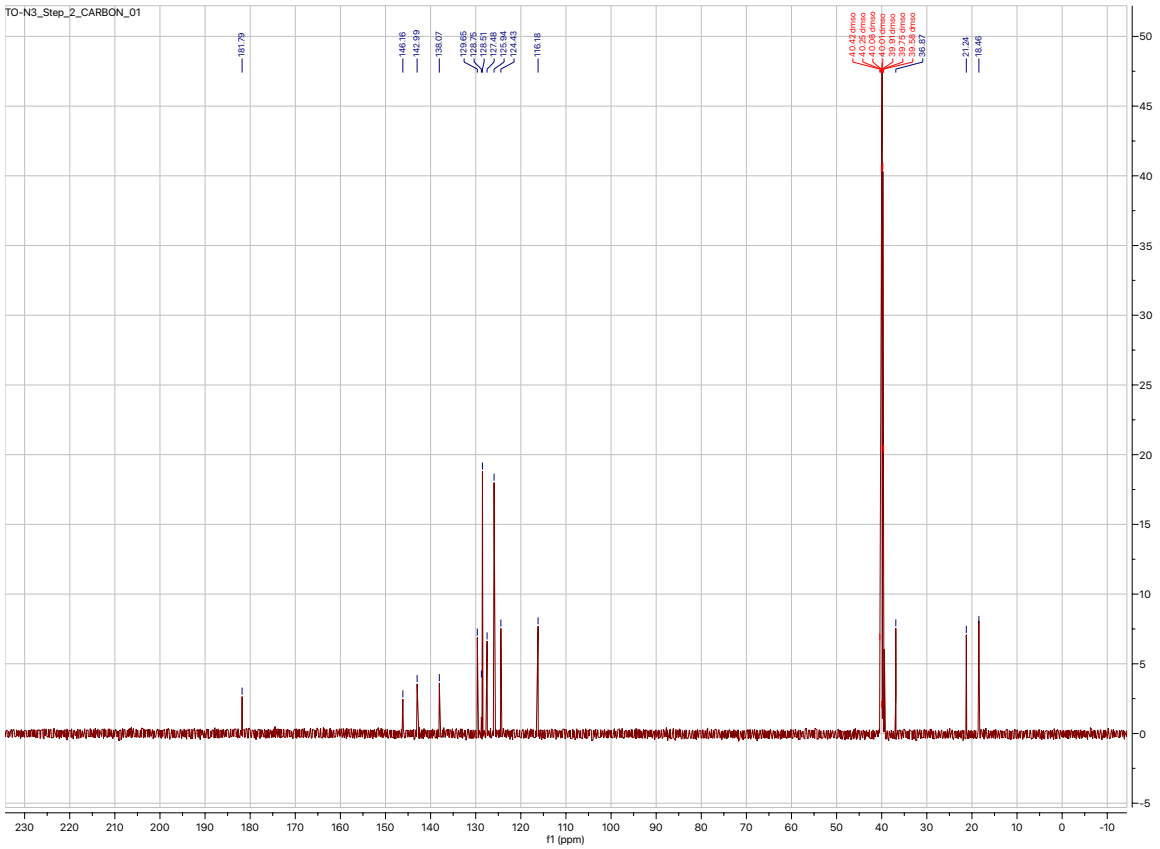

Figure 2.18. ^{13}C NMR Spectrum of **2**.

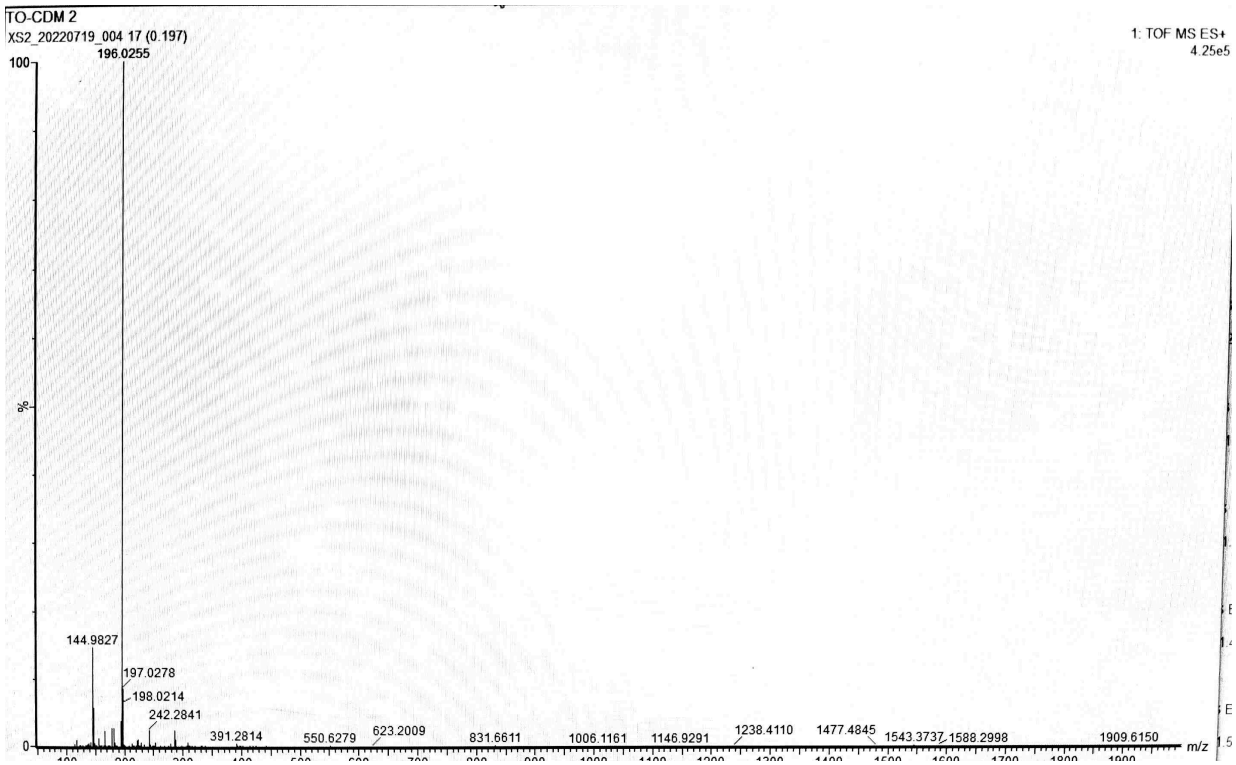

Figure 2.19. ESI-MS spectrum of **2**.

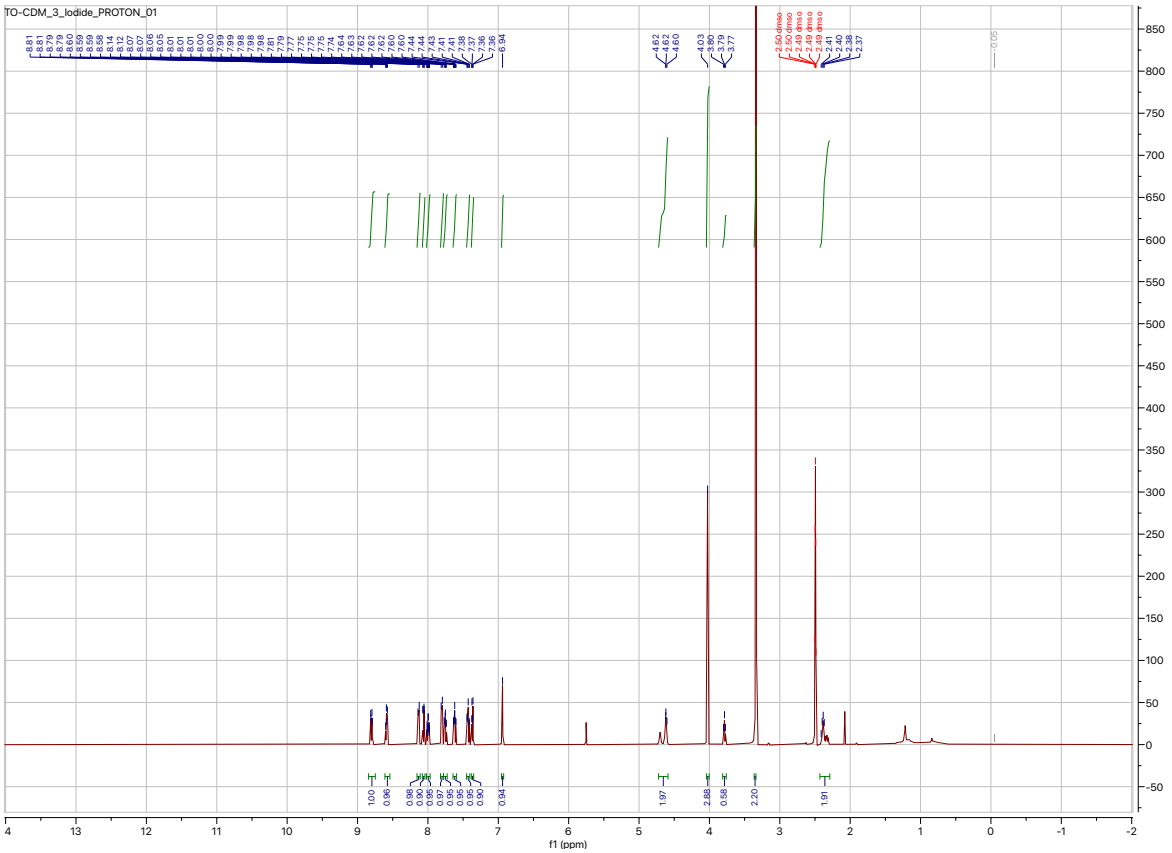

Figure 2.20. ^{1}H NMR Spectrum of **3**.

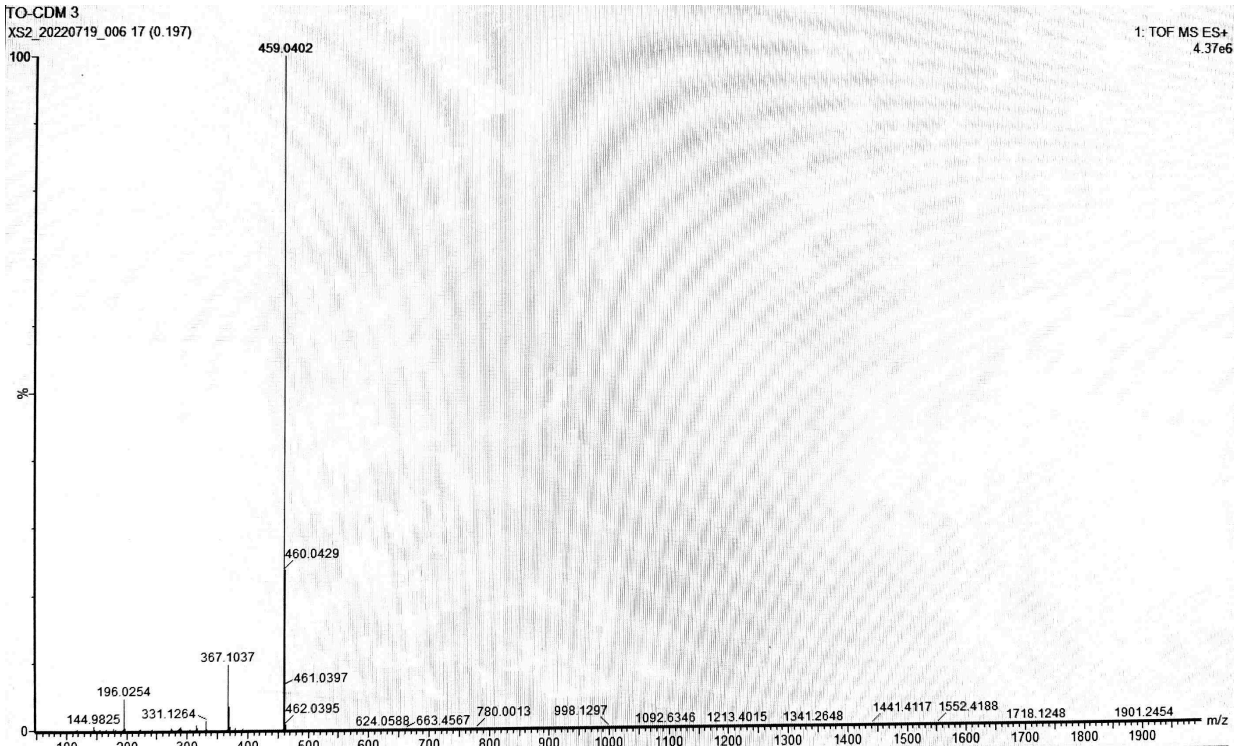

Figure 2.21. ESI-MS Spectrum of **3**.

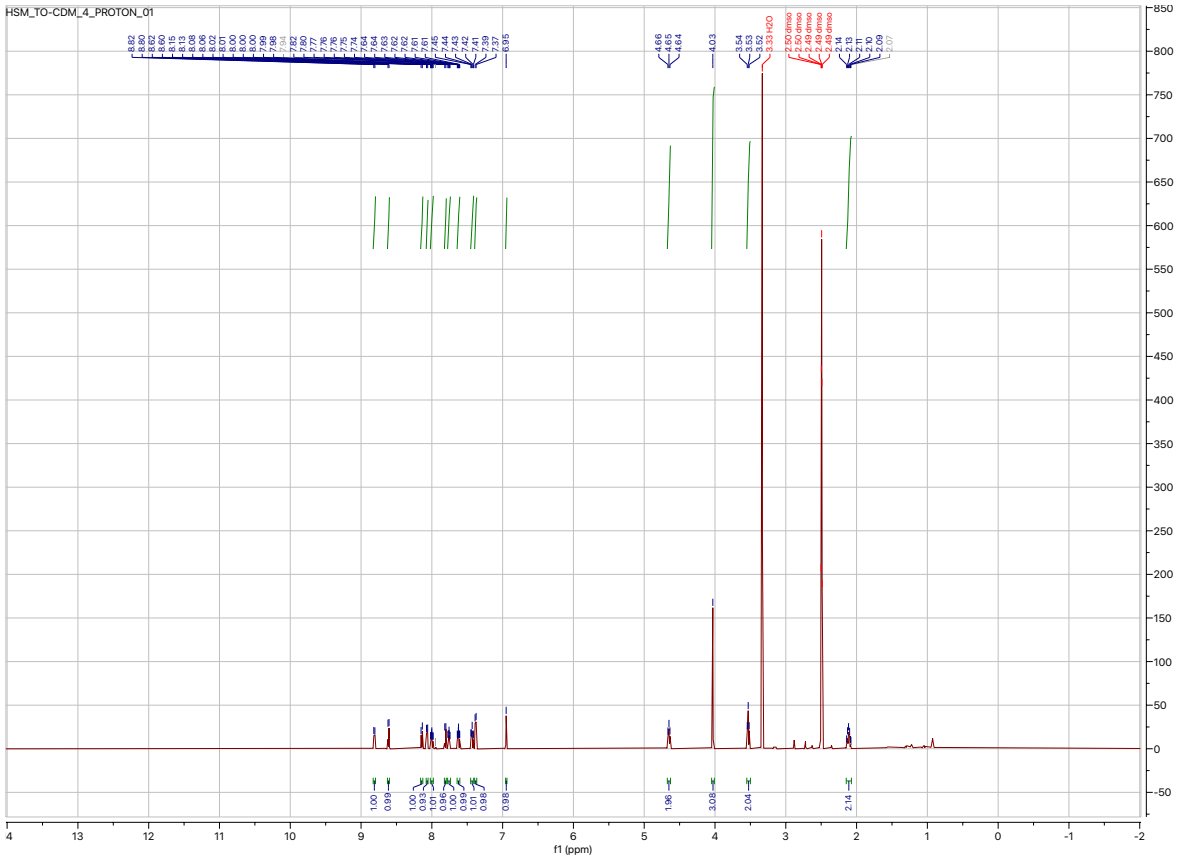

Figure 2.22. ^{1}H NMR Spectrum of **4**.

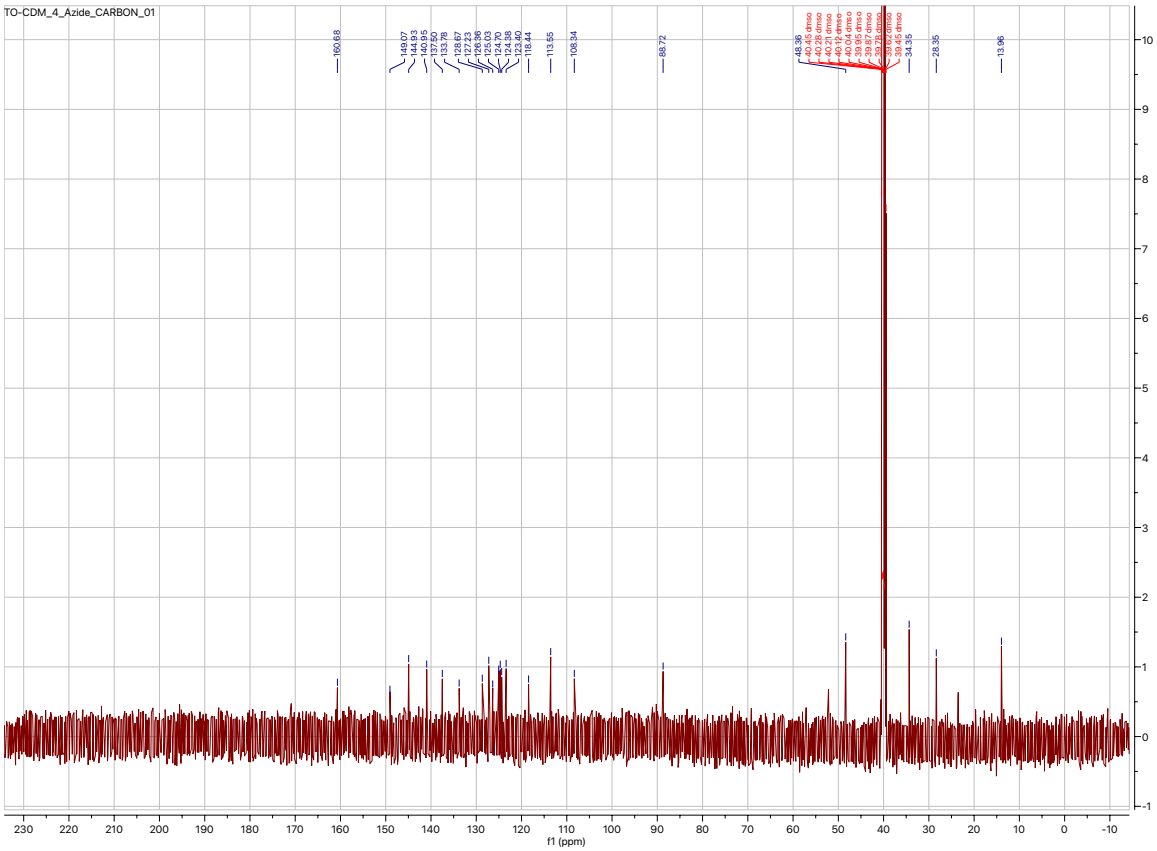

Figure 2.23. ^{13}C NMR Spectrum of **4**.

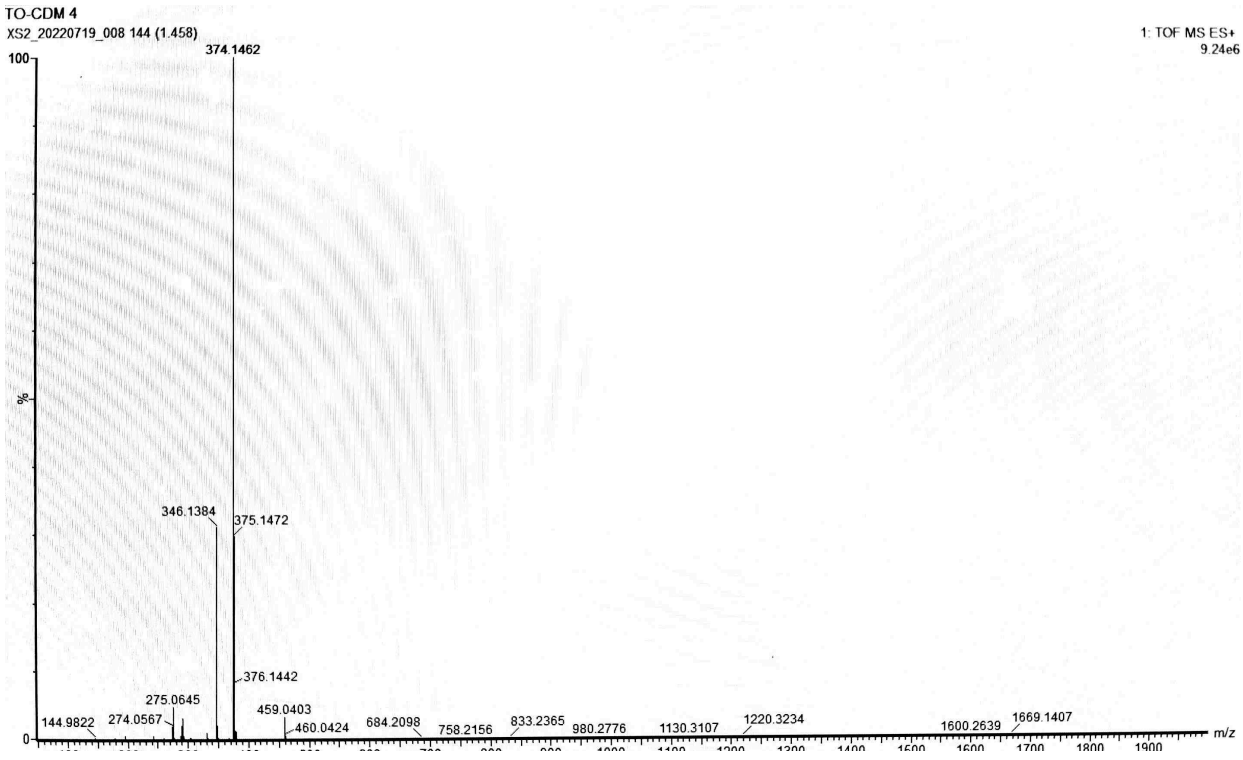

Figure 2.24. ESI-MS Spectrum of **4**.

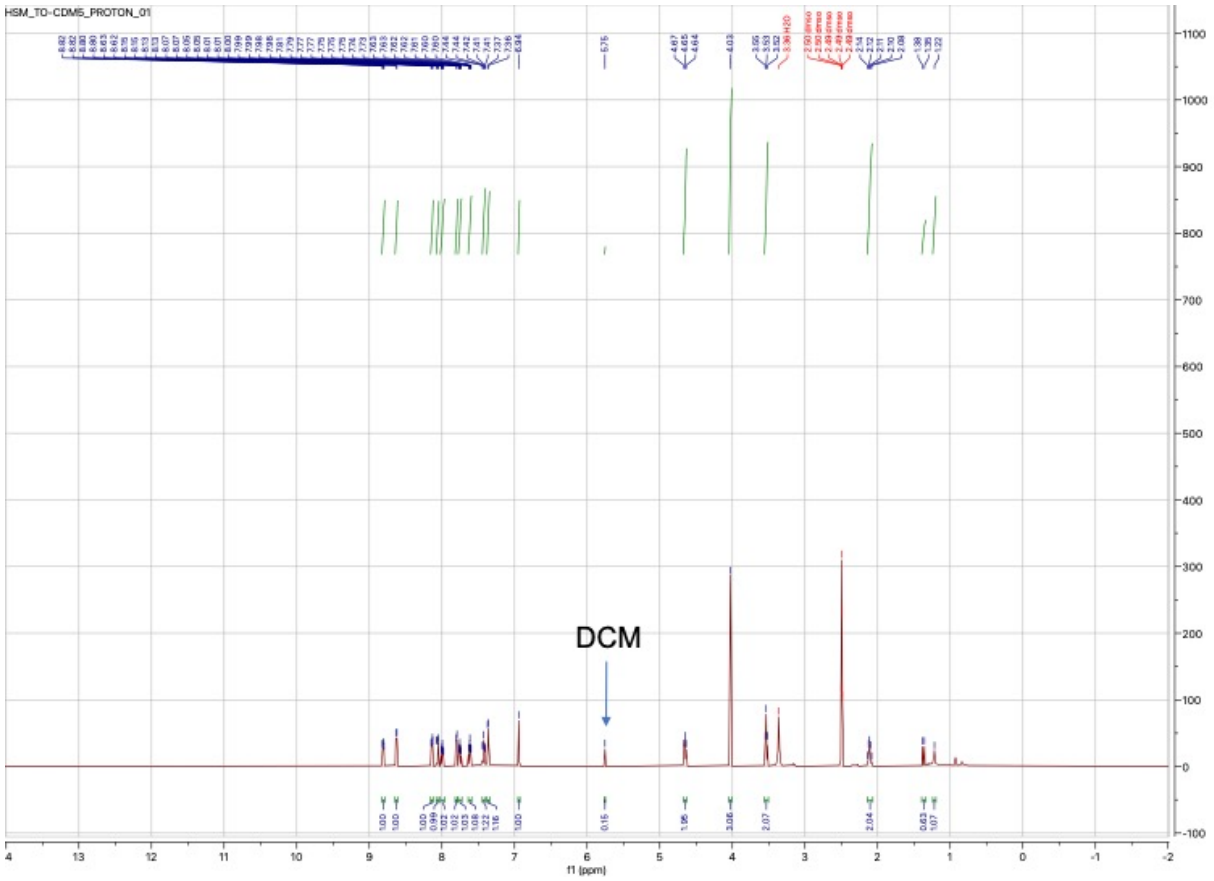

Figure 2.25. ^{1}H NMR Spectrum of **5**.

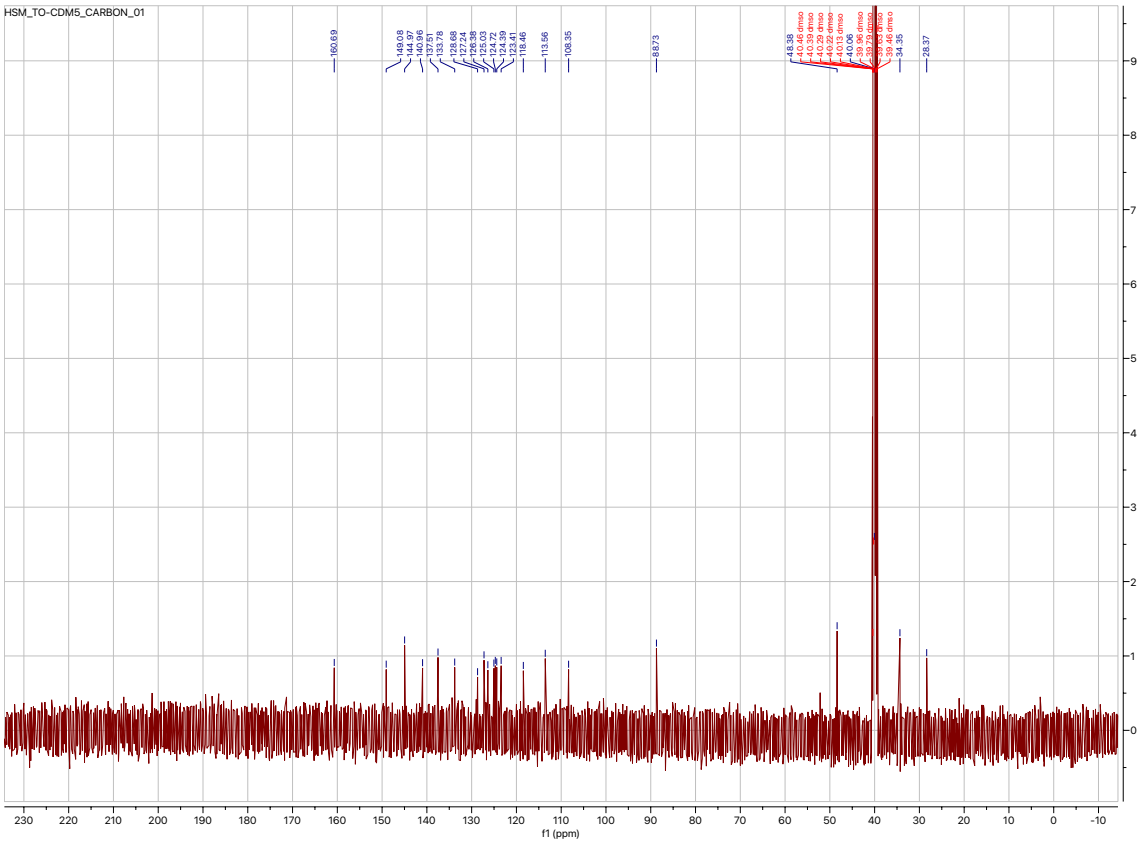

Figure 2.26. ^{13}C NMR Spectrum of **5**.

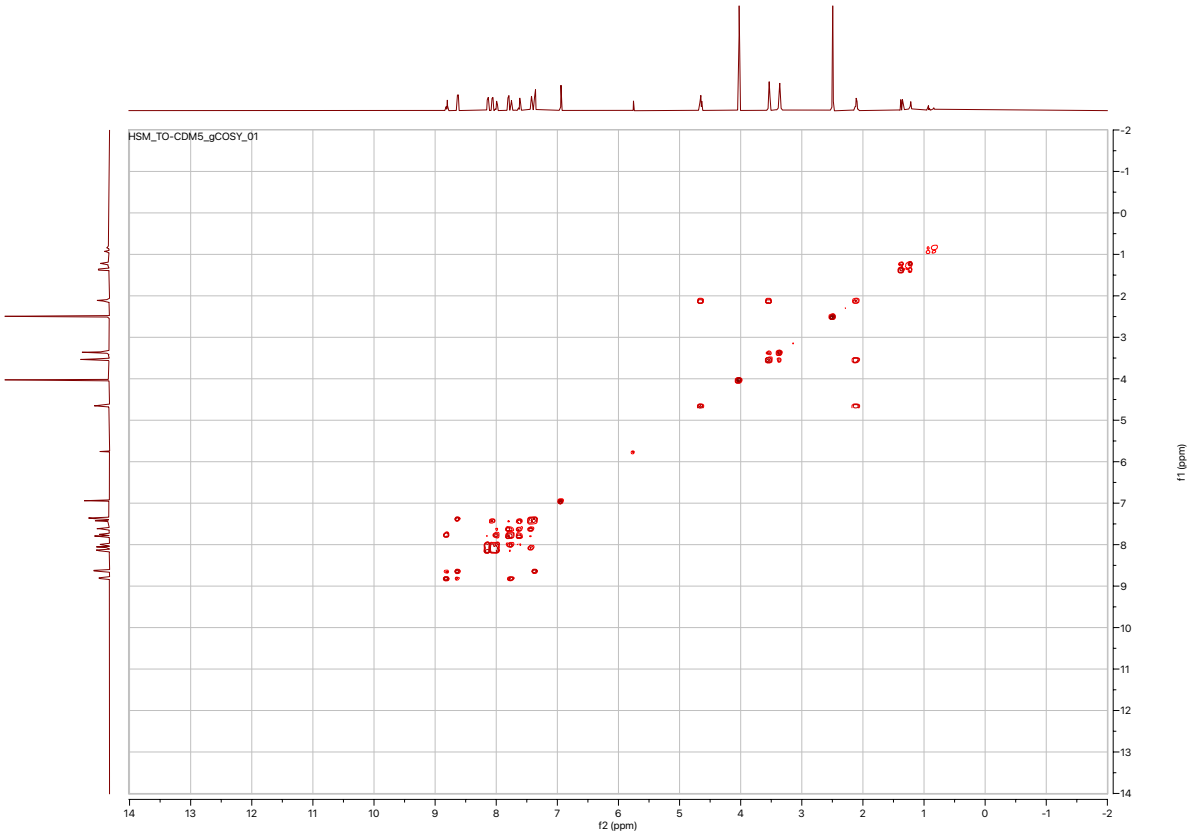

Figure 2.27. gCOSY Spectrum of **5**.

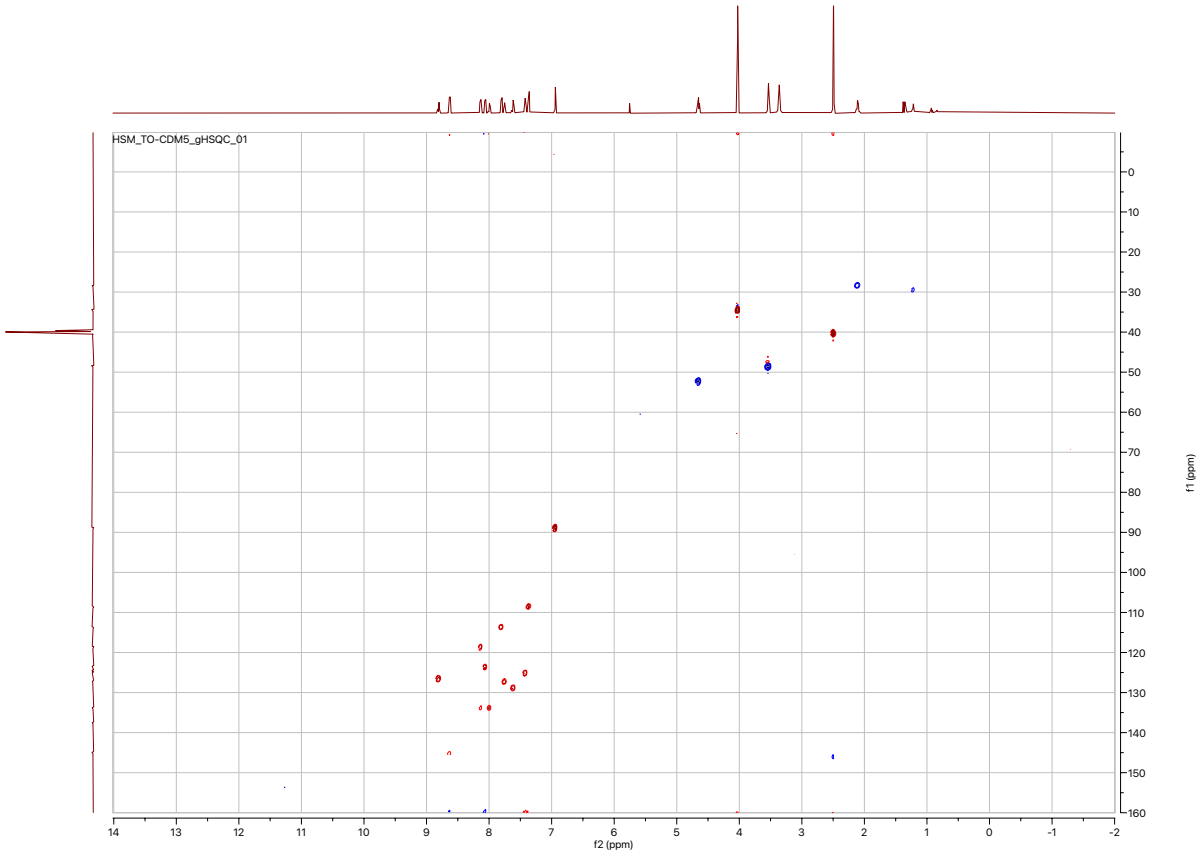

Figure 2.28. gHSQC Spectrum of **5**.

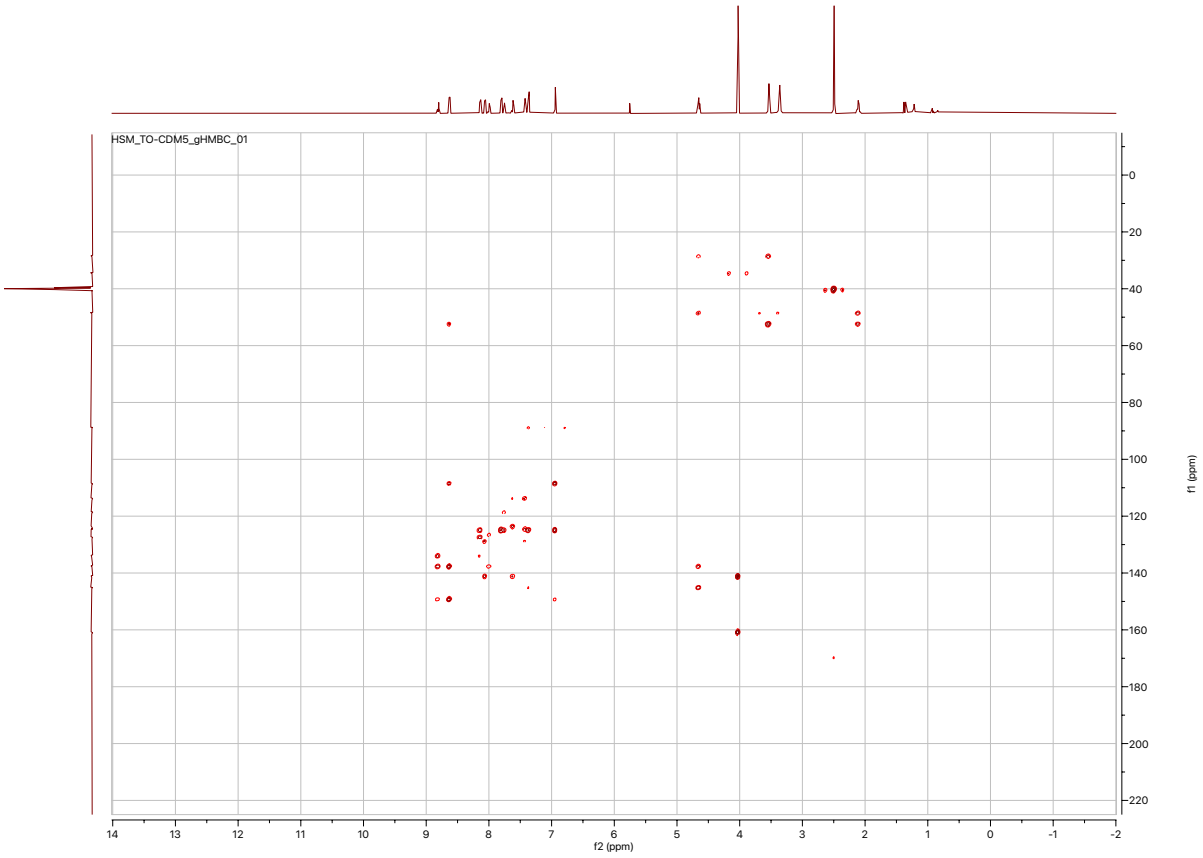

Figure 2.29. gHMBC Spectrum of **5**.

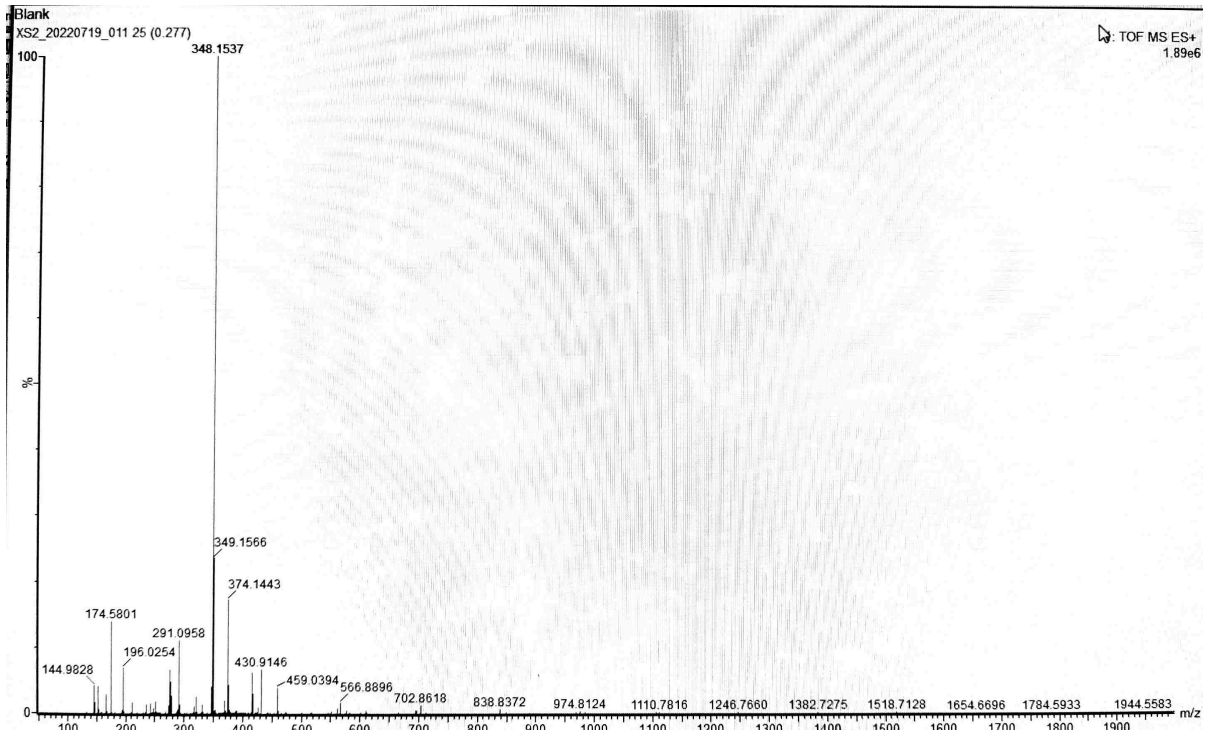

Figure 2.30. ESI-MS Spectrum of **5**.

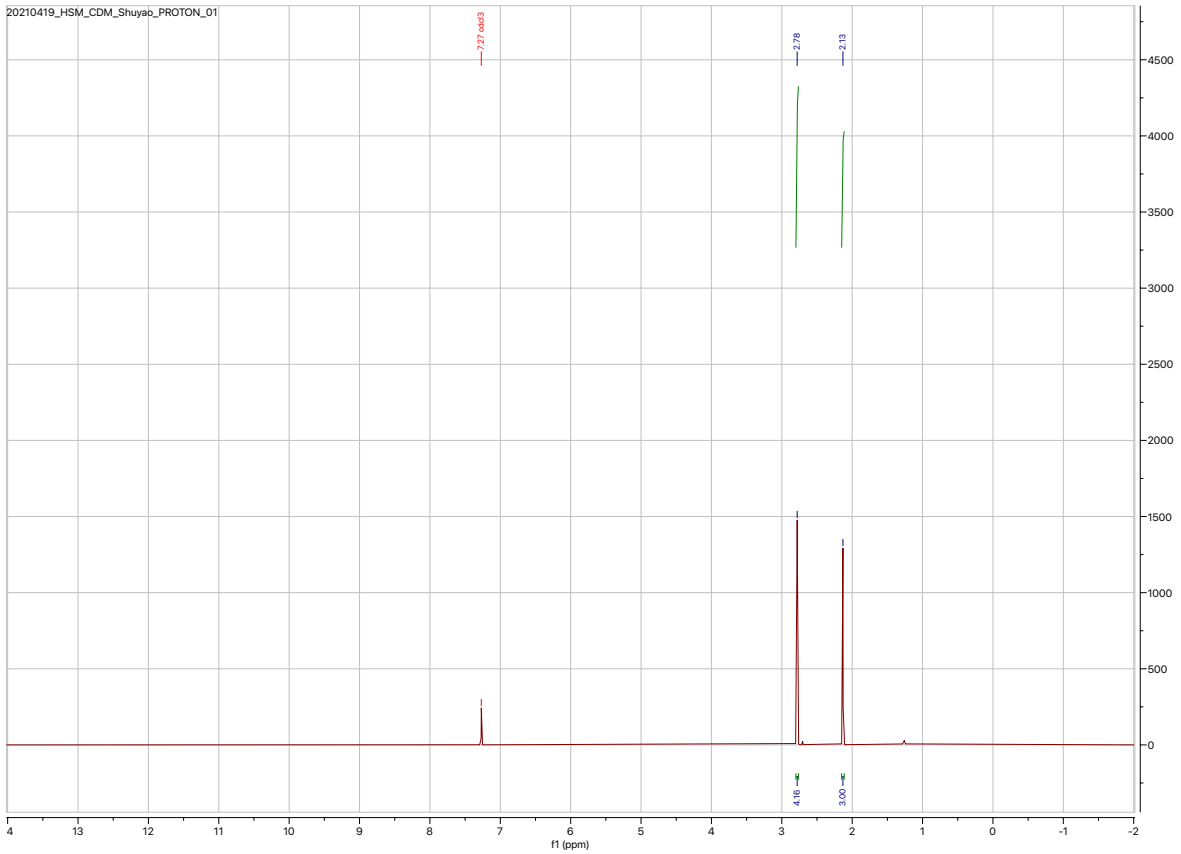

Figure 2.31. ^{1}H NMR Spectrum of **CDM**.

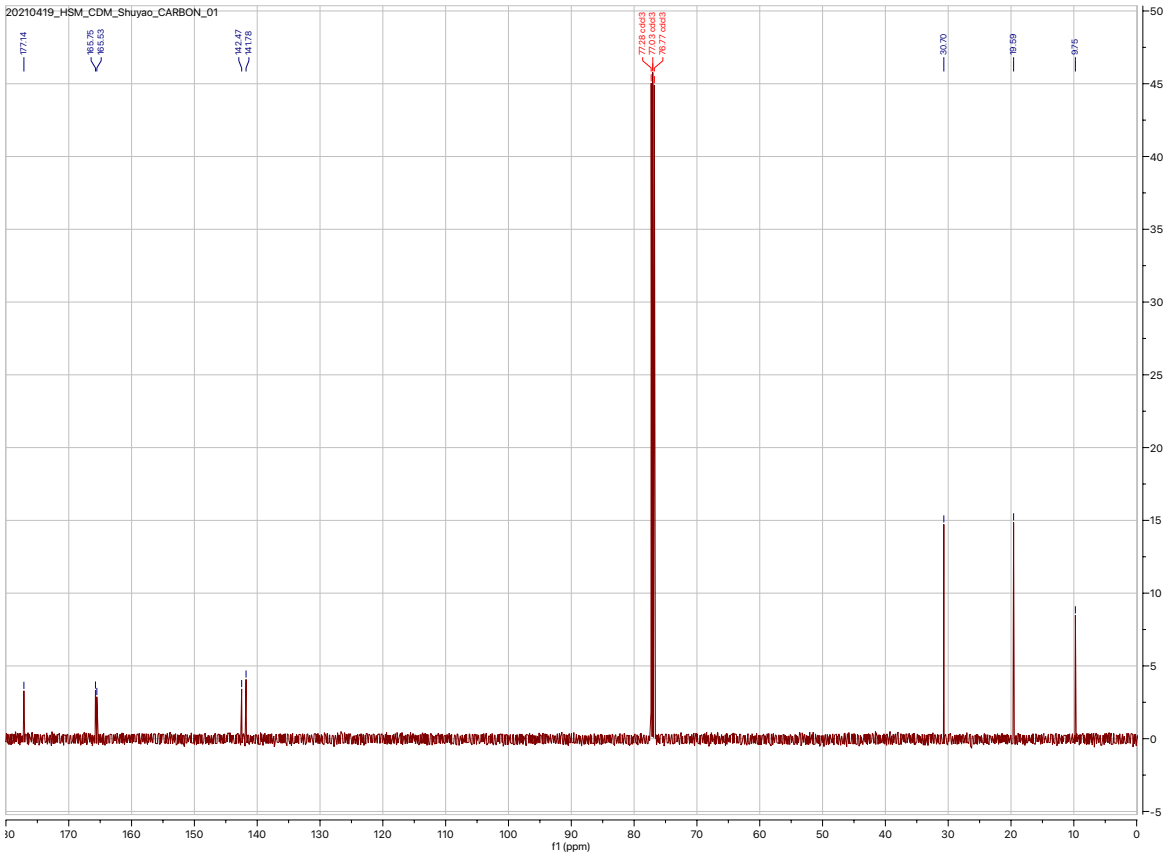

Figure 2.32. ^{13}C NMR Spectrum of **CDM**.

REFERENCES

REFERENCES

1. Sungsuwan, S.; Wu, X.; Shaw, V.; Kavunja, H.; McFall-Boegeman, H.; Rashidijahanabad, Z.; Tan, Z.; Lang, S.; Nick, S. T.; Lin, P.-H.; Yin, Z.; Ramadan, S.; Jin, X.; Huang, X., Structure Guided Design of the Bacteriophage Qβ Mutants as Next Generation Carriers for Conjugate Vaccines. *ACS. Chem. Biol.* **2022,** *XX*, XXXX-XXXX.

2. Rashidijahanabad, Z.; Kelly, M.; Kamruzzaman, M.; Qadri, F.; Bhuiyan, T. R.; McFall-Boegeman, H.; Wu, D.; Piszczek, G.; Xu, P.; Ryan, E. T.; Huang, X., Virus-like Particle Display of *Vibrio Cholerae O*-Specific Polysaccharide as a Potential Vaccine against Cholera. *ACS Infect. Dis.* **2022,** *8*, 574-583.

3. Bachmann, M. F.; Hengartner, H.; Zinkernagel, R. M., T helper cell-independent neutralizing B cell response against vesicular stomatitis virus: Role of antigen patterns in B cell induction? *Eur. J. Immunol.* **1995,** *25*, 3445-3451.

4. Jegerlehner, A.; Tissot, A.; Lechner, F.; Sebbel, P.; Erdmann, I.; Kündig, T.; Bächi, T.; Storni, T.; Jennings, G.; Pumpens, P.; Renner, W. A.; Bachmann, M. F., A molecular assembly system that renders antigens of choice highly repetitive for induction of protective B cell responses. *Vaccine* **2002,** *20*, 3104-3112.

5. Jegerlehner, A.; Stormi, T.; Lipowsky, G.; Schmid, M.; Pumpens, P.; Bachmann, M. F., Regulation of IgG Antibody Responses by Epitope Density and CD21-mediated Costimulation. *Eur. J. Immunol.* **2002,** *32*, 3305-3314.

6. Sungsuwan, S.; Wu, X.; Huang, X., Evaluation of Virus-Like Particle-Based Tumor-Associated Carbohydrate Immunogen in a Mouse Tumor Model. In *Methods Enzymol.*, Elsevier: New York, NY, 2017; Vol. 597, pp 359-376.

7. Yin, Z.; Comellas-Aragones, M.; Chowdhury, S.; Bentley, P.; Kaczanowska, K.; BenMohamed, L.; Gildersleeve, J. C.; Finn, M. G.; Huang, X., Boosting Immunity to Small Tumor-Associated Carbohydrates with Bacteriophage Q β Capsids. *ACS Chem. Biol.* **2013,** *8*, 1253-1262.

8. Braun, M.; Jandus, C.; Maurer, P.; Hammann-Haenni, A.; Schwarz, K.; Bachmann, M. F.; Speiser, D. E.; Romero, P., Virus-Like Particles Induce Robust Human T-Helper Cell Responses. *Eur. J. Immunol.* **2012,** *42*, 330-340.

9. Yin, Z.; Wu, X.; Kaczanowska, K.; Sungsuwan, S.; Aragones, M. C.; Pett, C.; Yu, J.; Baniel, C.; Westerlind, U.; Finn, M. G.; Huang, X., Antitumor Humoral and T Cell Responses by Mucin-1 Conjugates of Bacteriophage Qβ in Wild-type Mice. *ACS Chem. Biol.* **2018,** *13*, 1668-1676.

10. Schwarz, B.; Morabito, K. M.; Ruckwardt, T. J.; Patterson, D. P.; Avera, J.; Miettinen, H. M.; Graham, B. S.; Douglas, T., Viruslike Particles Encapsidating Respiratory Syncytial Virus M and M2 Proteins Induce Robust T Cell Responses. *ACS Biomater. Sci. Eng.* **2016,** *2*, 2324-2332.

11. Storni, T.; Ruedl, C.; Schwarz, K.; Schwendener, R. A.; Renner, W. A.; Bachmann, M. F., Nonmethylated CG Motifs Packaged into Virus-Like Particles Induce Protective Cytotoxic T Cell Responses in the Absence of Systemic Side Effects. *J. Immunol.* **2004,** *172*, 1777-1785.

12. Grotzke, J. E.; Sengupta, D.; Lu, Q.; Cresswell, P., The ongoing saga of the mechanism(s) of MHC class I-restricted cross-presentation. *Curr. Opin. Immunol.* **2017,** *46*, 89-96.

13. Pierce, S. K.; Liu, W., The Tipping points in the Initiation of B Cell Signalling; How Small Changes Make Big Differences. *Nat. Rev. Immunol.* **2010,** *10*, 767-777.

14. Kramer, K.; Al-Barwani, F.; Baird, M. A.; Young, V. L.; Larsen, D. S.; Ward, V. K.; Young, S. L., Functionalisation of Virus-Like Particles Enhances Antitumour Immune Responses. *J. Immunol. Res.* **2019,** *2019*, 5364632.

15. Lee, Y.-N.; Lee, Y.-T.; Kim, M.-C.; Gewirtz, A. T.; Kang, S.-M., A Novel Vaccination Strategy Mediating the Induction of Lung-Resident Memory CD8 T Cells Confers Heterosubtypic Immunity Against Future Pandemic Influenza Virus. *J. Immunol.* **2016,** *196*, 2637-2645.

16. Crossey, E.; Amar, M. J. A.; Sampson, M.; Peabody, J.; Schiller, J. T.; Chackerian, B.; Remaley, A. T., A Cholesterol-lowering VLP Vaccine that Targets PCSK9. *Vaccine* **2015,** *33*, 5747-5755.

17. Maphis, N. M.; Peabody, J.; Crossey, E.; Jiang, S.; Ahmad, F. A. J.; Alvarez, M.; Mansoor, S. K.; Yaney, A.; Yang, Y.; Sillerud, L. O.; Wilson, C. M.; Selwyn, R.; Brigman, J. L.; Cannon, J. L.; Peabody, D. S.; Chackerian, B.; Bhaskar, K., Qß Virus-like Particle-based Vaccine Induces Robust Immunity and Protects Against Tauopathy. *npj Vaccines* **2019,** *4*, 26.

18. Hovlid, M. L.; Lau, J. L.; Breitenkamp, K.; Higginson, C. J.; Lauder, B.; Manchester, M.; Finn, M. G., Encapsidated Atom-Transfer Radical Polymerization in Qβ Virus-Like Nanoparticles. *ACS Nano* **2014,** *8*, 8003-8014.

19. Rumnieks, J.; Tars, K., Crystal Structure of the Maturation Protein from Bacteriophage Qβ. *J. Mol. Biol.* **2017,** *429*, 688-696.

20. Lim, F.; Spingola, M.; Peabody, D. S., The RNA-binding Site of Bacteriophage Qβ Coat Protein. *J. Biol. Chem.* **1996,** *271* (50), 31839-31845.

21. Kirk, S. R.; Silverstein, T. P.; McFarlane Holman, K. L., Metal-Catalyzed Cleavage of $tRNA^{Phe}$. *J. Chem. Ed.* **2008,** *85*, 676-677.

22. Pan, T., Probing RNA Structure by Lead Cleavage. In *Current Protocols in Nucleic Acid Chemistry*, John Wiley & Sons Inc.: 2000; pp 6.3.1-6.3.9.

23. Sundaralingam, M.; Rubin, J. R.; Cannon, J. F., Non enzymatic Hydrolysis of RNA: Pb(II)-Catalyzed Site Specific Hydrolysis of Transfer RNA. The Role of the Tertiary Folding of the Polynucleotide Chain. *Int. J. Quantum Chem* **1984,** *11*, 355-366.

24. Batalia, M., A.; Collins, E. J., Peptide Binding by Class I and Class II MHC Molecules. *Peptide Sci.* **1997,** *43*, 281-302.

25. Emery, J. H. A. In *Analytic Control Strategy for a VLP-Peptide Conjugate Vaccine*, 17th Symposium on the Interface of Regulatory and Analytical Sciences for Biotechnology Health Products, Washington D.C., Washington D.C., 2013.

26. Karttunen, J.; Sanderson, S.; Shastri, N., Detection of Rare Antigen-Presenting Cells by the *lacZ* T-Cell Activation Assay Suggests an Expression Cloning Strategy for T-Cell Antigens. *Proc. Natl. Acad. Sci. USA* **1992,** *89*, 6020-6024.

27. Karttunen, J.; Shastri, N., Measurement of ligand-induced activation in single viable T cells using the *lacZ* reporter gene. *Proc. Natl. Acad. Sci. USA* **1991,** *88*, 3972-3976.

28. Cubas, R.; Zhang, S.; Kwon, S.; Sevick-Muraca, E. M.; Li, M.; Chen, C.; Yao, Q., Virus-Like Particle (VLP) Lymphatic Trafficking and Immune Response Generation After Immunization by Different Routes. *J. Immunother.* **2009,** *32*, 118-128.

29. McFall-Boegeman, H.; Huang, X., Mechanisms of Cellular and Humoral Immunity Through the Lens of VLP-Based Vaccines. *Expert Rev. Vaccines* **2022,** *21*, 453-469.

30. Carreon, J. R.; Mahon, K. P.; Kelley, S. O., Thiazole orange-Peptide Conjugates: Sensitivity of DNA Binding to Chemical Structure. *Org. Lett.* **2004,** *6*, 517-519.

31. Fei, X.; Gu, Y.; Ban, Y.; Liu, Z.; Zhang, B., Thiazole Orange Derivatives: Synthesis, Fluorescence Properties, and Labeling Cancer Cells. *Bioorg. Med. Chem.* **2009,** *17*, 585-591.

32. Das, S.; Yau, M.-K.; Noble, J.; De Pascalis, L.; Finn, M. G., Transport of Molecular Cargo by Interaction with Virus-Like Particle RNA. *Angew. Chem. Int. Ed.* **2022,** *61*, e202111687.

33. Yin, Z.; Chowdhury, S.; McKay, C.; Baniel, C.; Wright, W. S.; Bentley, P.; Kaczanowska, K.; Gildersleeve, J. C.; Finn, M. G.; BenMohamed, L.; Huang, X., Significant Impact of Immunogen Design on the Diversity of Antibodies Generated by Carbohydrate-Based Anticancer Vaccine. *ACS Chem. Biol.* **2015,** *10* (10), 2364-2372.

34. Bijker, M. S.; van den Eeden, S. J. F.; franken, K. L.; Melief, C. J. M.; van der Burg, S. H.; Offringa, R., Superior Induction of Anti-Tumor CTL Immunity by Extended Peptide Vaccines Involves prolonged, DC-Focused Antigen Presentation. *Eur. J. Immunol.* **2008,** *38*, 1033-1042.

35. Craiu, A.; Akopian, T.; Goldberg, A.; Rock, K. L., Two Distinct Proteolytic processes in the Generation of a Major Histocompatibility Complex Class I-Presented Peptide. *Proc. Natl. Acad. Sci. USA* **1997,** *94*, 10850-10855.

36. Rosalia, R. A.; Quakkelaar, E. D.; Redeker, A.; Khan, S.; Camps, M.; Drijfhout, J. W.; Silva, A. L.; Jiskoot, W.; van Hall, T.; van Veelen, P. A.; Janssen, G.; Franken, K.; Cruz, L. J.; Tromp, A.; Oostendorp, J.; van der Burg, S. H.; Ossendorp, F.; Melief, C. J. M., Dendritic Cells Process Synthetic Long Peptides Better than Whole Protein, Improving Antigen Presentation and T-Cell Activation. *Eur. J. Immunol.* **2013,** *43*, 2554-2565.

37. Presolski, S. I.; Hong, V. P.; Finn, M. G., Copper-Catalyzed Azide-Alkyne Click Chemistry for Bioconjugation. *Curr. Protoc. Chem. Biol.* **2011,** *3*, 153-162.

38. Willkomm, D. K.; Hartmann, R. K., 3'-Terminal Attachment of Fluorescent Dyes and Biotin. In *Handbook of RNA Biochemistry*, Hartmann, R. K.; Bindereif, A.; Schön, A.; Westhof, E., Eds. Wiley-VCH Verlag GmbH & Co. KGaA: Weinheim, 2005; pp 86-94.

39. Jin, D.; Sprent, J., GM-CSF Culture Revisited: Preparation of Bulk Populations of Highly Pure Dendritic Cells from Mouse Bone Marrow. *J. Immunol.* **2018,** *201*, 3129-3139.

40. Matheu, M. P.; Sen, D.; Cahalan, M. D.; Parker, I., Generation of Bone Marrow Derived Murine Dendritic Cells for Use in 2-Photon Imaging. *J. Vis. Exp.* **2008,** *17*, e773.

41. Kavunja, H. W.; Lang, S.; Sungsuwan, S.; Yin, Z.; Huang, X., Delivery of foreign cytotoxic T lymphocyte epitopes to tumor tissues for effective antitumor immunotherapy against pre-established solid tumors in mice. *Cancer Immunol. Immunother.* **2017,** *66*, 451-460.

42. Lang, S.; Tan, Z.; Wu, X.; Huang, X., Synthesis of Carboxy-Dimethylmaleic Amide Linked Polymer Conjugate Based Ultra-pH-Sensitive Nanoparticles for Enhanced Antitumor Immunotherapy. *ACS Macro Lett.* **2020,** *9*, 1693-1699.

CHAPTER 3 A VLP-BASED CONJUGATE VACCINE TO PREVENT TAU OLIGOMERIZATION IN ALZHEIMER'S DISEASE

3.1 Introduction

Alzheimer's disease is one of the most common forms of dementia. It is characterized by progressive neurodegeneration resulting in loss of memory and independence. Beyond the emotional and personal tragedies associated with the disease, the care needed, as patients lose their independence, is estimated to cost the United State $321 billion/year.[1] The human and financial tolls suggest a need for effective treatments to cure or at least slow the disease progression.

One of the hallmarks of Alzheimer's disease is the build-up of neurofibrillary tangles (NFTs) made up of tau[2]. Tau is an intrinsically disordered protein that in healthy tissue plays a role in stabilizing microtubules in axons. In patients with Alzheimer's disease, tau has been found to be hyperphosphorylated. It is believed that the increased negative charge causes unfolding, exposing hydrophobic regions. Inside the hydrophobic regions are the microtubule binding regions (MTBRs). When exposed, MTBRs on soluble tau can interact leading to dimerization. Following dimerization, aggregation can continue to increase through interactions between tau's MTBRs forming small soluble oligomers (tauO) and eventually NFTs (**figure 3.1 A**).

Because of their large size and correlation with disease progression in post-mortem analysis, it was initially believed that NFTs were the cytotoxic tau species. Although recent advances have shown that the actual cytotoxic tau species is tauO.[3, 4] In animal models, deposition of tauO has induced tau misfolding and disease progression.[5] Prevention of tauO formation is an interesting therapeutic target (**figure 3.1 B**). Kontsekova and coworkers

identified protective epitopes in tau's MTBRs. The minimal epitope sequence identified was HXPGGG.[6]

A monoclonal antibody that recognized the protective epitope decreased tau oligomerization *in vitro* and *in vivo*.[6] Monoclonal antibody therapeutics require large doses and administration by trained professionals. The long-term need for treatment and difficulty in diagnosing Alzheimer's disease work against monoclonal therapies. Instead, vaccines capable of providing protective immune responses are of extreme interest. A keyhole limpet hemocyanin (KLH)-based conjugate vaccine targeting the MTBRs in tau has shown promising results in phase I and II clinical trials.[7-10]

The body naturally selects against immune cells that can recognize self-antigens like tau. In order to overcome that negative selection pressure, vaccines against self-antigens usually require the antigen to be conjugated to an immunologically active carrier. The structure and identity of the carrier can have an effect on the immune response generated. This is important in targeting antigens in the CNS as it is believed that only 0.1% of antibodies cross the blood-brain barrier (BBB).[11] Herein we report the ability of bacteriophage Qβ-based conjugate vaccine to elicit high titers of antibodies capable of preventing tau oligomerization and providing protection *in vitro*. The vaccine induced titers an order of magnitude higher than the current gold standard carrier, KLH.

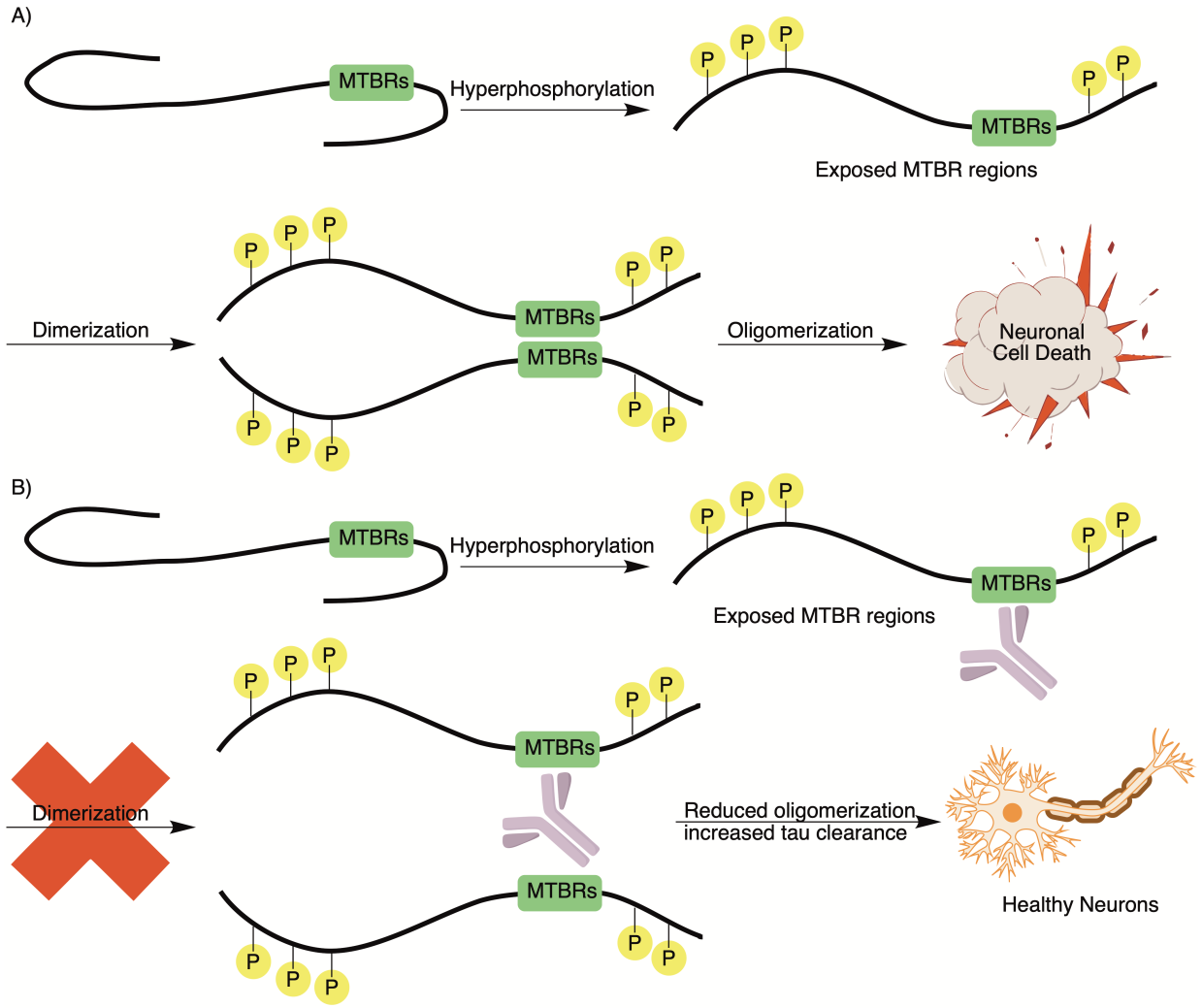

Figure 3.1 (A) In Alzheimer's disease hyperphosphorylation of tau leads to the exposure of microtubule binding regions (MTBRs). Tau dimerizes and continues to oligomerize through interactions between MTBRs, leading to neuronal cell death. (B) Antibodies against the MTBR region should block MTBR interactions preventing dimerization/oligomerization and increase the clearance of disease associated tau resulting in healthy neurons.

3.2 Results and Discussion

3.2.1 Synthesis and Characterization of Vaccine Constructs

Bacteriophage Qβ is virus that infects *e. coli*. Recombinant expression of the coat protein (CP) results in spontaneous assembly of a capsid containing 180 copies of the CP and an RNA core.[12, 13] Conjugation of antigens to the surface of Qβ has been shown to result in

enhanced immune responses towards the antigen compared with the antigen on its own.[14-16] For this study we functionalized the surface lysines on Qβ. Qβ was first incubated with 4-maleimidobutyric acid *N*-hydroxysuccinimide ester (GMBS) (**scheme 3.1a**). Following centrifuge filtration to remove unreacted GMBS, the peptide, $tau_{294-305}$, with an added *N*-terminal cystiene, was conjugated to Qβ through the maleimide moiety on the linker. ESI-TOF mass spectrometry showed Qβ-GMBS-Tau to have an average loading of 401 antigens/CP, for an average of 2.2 antigens per capsid (**figure 3.10**). KLH-GMBS-Tau was synthesized as previously reported (**scheme 3.1b**).

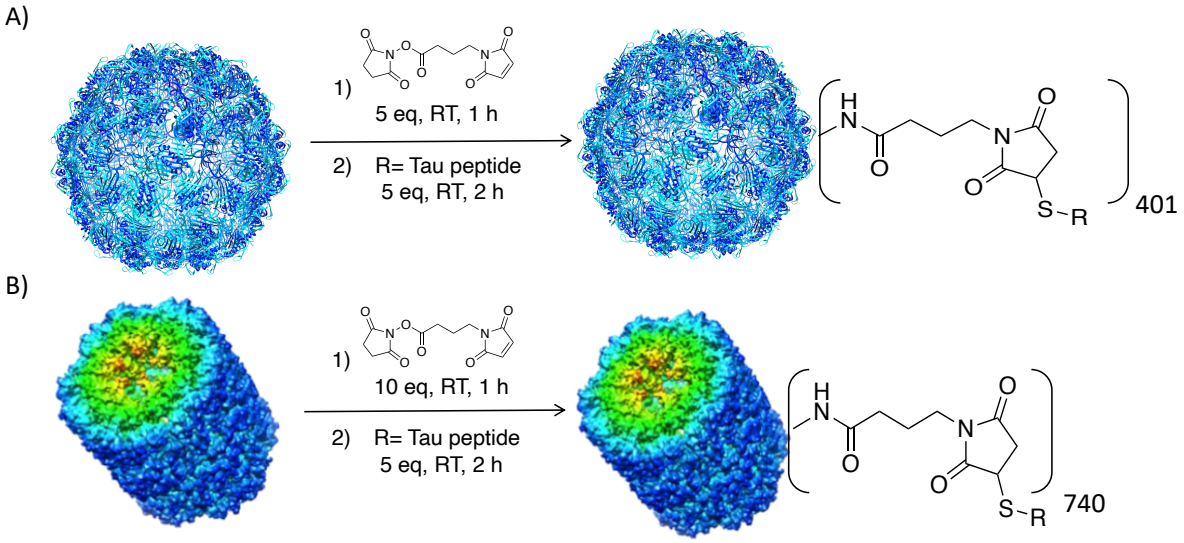

Scheme 3.1. (A) Reaction scheme for synthesis of Qβ-GMBS-Tau. Average loading was determined by ESI-MS (B) Reaction scheme for synthesis of KLH-GMBS-Tau.

3.2.2 Vaccination Induces Long Lasting Immune Responses

With vaccine constructs in hand, we investigated the ability of the vaccine constructs ability to elicit immune responses against the MTBR and tau in general. C57BL/6J mice were immunized with either Qβ-GMBS-Tau or KLH-GMBS-Tau (9.6 nmol of antigen) with Alum as adjuvant, according to the vaccination schedule in **scheme 3.2.**

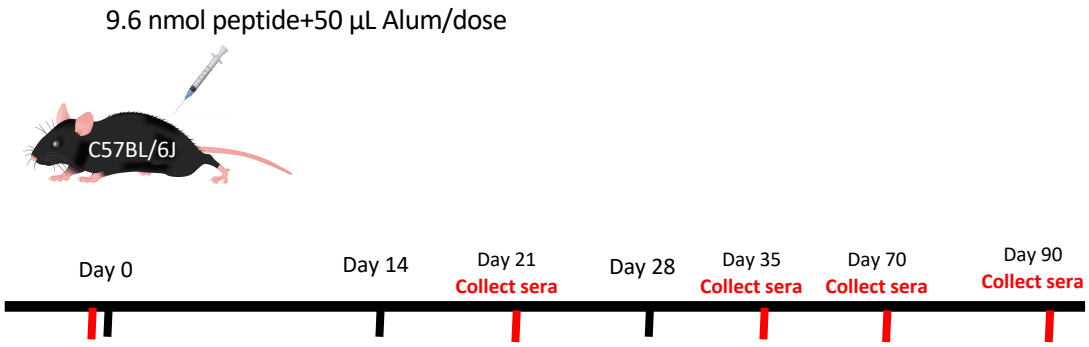

Scheme 3.2. Immunization schedule. Groups of 5 C57BL/6J mice were immunized 3 times bi-weekly with 9.6 nmol of peptide, as either Qβ-GMBS-Tau or KLH-GMBS-Tau, with 50 µL of alum as an adjuvant. Serum was collected on days 0 (pre-immunization), 21, 35, 70, and 90.

Mice immunized with Qβ-GMBS-Tau elicited super high titers of IgG antibodies against the targeted epitope. At day 35, Qβ-GMBS-Tau vaccinated mice produced titers over an order of magnitude (OOM) higher than mice immunized with KLH-GMBS-Tau (**figure 3.2A**). The OOM difference in titer response was maintained at all time points tested (**figure 3.2A**). As only ~0.1% of antibodies cross the BBB, high titers are critical for humoral immune responses aimed at diseases of the central nervous system (CNS). The difference in titer responses, between Qβ-GMBS-Tau and KLH-GMBS-Tau, encourages continued research into Qβ as a potential replacement for the current gold-standard KLH.[11]

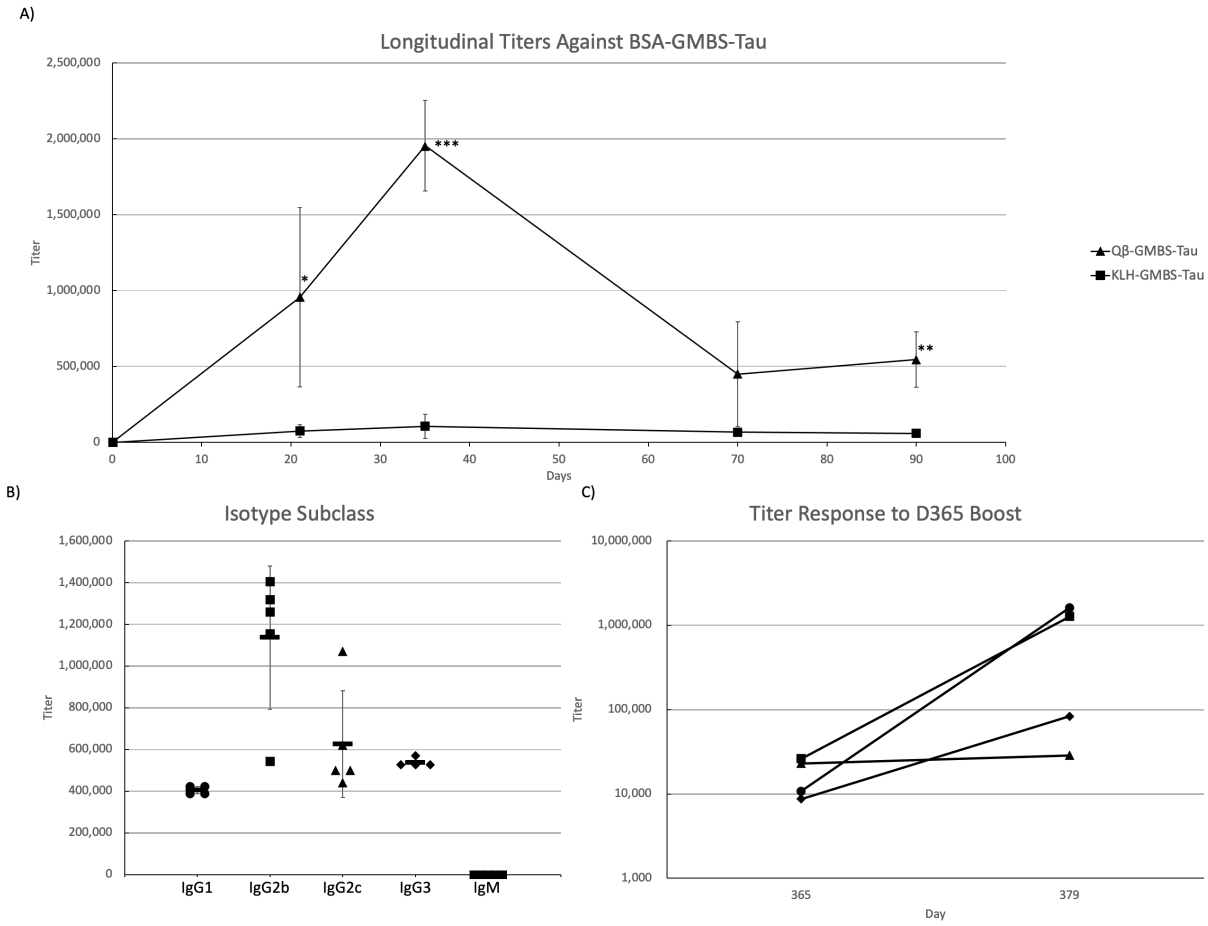

Figure 3.2. Immunization with Qβ-GMBS-Tau produced superior titers to immunization with KLH-GMBS-Tau. The antibodies elicited were mainly of IgG subtypes and mice responded to booster injections. (A) Longitudinal titers from mice (N = 5) immunized with either Qβ-GMBS-Tau or KLH-GMBS-Tau. (B) Immunoglobulin subtyping of D35 sera from mice immunized with Qβ-GMBS-Tau. (C) Pre- and post-boost titers from mice (N = 4) immunized with Qβ-GMBS-Tau that received another booster on D365.Titers were determined as the fold of dilution that gave an absorbance value above the average + 3*S.D. of the blank. All measurements were made in quadruplicates. *p*-values were calculated by a one-tailed *t*-test. *$p < 0.05$, **$p < 0.01$, ***$p < 0.001$.

One of the advantages of using Qβ as a carrier in conjugate vaccines is that it contains helper T cell epitopes. The presence of these epitopes helps direct the immune response towards a long-term humoral memory response through isotype switching. The predominant subtypes were from long-lasting IgG subtypes and very little IgM was observed (**figure 3.2B**)

As Alzheimer's is a long-term disease, it is important to ensure that if protection wanes it can be regained through boosting. To that end, sera from immunized mice were collected at D365 and mice were given a 3rd booster of the Qβ-GMBS-Tau vaccine on the same day. Two weeks later sera were collected again, and pre- and post-booster titers were compared (**figure 3.2C**). Three out of the four mice responded to the boost with two returning to titer levels near their D35 peak. This suggests that immunization with Qβ-GMBS-Tau generated long-lived memory B cells that could be reactivated following another booster if protection starts to wane.

3.2.3 Antibodies Produced are Capable of Recognizing Hyperphosphorylated, Monomeric, and Oligomeric Tau

With knowledge that sera from immunized mice were capable of recognizing the peptide used for immunization, we next investigated whether the sera could recognize tau species associated with Alzheimer's disease. Western blotting confirmed that the antibodies generated during immunization could recognize hyperphosphorylated tau, monomeric and oligomer tau but not another Alzheimer's disease associated protein, Aβ42 (**figure 3.3**).

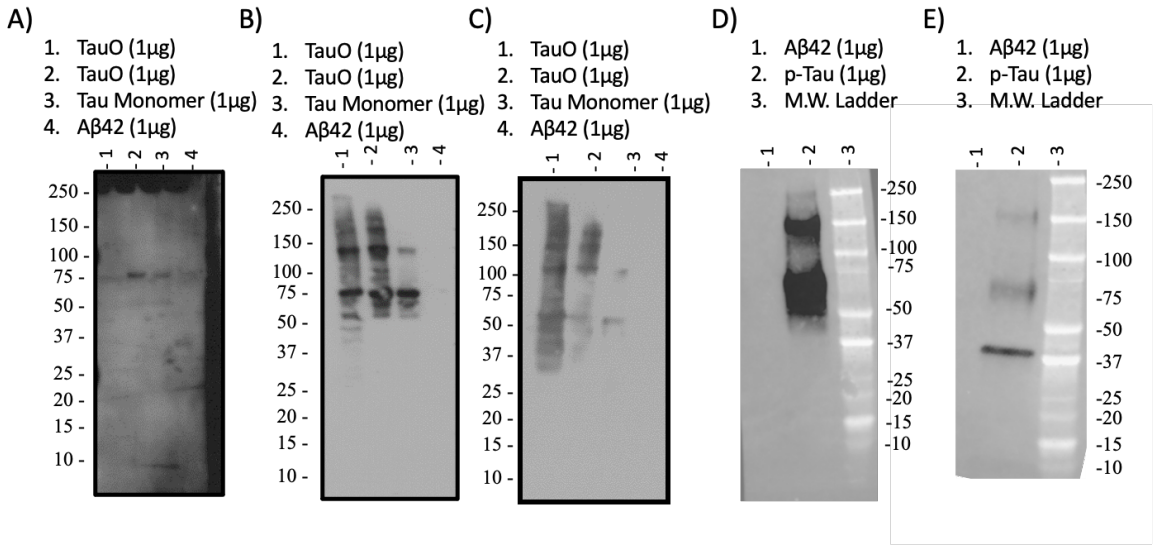

Figure 3.3. Western Blotting against various tau constructs. Aβ42 was used as a negative control. (A) Sera from mice immunized with Qβ alone were unable to recognize oligomeric tau (tauO) or monomeric tau. (B) Sera from mice immunized with Qβ-GMBS-Tau recognized both tauO and monomeric tau. (C & D) positive controls using a commercial pan tau antibody (Tau5). (E) Sera from mice immunized with Qβ-GMBS-Tau were capable of recognizing hyperphosphorylated tau (p-tau). All tau species were based on the 2N4R isoform. Serum was used at a 1:500 dilution. Tau5 was used at a 1:1000 dilution. Goat anti-mouse-HRP was used as the secondary antibody at a 1:1000 dilution. Gels A-C were kindly performed by the Kayed lab.

We next examined the ability of the induced antibodies to recognize different models of healthy and disease associated tau. D35 titers against, $tau_{151\text{-}391}$, p-tau, and the 2N4R tau isoform were calculated (**figure 3.4**). $Tau_{151\text{-}391}$ is a truncated version of the 2N4R isoform. With the *N*- and *C*-termini removed, the MTBR regions are exposed making it capable of initiating the oligomerization process. As it contains four copies of the minimal epitope we are targeting, it makes sense that the average titer against $tau_{151\text{-}391}$ is similar to that obtained against our BSA-GMBS-Tau construct that contains multiple copies of the antigen per BSA.

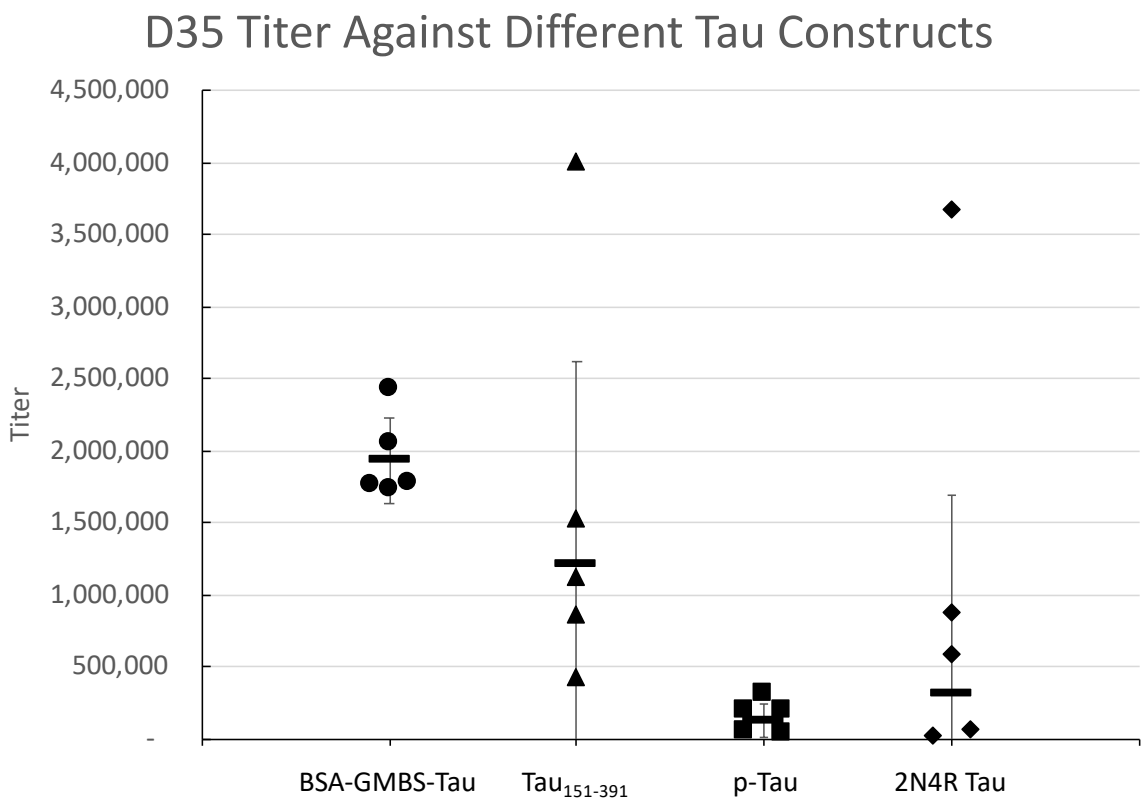

Figure 3.4. D35 titers against various tau constructs. Individual sera (N = 5) from D35 mice immunized with Qβ-GMBS-Tau. ELISA plates were coated with the antigen indicated on the x-axis. Titer values were calculated as the value that gave a signal greater than Ave.+3*S.D. of the blank.

To obtain titer data against an even more disease relevant form of tau, ELISA against p-tau was performed. Theoretically the hyperphosphorylation should lead to more exposure of the MTBR regions similar to the $tau_{151-391}$. Interestingly the D35 titer against p-tau was more similar to the D35 titer against "healthy" 2N4R tau than the D35 titer against $tau_{151-391}$ (**figure 3.4**). This form of p-tau does not contain phosphorylation in the epitopes targeted by immunization, so alteration of the epitopes should not explain the difference in titers.[17] One plausible mechanism then is that although the increased negative charge from hyperphosphorylation is thought to cause conformational changes in tau exposing the MTBR

regions, this is probably more dynamic in how exposed the MTBRs are unlike the “fully” exposed MTBRs from $tau_{151-391}$. Although it is tempting to compare these titers directly differences in binding affinity and orientation with the wells complicate the analysis.

To investigate this further, competitive ELISA was performed. ELISA plates were coated with BSA-GMBS-Tau and either 2N4R tau, $tau_{151-391}$, or p-tau was pre-incubated with D35 pooled sera. As expected from the ELISA results, the IC_{50} values for $tau_{151-391}$ (88.2 nM),p-tau (22.4 µM), 2N4R tau (>100 µM) followed the expected trend, if the titer differences were due to epitope availability based on tau conformation changes. Based on the ELISA and Competitive ELISA results our sera has a preference for disease associated forms of tau even as it retains the ability to recognize most forms of tau.

3.2.4 Immunized Serum Recognizes Tau in Patient Brain Tissue

To ensure that elicited antibodies were capable of staining tau in human tissue, immunohistochemistry (IHC) was performed on brain tissue samples from patients with Alzheimer’s disease. Slides were stained with either Qβ immunized serum (negative ctrl), Qβ-GMBS-Tau immunized serum, or a total tau monoclonal atibody (Tau5, positive ctrl). Qβ immunized serum showed little to no staining (**figure 3.5**). Whereas both Qβ-GMBS-Tau immunized serum and Tau5 strongly stained the slides.

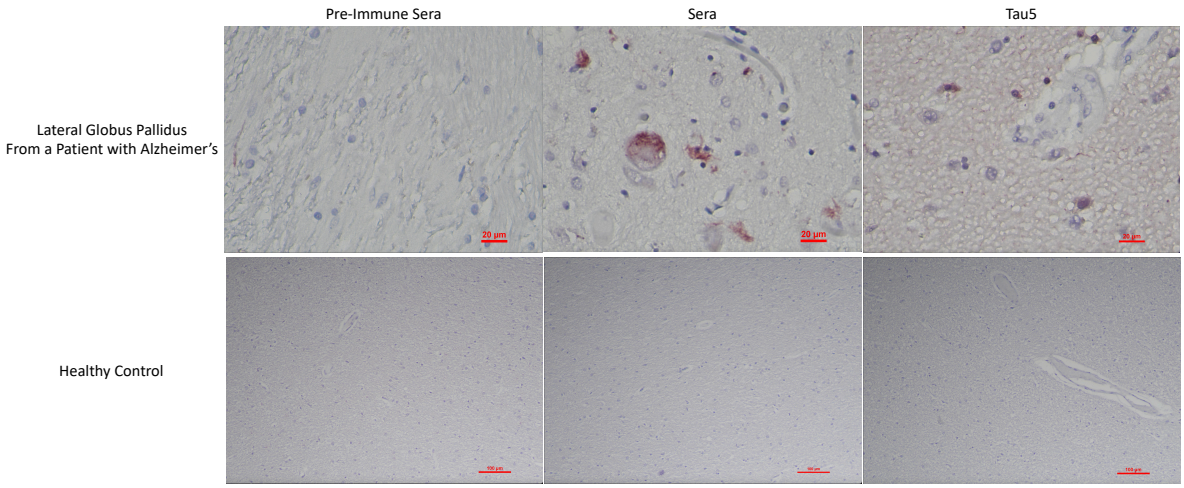

Figure 3.5. Immunohistochemistry (IHC) of human brain tissue from a patient with Alzheimer's disease or a healthy control. Slides were stained with either pre-immunization sera, D35 pooled sera from mice immunized with Qβ-GMBS-Tau, or the pan tau monoclonal antibody Tau5. Sera showed a similar staining patter to a commercial anti-tau antibody in diseased tissue and no staining in healthy tissue.

To confirm the IHC staining results showing similar punctate staining between Qβ-GMBS-Tau immunized serum and Tau5, immunofluorescense (IF) was performed. IF staining of patient's with Alzheimer's disease showed excellent correlation between Qβ-GMBS-Tau immunized serum and polyclonal total tau antibodies, suggesting that the sera are specific for tau. As a negative control healthy age and gender matched controls were also stained, which resulted in very little staining by either Qβ-GMBS-Tau immunized serum or Tau5 (**figure 3.6**)

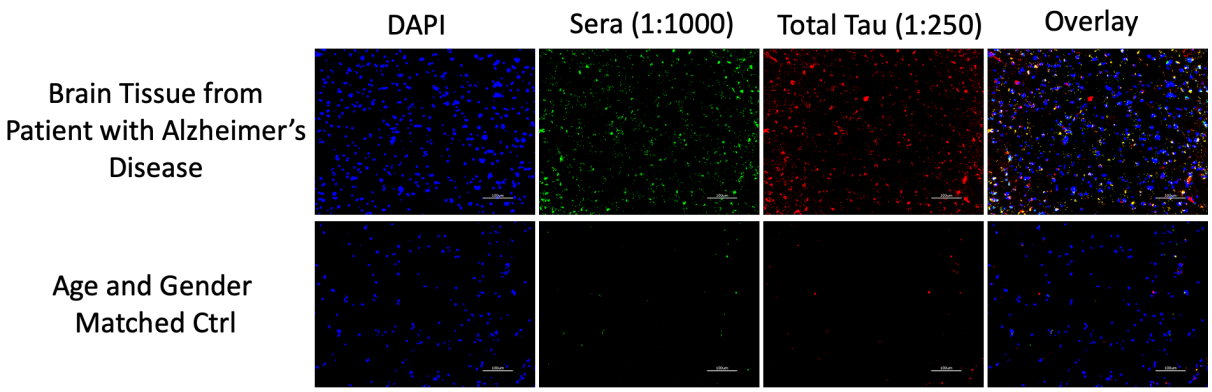

Figure 3.6 Immunofluorescence staining of brain tissue from either a patient with Alzheimer's disease or a healthy age and gender matched control. Tissue was stained with DAPI, D365 pooled sera from mice immunized with Qβ-GMBS-Tau, or polyclonal anti-tau rabbit sera. To visualize the staining, serum antibodies were stained with either goat-anti-mouse-Alexa Fluor 488 or goat-anti-rabbit-Alexa Fluor 568. Sera and a commercial anti-tau antibody tended to overlap in diseased tissue and showed minimal staining in healthy tissue.

3.2.5 *In Vitro* Protection Testing

Thioflavin based assays have been used to quantify the amount of tau aggregation, which interacts with β-sheets present in the aggregates and undergoes a spectral change upon binding.[18] Unfortunately, thioflavin is not specific for tau aggregation. It binds and interacts with other beta-sheet rich proteins prone to aggregation including serum albumin. Initial aggregation studies using serum from vaccinated mice and thioflavin S (ThS) showed that ThS interacting with albumin in the serum overpowered the signal from tau aggregate-ThS interactions (data not shown).

To test the ability of induced antibodies to prevent aggregation albumin must be removed from the serum. Ammonium sulfate cut is a technique used as part of antibody purification protocols.[19] As the amount of ammonium sulfate in solution increases, different proteins precipitate out of solution. IgG antibodies and serum albumin precipitate at different ammonium sulfate solutions.[20] Ammonium sulfate (NH_4SO_4) cut was used to remove serum

albumin leaving the intact IgG (**figure 3.11**). Antibodies that precipitated between 25%-50% (v/v) NH_4SO_4 were collected and resuspended in PBS. Purified antibodies retained activity as measured by the ability to generate a signal in an ELISA experiment (**figure 3.12**)

Using the purified IgG, the ThS-based aggregation assay was performed. The literature supporting these aggregation assays indicates that they are mainly used for testing of small drug-like molecules, and if they do utilize antibody-based therapeutics they are monoclonal antibodies. After troubleshooting the assay by purifying the crude sera and changing the ratio of antibody:p-tau ratio, we were unable to see any protective effects (**figure 3.7**). This is not to say that our sera did not have any protective effects, but instead the results are likely a limitation of the experimental design. Effective blocking of MTBR interaction by antibodies would require near stoichiometric equivalents of antibodies and p-tau and effectively measuring the ratio of antigen specific to non-specific antibodies in polyclonal serum is not a trivial exercise.[6] The challenges combined make the current *in vitro* studies ill-suited to examining the protective effects of antibodies elicited by immunization. With that in mind we moved to *in vivo* studies.

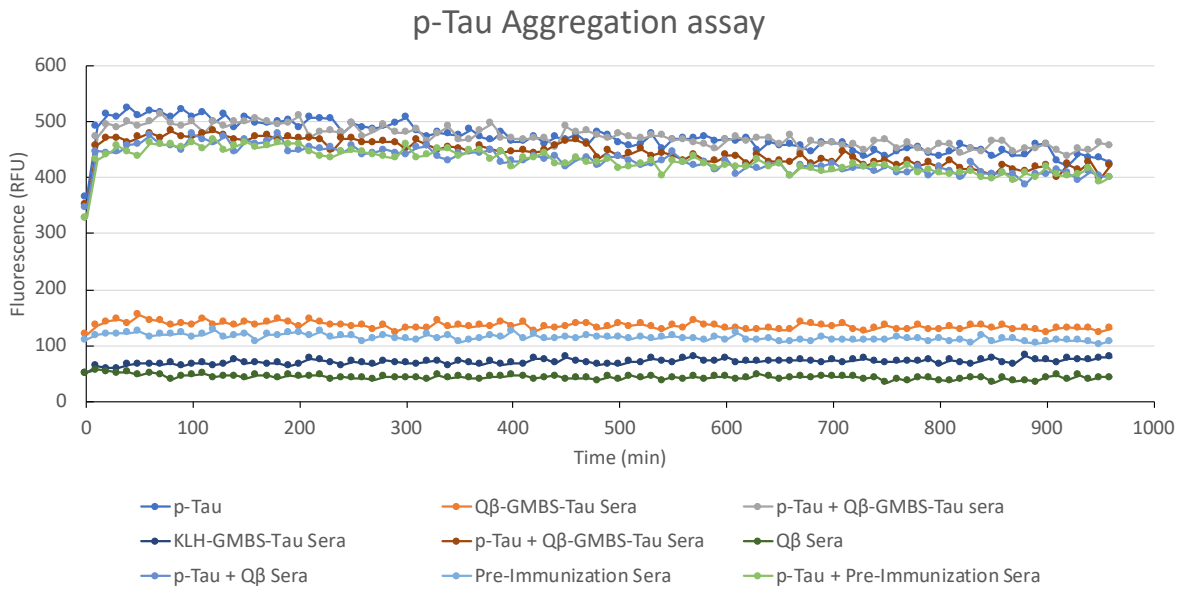

Figure 3.7. p-Tau aggregation assay results. Hyperphosphorylated tau (p-tau) was incubated with thioflavin S (ThS) and purified sera from mice immunized with either KLH-GMBS-Tau, Qβ-GMBS-Tau, Qβ, or pre-immunization sera. None of the tested sera showed a difference in p-tau aggregation compared to p-tau alone.

3.2.6 Examination of a Qβ Mutant as an Improved Carrier

Sungsuwan and coworkers recently reported a Qβ mutant (mQβ) with the following mutations A38K/A40C/D102C. This mutant has shown the potential to inhance the immune response by reducing anti-carrier antibody responses and increasing the stability of the capsid.[21] An mQβ-GMBS-Tau vaccine was synthesized with an average loading of 243 antigens/VLP (1.4 antigens/CP) (**figure 3.13**). Comparison of longitudinal titer data of C57BL/6J mice immunized with either mQβ-GMBS-Tau or Qβ-GMBS-Tau (**scheme 3.2**) showed significant anti-tau titer differences at all times measured (**figure 3.8A**). Additionaly there was approximatelly 5 times fewer anti-carrier antibodies elicited when using mQβ vs when wt Qβ was used as the carrier (**figure 3.8B**). Taken together the data supports the enhanced immunostimmulatory effect of mQβ compared to Qβ.

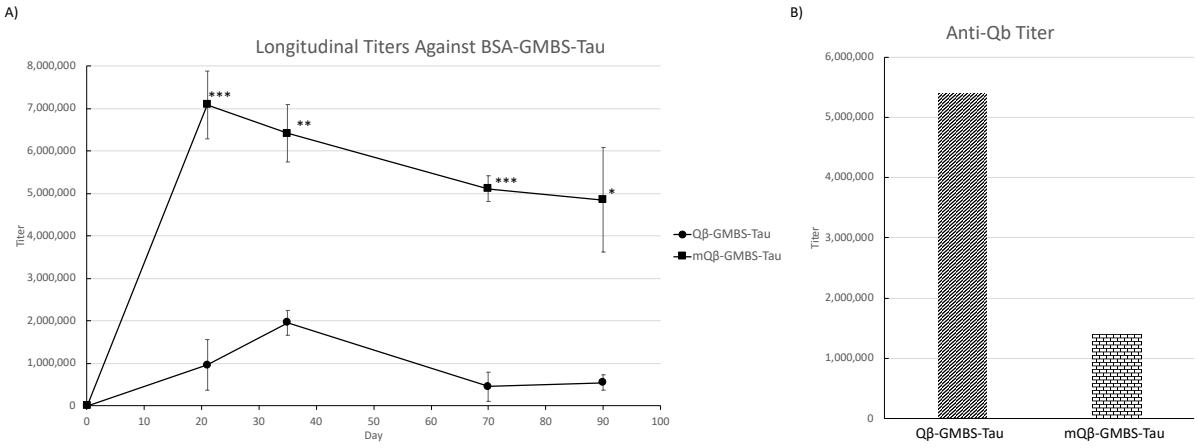

Figure 3.8. Immunization with mQβ-GMBS-Tau induced superior titers compared with Qβ-GMBS-Tau and resulted in 5 timesfewer anti-carrier antibodies. (A) Longitudinal ELISA titers against BSA-GMBS-Tau from mice (N = 5) immunized with either Qβ-GMBS-Tau or mQβ-GMBS-Tau. (B) D35 ELISA titers against Qβ from pooled sera from mice (N = 5) immunized with either Qβ-GMBS-Tau or mQβ-GMBS-Tau. The titers were calculated as the dilution that gave an absorbance > ave. + 3*S.D. of a blank. *p*-values were calculated by a one-tailed *t*-test. *$p < 0.05$, **$p < 0.01$, ***$p < 0.001$.

3.2.7 *In Vivo* Protection Studies

The mQβ-GMBS-Tau vaccine, with a higher loading 393 antigens/capsid (2.2 antigens/CP), was used in the in vivo studies (**figure 3.14)**. The higher loading was accomplished by increasing the equivalents of linker and peptide used during the conjugation reactions. Tauopathy prone transgenic mice (rTg510) were utilized for the in vivo studies. These mice were chosen because they start to display cognitive and behavioral symptoms at ~10 weeks of age.[22] The cognitive and behavioral deficits are even more apparent at ~16 weeks.[23] 8 week old mice are currently undergoing the same immunization schedule as wt mice with either mQβ-GMBS-Tau, mQβ/$tau_{294-305}$ admixed, or vehicle control. At 16 weeks of age, mice will undergo cognitive testing and non-invasive imaging to examine the protective effects of vaccination.

3.2.8 Development of a Monoclonal Nanobody

Despite the relatively high cost and the need for administration in a medical office, there has been a renewed interest in monoclonal antibodies for therapies against Alzheimer's disease after the approval of aducanumab.[24] With our construct's ability to elicit super high titers of IgG antibodies, we were interested in using our vaccine construct to develop a monoclonal nanobody. Nanobodies are single domain antibodies generaly produced in camelids.[25]

Unlike traditional IgG subtypes where the antigen binding domain consists of 2 chains (the variable heavy (V_H) and variable light (V_L) chains), camelids can produce an IgG subtype (IgG2/3) containing only a single variable heavy chain (VHH) making up the antigen binding domain.[26] After clonal selection and sequencing of an antigen specific IgG2/3 antibody, the VHH domain can be expressed on its own as a nanobody.

The small size of the nanobody (~15 kDA) compared to traditional monoclonal antibodies (~150 kDA) is part of their appeal.[25] There is evidence that they are better able to cross the BBB than traditional antibodies.[27] That penetration can be further increased by the alteration of the nanobody's pI.[28]

There have been nanobodies developed against tau in the past, although they have been developed from pre-existing VHH libraries instead of by active immunization.[29, 30] Use of mQβ-GMBS-Tau may allow for more specific generation of nanobodies recognizing the desired epitopes.

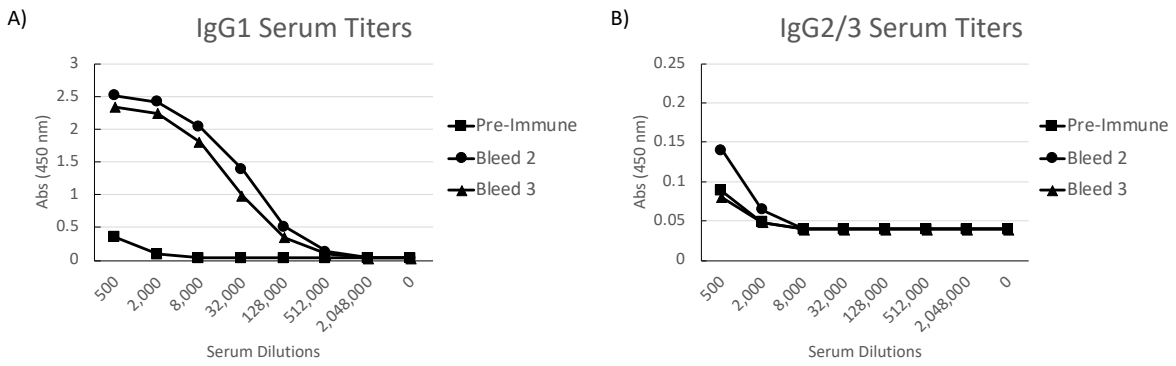

Figure 3.9. (A) IgG1 ELISA data from a llama immunized with mQβ-GMBS-Tau. (B) IgG2/3 ELISA data from a llama immunized with mQβ-GMBS-Tau.

A llama was immunized four times each with mQβ-GMBS-Tau. Blood was collecte pre-immunization, between dose 3 and 4 (bleed 2), and after dose 4 (bleed 3). mQβ-GMBS-Tau succesfully elicited traditional antibodies as measured by the IgG1 titers with stable titers developing after the 3rd immunization (**figure 3.9A**). Unfortunately mQβ-GMBS-Tau induced only low levels of IgG2/3 antibodies against tau (**figure 3.9B**).

The lack of IgG2/3 is likely due to the type of epitope targeted. Nanobodies have half the complementary determing region (CDR) loops compared to standard antibodies. This results in smaller paratope surface area allowing for access to privledged epitopes on the target.[31] The nanobodies can act more like a key in a lock, in the nanobody-antigen interaction, while traditional antibodys may be more like a glove holding a baseball. This suggests nanobodies might be worse at recognizing linear peptide epitopes like the one we targeted. Our results support this hypothesis.

3.3 Conclusions and Future Work

Herein we report the development of a Qβ conjugate vaccine targeting the MTBR region of tau to prevent oligomerization in Alzheimer's disease. The Qβ-GMBS-Tau elicited higher

titers than the current carrier gold-standard KLH. The antibodies elicited were associated with long-term immunological memory and could be boosted with another vaccine dose. The antibodies elicited showed a preference for tau with exposed MTBR regions mimicking aggregation prone tau. Additionally immunostaining showed elicited antibodies were capable of recognizing tau in human patients with Alzheimer's disease. With these promising initial results, there are on-going efforts to examine the ability of vaccination to provide protection and slow disease progression an a transgenic mouse model of Alzheimer's disease.

3.4 Materials and Methods

3.4.1 General Methods

Centrifugal filter units of 10,000 and 100,000 molecular weight cut-off (MWCO) were purchased from EMD Millipore. Fast protein liquid chromatography (FPLC) was performed on a GE ÄKTA Explorer (Amersham Pharmacia) instrument equipped with a Superose-6 column. For characterization of Qβ constructs, liquid chromatography-mass spectrometry (LCMS) analysis was performed. The samples for LCMS were prepared as follows: 1:1 v/v of 40 μg mL^{-1} of sample stock solution and 100 mM DTT was mixed and incubated in a water bath at 37 °C for 30 min. One drop of 50% formic acid was added to the mixture. LCMS was performed on Waters Xevo G2-XS quadrupole/time-of-flight UPLC/MS/MS. The liquid chromatography was done on ACUITY UPLC® Peptide BEH C18 column, 130Å, 1.7 μm, 2.1 mm x 150 mm, using gradient eluent from 95% 0.1% formic acid in CH_3CN (0.3 mL min^{-1} flowrate) at a column temperature of 40 °C. The spectra were deconvoluted using MaxEnt1. Protein concentration was measured using the Coomassie Plus Protein Reagent (Bradford Assay, Pierce) with BSA as the standard. p-Tau was a kind gift from Dr. Min-Hao Kuo. Human tissue was obtained from the NIH NeuroBioBank.

3.4.2 Synthesis of Qβ-GMBS-Tau and mQβ-GMBS-Tau

Qβ and mQβ were expressed and purified as previously discribed.[32] GMBS (0.2 mg, 0.71 mmol, 5 equiv with respect to CP) was dissolved in DMSO (10 uL). The solution was slowly added to a solution of Qβ/mQβ (10 mg mL^{-1} in PBS, pH = 7, 0.1 mL). The reaction was mixed on a nutating mixer in the dark for 1 hr at room temperature. The Qβ-GMBS/mQβ-GMBS was washed twice by centrifuge filtration using amicron ultra 0.5 mL centrifuge filters (MWCO = 10 kDa). Tau peptide (0.46mg, 0.35 mmol, 5 equiv with respect to CP) was dissolved in DMSO (10 µL). The solution was added to the solution of Qβ-GMBS/mQβ-GMBS (10 mg mL^{-1} in PBS, pH = 7, 0.1 mL). The reaction was mixed on a nutating mixer in the dark for 2 hrs at room temperature. The Qβ-GMBS-Tau/mQβ-GMBS-Tau was purified by centrifuge filtration using amicron ultra 0.5 mL centrifuge filters (MWCO = 10 kDa). Mass recovery of Qβ-GMBS-Tau/mQβ-GMBS-Tau was typically >90% as measured by bradford assay using BSA as a standard. The degree of functionalization was 390 antigens per Qβ (an average of 2.2 antigens per CP, **figure 3.10**) or 244 antigens per mQβ (an average of 1.4 antigens per CP, **figure 3.13**) as determined by ESI-TOF. Increasing the equivalents of GMBS (15 equiv.) and tau peptide (10 equiv.) increased the loading level of mQβ-GMBS-Tau to 393 antigens per mQβ (an average of 2.2 antigens per CP, **figure 3.14**).

3.4.3 Synthesis of KLH-GMBS-Tau

Synthesis of KLH-GMBS-Tau was performed as previously described.[7] A solution of GMBS (40 mg mL^{-1} in DMSO, 50 µL) was added to a solution of KLH (10 mg mL^{-1} in PBS, pH = 7, 1 mL). The reaction was mixed on a nutating mixer in the dark for 2 hrs at room temperature. The KLH-GMBS was washed twice by centrifuge filtration using amicron ultra 0.5 mL centrifuge

filters (MWCO = 10 kDa). The solution was adjusted to a final volume of 0.95 mL. A solution of tau peptide (400 mg mL^{-1} in DMSO, 50 µL) was added to the solution and the reaction was mixed on a nutating mixer in the dark for 2 hrs at room temperature. The KLH-GMBS-Tau was purified by centrifuge filtration using amicron ultra 0.5 mL centrifuge filters (MWCO = 10 kDa).

3.4.4 Synthesis of BSA-GMBS-Tau

GMBS (2.12 mg, 7.58 mmol, 50 equiv with respect to BSA) was dissolved in DMSO (100 uL). The solution was slowly added to a solution of mQβ (10 mg mL^{-1} in PBS, pH = 7, 1 mL). The reaction was mixed on a nutating mixer in the dark for 1 hr at room temperature. The mQβ-GMBS was washed twice by centrifuge filtration using amicron ultra 0.5 mL centrifuge filters (MWCO = 10 kDa). Tau peptide (4.97 mg, 3.79 mmol, 25 equiv with respect to BSA) was dissolved in DMSO (100 uL). The solution was added to the solution of BSA-GMBS (10 mg mL^{-1} in PBS, pH = 7, 1 mL). The reaction was mixed on a nutating mixer in the dark for 2 hrs at room temperature. The BSA-GMBS-Tau was purified by centrifuge filtration using amicron ultra 0.5 mL centrifuge filters (MWCO = 10 kDa). Mass recovery of BSA-GMBS-Tau was typically >90% as measured by the Bradford assay using BSA as a standard. The degree of functionalization was 17.5 antigens per BSA as determined by MALDI-TOF (**figure 3.15**)

3.4.5 Expression and Purification of $Tau_{151-391}$ and 2N4R Tau

BL21 (DE3) *e. coli.*transfected with a PET28b plasmid containing the gene for either $tau_{151-391}$ with a TEV cleavable His-tag or 2N4R tau were grown in LB media supplemented with kanamyacin (20 mg/L) to an OD_{600} of 0.7-1.0. Expression was induced by addition of IPTG (1 mM) and expression was run for 6 hrs at 37°C with shaking. Cells were pelleted by centrifugation at 7000 x g for 20min. Pelleted cells were resuspended in lysis buffer (20 mM

Tris, 100 mM NaCl, 1 mM EDTA, 1 mM PMSF, 20 mL/L of culture) and stored at -80^{o}C until purification.

Cells were thawed and all subsequent steps were performed at 4^{o}C. Cells were sonicated at 30% power for 10 min with 10 sec on and 10 sec off (total = 20 min). The lysate was centrifuged at 10,000 xg for 10 min. The superatant was collected and heated in a boiling water bath for 30 min. Centrifuged for 10 min at 10,000 xg and the supernatant collected. The pH value of the supernatant was adjusted to pH = 8 and loaded onto a nickel column. The column was washed twice with 5 column volumes with washing buffer (20 mM Tris HCl, 500 mM NaCl, pH 8). The protein of interest was then eluted twice using 5 column volumes of elution buffer (20 mM Tris HCl, 500 mM NaCl, 100 mM imidazole, 8 M urea). Fractions containing the protein of interest were snap frozen in liquid nitrogen and lyophilized (**figures 3.16-3.17**). Before use samples were resuspended in PBS washed with a 10 or 30 kDa MWCO centrifuge filter to remove elution buffer.

3.4.6 Western Blotting

1 µg of various tau constructs (tauO, monomeric tau, or p-tau) were run on a 4-15% SDS-PAGE gel under reducing conditions (220 V for 30 min at RT). Following gel electrophoresis proteins were transferred to a pre-wetted PVDF membrane (60 V for 90 min at 4 ^{o}C). Transfer was confirmed by the use of a pre-stained M.W. ladder. Blots were blocked overnight using blocking buffer (EveryBlot, Bio-Rad). After blocking, blots were washed 3 times with TBST for 15 min. each wash. Blots were stained with primary antibodies (immunized sera or Tau5) diluted (1:500 or 1:1000 respectively) in blocking buffer for 2 hrs at RT. Unbound primary antibodies were removed by washing 3 times with TBST for min. each wash. Primary antibodies were

detected by staining with HRP-conjugated goat anti-mouse IgG diluted (1:1000) in blocking buffer for 1 hr and washed 3 times with TBST for 15 min. each wash. Staining was detected using ECL spray (Prometheus Protein Biology, catalog # 20-300S) and a ChemiDoc imaging system (Bio-Rad).

3.4.7 Immunohistochemistry

Specimens were processed, embedded in paraffin and sectioned on a rotary microtome at 4μ's. Sections placed on charged slides and dried at 56°C overnight. The slides were subsequently deparaffinized in Xylene and hydrated through descending grades of ethyl alcohol to distilled water. Slides were placed in Tris Buffered Saline pH 7.4 (Scytek Labs – Logan, UT) for 5 minutes for pH adjustment. Following TBS, Heat Induced Epitope Retrieval in Citrate Plus pH 6.0 (Scytek) performed in vegetable steamer at 100°C – 30 minute; followed by 10 minute room temperature incubation and rinses in several changes of distilled water. Endogenous Peroxidase was blocked utilizing 3% Hydrogen Peroxide / Methanol bath for 30 minutes followed by running tap and distilled water rinses. Following pretreatments, standard micro-polymer complex staining steps performed at room temperature on the IntelliPath™ Flex Autostainer. All staining steps followed by rinses in TBS Autowash buffer (Biocare Medical – Concord, CA). After blocking for non-specific protein with IP FLX Background Punisher (Biocare) for 5 minutes; sections were incubated with specific primary (1:300 Tau5, 1:1000 D35 sera, or 1:1000 pre-immune sera) in normal antibody diluent (NAD-Scytek). MACH3™ Mouse Probe and Polymer (Biocare) incubated for 10 minutes each followed by reaction development with Romulin AEC™ (Biocare) – 5 minutes and counterstained with Cat Hematoxylin – 5 minutes.

3.4.8 Immunofluorescence

Tissue sections were fixed in chilled methanol for 10 min and washed 3 times in PBS supplemented with 0.25% Triton X-100 (0.25% PBST) for 5 min. Following the washing sections were washed in 70% ethanol (EtOH). Auto-fluorescence was blocked by treating tissue sections with TrueBlack (Biotium, catalog # 23007) for 5 min. then washed with 70% EtOH three times for 1 min and once with 0.25% PBST for 10 min. Tissue sections were blocked with 5% goat serum in incubation buffer (0.25% PBST supplemented with 5% BSA) for 1 hr in a humidity chamber and washed 3 time in 0.25% PBST for 5 min. Tissue sections were incubated with primary antibodies diluted in incubation buffer overnight at 4 ^{o}C in a humidity chamber and washed 3 times in 0.25% PBST for 5 min. Primary antibodies were stained using goat anti-mouse IgG Alexa Fluor-488 and goat anti-rabbit IgG Alexa Fluor-568 diluted in incubation buffer for 1 hr at RT in a humidity chamber and washed 3 times with 0.25% PBST for 10 min. Nuclei were stained by incubation with DAPI in incubation buffer for 5 min at RT in a humidity chamber and washed 3 times with 0.25% PBST for 5 min. Coverslips wer mounted using Fluoromount G and sealed with nail polish.

3.4.9 p-Tau Aggregation Assay

Aggregation assays were performed as previously reported.[17] In short, p-tau was thawed on ice. Experiments were performed on a 384-well low-volume plate. For each sample p-tau (6 or 3 µM), 20 mM Tris (pH 7.4), thioflavin S (ThS) (20 µM), and sera were mixed in a microcentrifuge tube (final volume = 40 µL). Reactions were run in triplicate (10 µL/well). The plate was covered by an Optical Adhesive Film to minimize evaporation during the assay. ThS fluorescence was measured every 10 min (ex. 440 nm; em. 490) for 16 hrs. During the

measurement phase, the temperature was held at 37°C. Only assays conducted at the same time were plotted in the same graph.

3.4.10 Immunization of Mice

Female mice (C57BL/6 or rTg510)aged 6−10 weeks were used for studies. All animal experiments were performed in accordance with the guidelines of the Institutional Animal Care and Use Committee (IACUC) of Michigan State University. The animal usage protocol number is PROTO201900423.

In all studies, mice were subcutaneously injected under the scruff on day 0 with 0.1 mL of various vaccine constructs in PBS containing Alum (Imject Alum™, Thermo Scientific, catalog #: 77161) (50 µL) for each mouse. Vaccine doses were prepared by vortexing the mixture at 4 °C until an emulsion formed. Boosters were given subcutaneously at the same amounts of vaccines with Alum under the scruff on days 14 and 28. All vaccine doses had the same amounts of antigen (9.6 nmol). Serum samples were collected on days 0 (before immunization), 21, 35, 70, and 90. The final bleeding was performed through cardiac bleed.

3.4.11 Evaluation of Antibody Titers by ELISA

The Nunc MaxiSorp® flat-bottom 96-well microtiter plates were coated with 10 µg mL^{-1} of the corresponding BSA-GMBS-Tau, 2N4R Tau, $Tau_{151-394}$ or p-Tau (100 µL/well) in $NaHCO_3/Na_2CO_3$ buffer (0.05 M, pH 9.6) by incubation at 4°C overnight. The coated plates were washed with PBS/0.5% Tween-20 (PBST) (4 × 200 µL) and blocked with 1 % BSA in PBS (100µL/well) at rt for 1 h. The plates were washed again with PBST (4 × 200 µL) and incubated with serial dilutions of mouse sera in 0.1 % BSA/PBS (100 µL/well, 4 wells for each dilution). The plates were incubated for 2 h at 37 °C and then washed with PBST (4 × 200 µL). A 1:2000

dilution of HRP-conjugated goat anti-mouse IgG, IgG1, IgG2b, IgG2c, IgG3 or IgM (Jackson ImmunoResearch Laboratory) or HRP-conjugated goat anti-alpaca IgG1 or IgG2/3 (Jackson ImmunoResearch Laboratory) in 0.1% BSA/PBS (100 µL) was added to the wells respectively to determine the titers of antibodies generated. The plates were incubated for 1 h at 37 °C and then washed with PBST (4 × 200 µL). A solution of enzymatic substrate 3,3',5,5'-tetramethylbenzidine (TMB, 200 µL) was added to the plates (for one plate: 5 mg of TMB was dissolved in 2 mL of DMSO plus 18 mL of citric acid buffer containing 20 µL of H_2O_2). Color was allowed to develop for 15 min and then quenched by adding 50 µL of 0.5 M H_2SO_4. The readout was measured at 450 nm using a microplate reader. The titer was determined as the highest fold of dilution giving the optical absorbance value equal to the average of the blank well plus three times the standard deviation.

3.4.12 Competitive ELISA

The procedure was adapted from the literature.[33] The Nunc MaxiSorp® flat-bottom 384-well microtiter plates were coated with 10 µg mL^{-1} of BSA-GMBS-Tau, (50 µL/well) in $NaHCO_3/Na_2CO_3$ buffer (0.05 M, pH 9.6) by incubation at 4°C overnight. The coated plates were washed with PBST (4 × 100 µL) and blocked with 1 % BSA in PBS (50µL/well) at rt for 1 h. The plates were washed again with PBST (4 × 100 µL). D35 pooled serum was diluted to a dilution that was known to give a final signal of ~1.0-1.5 in ELISA experiments with incubated with serial dilutions of varying tau constructs ($tau_{151-391}$, p-Tau, or 2N4R, starting conc. = 100 µM) in 0.1 % BSA/PBS, for 30 min at rt. The samples were centrifuged for 3 min at 14,000 x g to remove any precipitate. Samples were added to each plate (50 µL/well, 4 wells for each dilution). The plates were incubated for 2 h at rt and then washed with PBST (4 × 100 µL). A 1:2000 dilution of HRP-

conjugated goat anti-mouse IgG (Jackson ImmunoResearch Laboratory) in 0.1% BSA/PBS (50 µL) was added to the wells. The plates were incubated for 1 h at rt and then washed with PBST (4 × 100 µL). A solution of enzymatic substrate 3,3',5,5'-tetramethylbenzidine (TMB, 75 µL) was added to the plates (for one plate: 10 mg of TMB was dissolved in 4 mL of DMSO plus 36 mL of citric acid buffer containing 40 µL of H_2O_2). Color was allowed to develop for 15 min and then quenched by adding 25 µL of 0.5 M H_2SO_4. The readout was measured at 450 nm using a microplate reader.

3.4.13 Ammonium Sulfate Cut

The procedure was adapted from literature.[19] D35 serum (10 µL) from each mouse (n=5) was mixed in an eppendorf tube (total volume = 50 µL). A saturated ammonium sulfate solution (16.6 µL) was slowly added to the pooled serum until the concentration of ammonium sulfate was 25% (v/v). The solution was incubated at 4°C for 12hrs. Precipitate was removed by centrifugation at 3000g for 30 min at 4°C. The supernatant was collected, and saturated ammonium sulfate (22.2 µL) was added until the concentration was ~50% (v/v). The solution was incubated at 4°C for 6hrs. The precipitate was collected by centrifugation at 3000g for 30 min at 4°C. The supernatant was discarded, and the pellet was resuspended in PBS (50 µL). The resuspended pellet was dialyzed for 48hrs using a Pur-A-Lyzer™ Midi 6000 dialysis kit (6-8 kDa MWCO) against 3x changes of PBS. Following dialysis, the purified antibodies were stored at 4°C in PBS.

3.4.14 Llama Immunization

All work was completed under contract by ProSci Inc. A llama was immunized on day 0 with 200 µg of mQβ-GMBS-Tau (244 peptides/capsid) and Complete Freund's Adjuvant. On days 21, 49,

and 77, the llama was boosted with 100 µg of mQβ-GMBS-Tau (244 peptides/capsid) and Incomplete Freund's Adjuvant. On days 0, 28, 56, and 84, blood was collected and PMBC and sera were collected.

APPENDIX

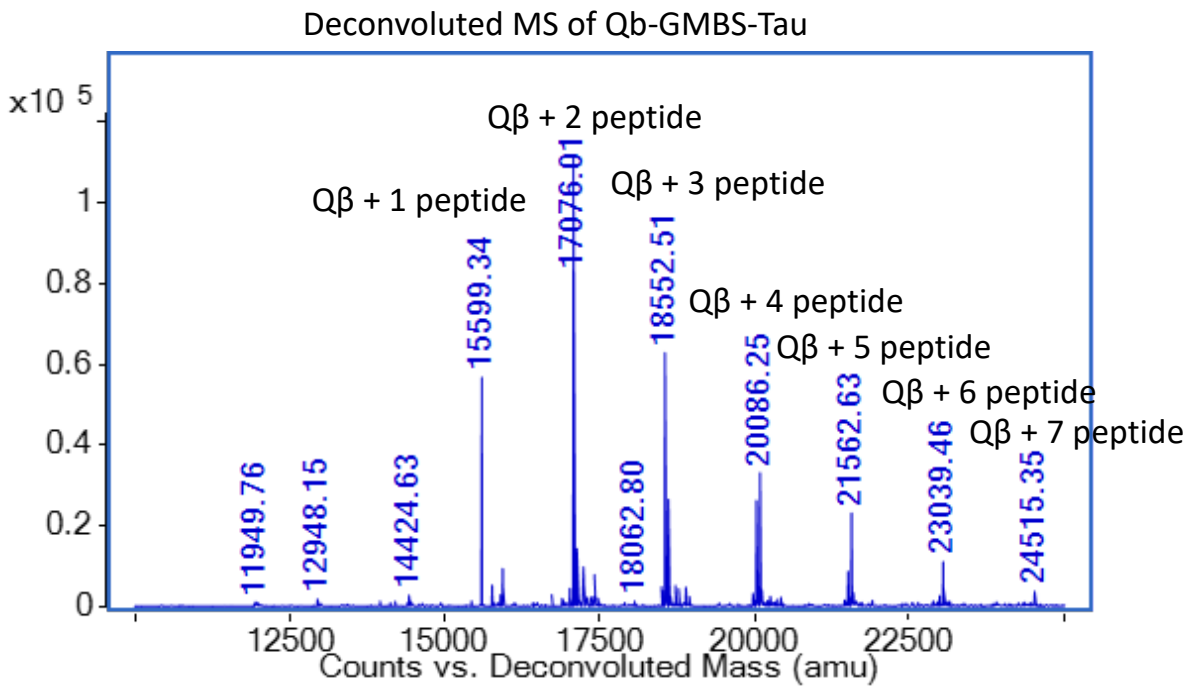

Figure 3.10. Deconvoluted mass spectrum from Qβ-GMBS-Tau. Analysis of the peak intensities showed an average loading of 390 antigens per capsid or 2.2 antigens per coat protein (CP).

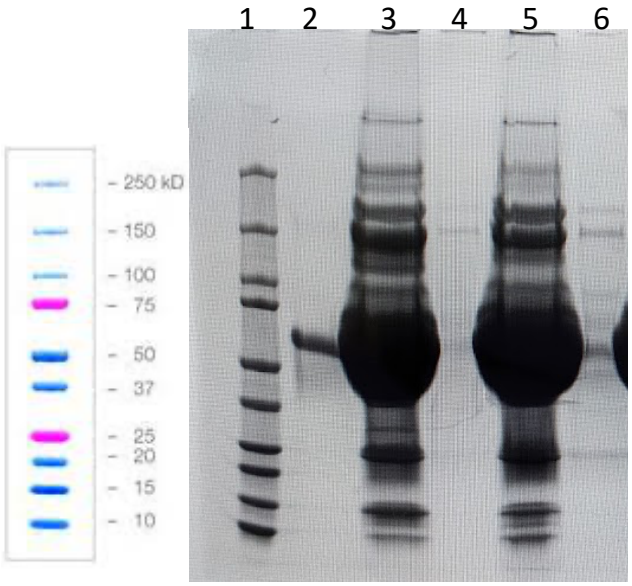

1: ladder
2: Serum albumin standard
3: Pre-Sulfate Anti-QB-GMBS-Tau Sera
4: Post-Sulfate Anti-QB-GMBS-Tau Sera
5: Pre-Sulfate Anti-QB Sera
6: Post-Sulfate Anti-QB Sera

Figure 3.11. SDS PAGE gel of Serum pre- or post- purification. 5 µL of pre- and post-precipitation samples were run on a non-reducing SDS-PAGE gel. Protein was visualized using Coomassie Blue stain.

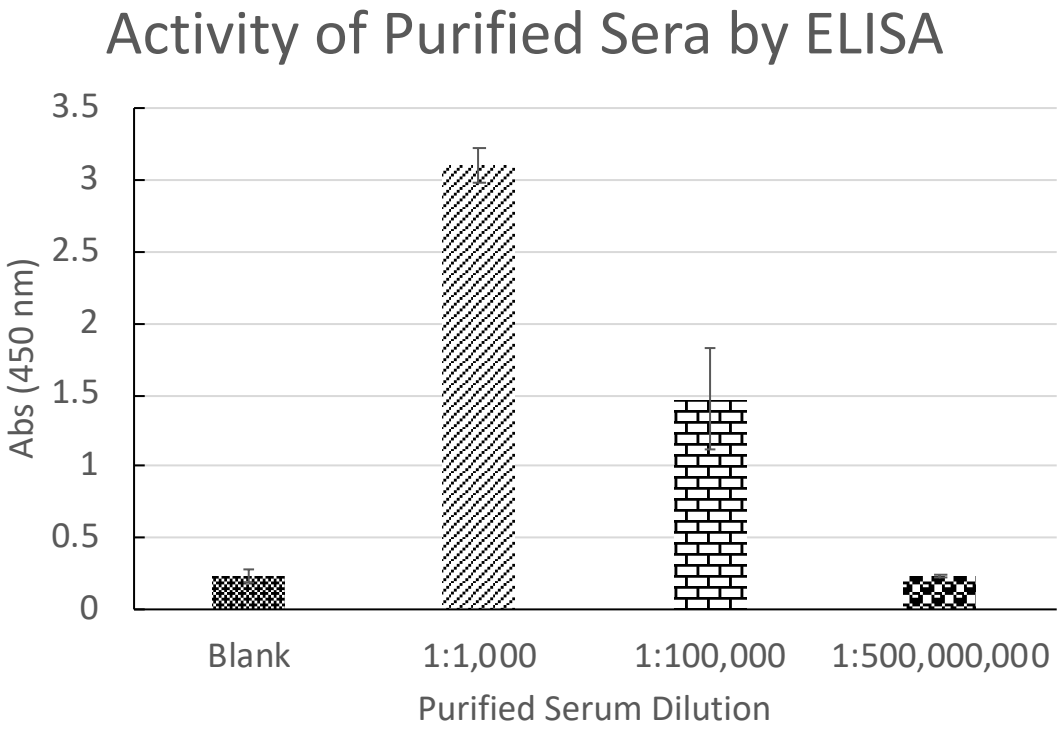

Figure 3.12. Sera purified by ammonium sulfate cut retained their activity. ELISA plates were coated with BSA-GMBS-Tau. Purified D35 sera from mice immunized with Qβ-GMBS-Tau was incubated at different dilutions. Antibody binding was observed using a goat anti-mouse HRP conjugated secondary antibody and TMB. The absorbance was measured at 450 nm. All samples were run in quadruplicate.

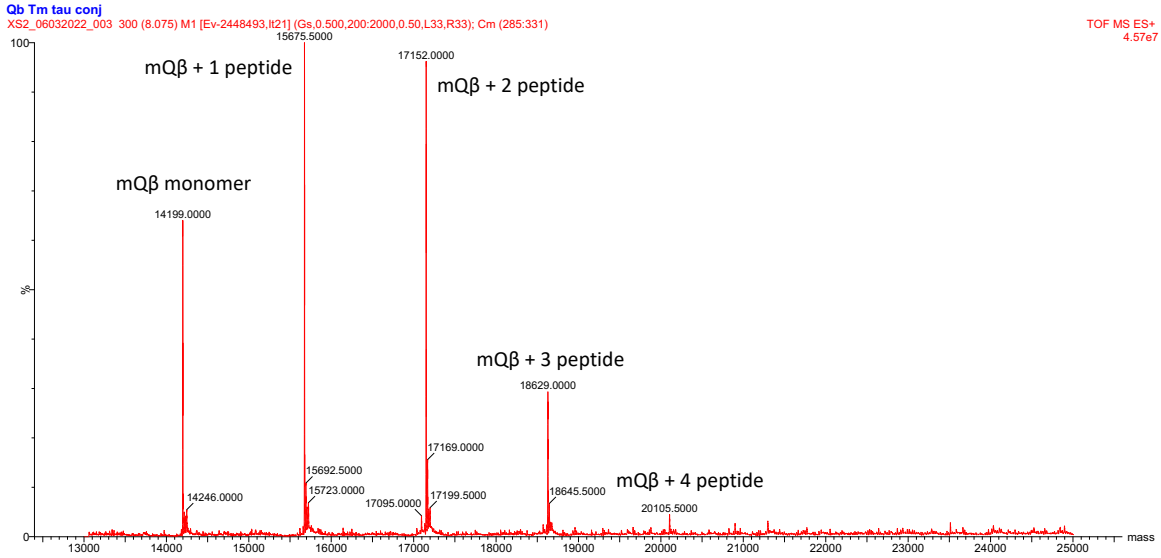

Figure 3.13. Deconvoluted mass spectrum from mQβ-GMBS-Tau synthesized using 5 eq. GMBS and 5 eq. of peptide. Analysis of the peak intensities showed an average loading of 244 antigens per capsid or 1.4 antigens per coat protein (CP). mQβ-GMBS-Tau with this loading was using in immunization studies with C57BL/6 mice.

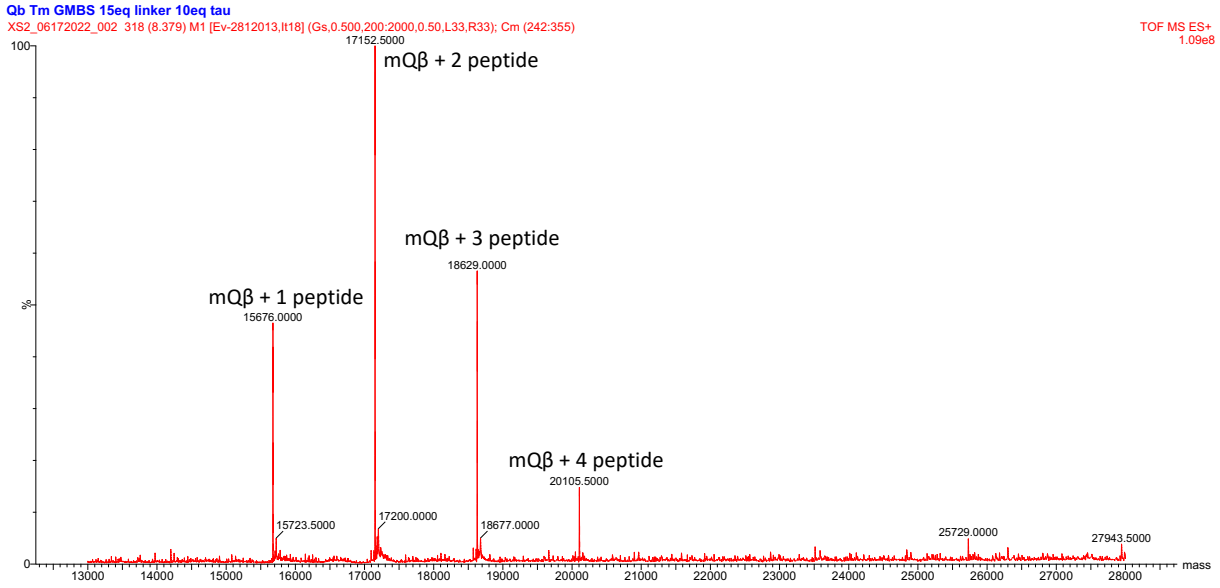

Figure 3.14. Deconvoluted mass spectrum from mQβ-GMBS-Tau synthesized using 10 eq. og GMBS and 15 eq. of peptide. Analysis of the peak intensities showed an average loading of 393 antigens per capsid or 2.2 antigens per coat protein (CP). mQβ-GMBS-Tau with this loading was used in immunization studies with rTg510 mice.

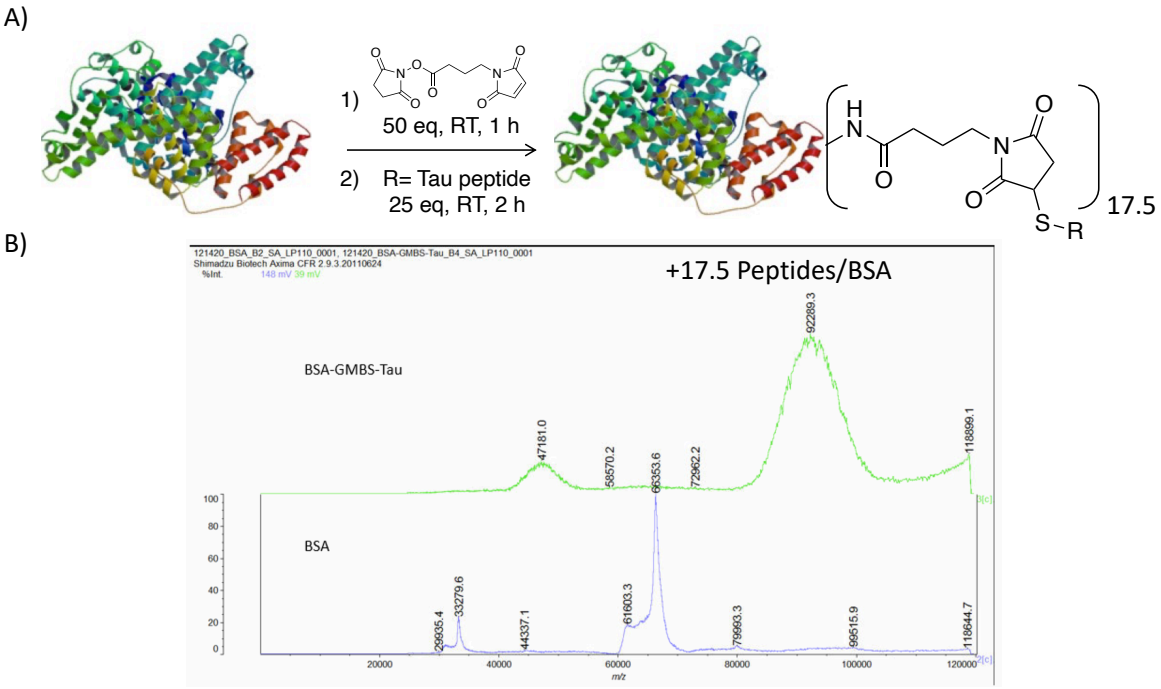

Figure 3.15. (A) Reaction conditions for the synthesis of BSA-GMBS-Tau. (B) MALDI TOF MS spectra showing BSA-GMBS-Tau and unmodified BSA. The peak shift shows an average loading of 17.5 antigens per BSA.

- Ln 1: Ladder
- Ln 2: Sonication
- Ln 3: Boil
- Ln 4: Flow Thru
- Ln 5: Wash 1
- Ln 6: Wash 2
- Ln 7: Elute 1
- Ln 8: Elute 2

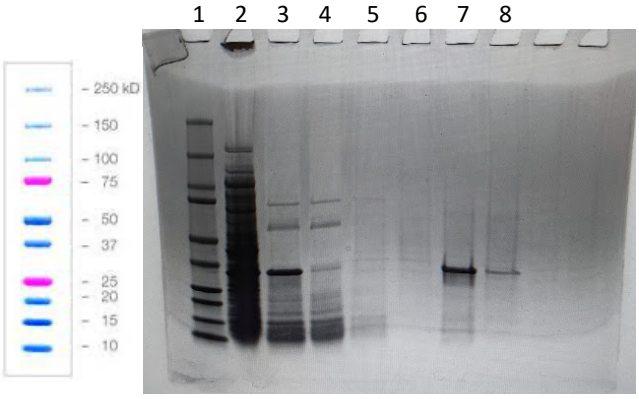

Figure 3.16. SDS-PAGE gel of $Tau_{151-391}$-TEV-HIS purification. 10 µL of sample from each step was retained and run on a reducing SDS-PAGE gel. Protein was visualized using Coomassie Blue stain.

- Ln 1: Ladder
- Ln 2: Sonication
- Ln 3: Boil
- Ln 4: Flow Through
- Ln 5: Wash
- Ln 6: Elute 1
- Ln 7: Elute 2

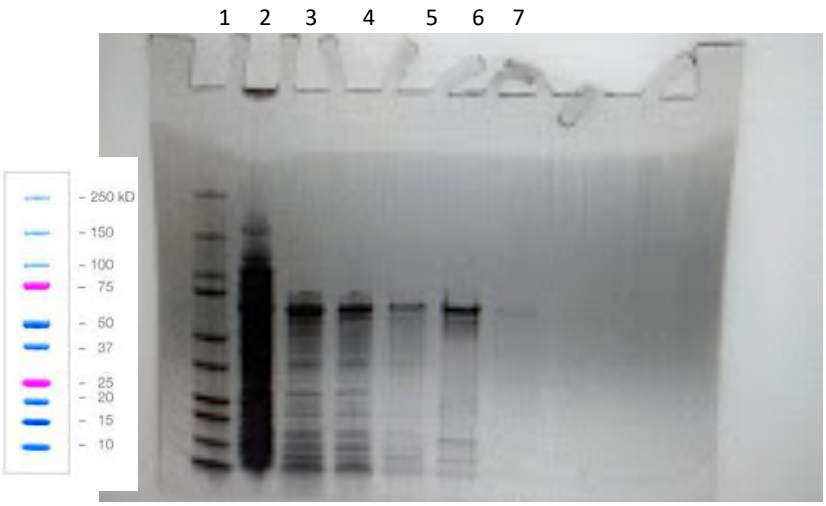

Figure 3.17. SDS PAGE gel of Tau_{1-441} Purification. 10 µL of sample from each step was retained and run on a reducing SDS-PAGE gel. Protein was visualized using Coomassie Blue stain.

REFERENCES

REFERENCES

1. Alzheimer's Association *Alzheimer's Disease Facts and Figures*; 2022; p 18.

2. Moloney, C. M.; Lowe, V. J.; Murray, M. E., Visualization of Neurofibrillary Tangle Maturity in Alzheimer's Disease: a Clinicopathologic Perspective for Biomarker Research. *Alzheimers Dement.* **2021,** *17*, 1554-1574.

3. Cowan, C. M.; Mudher, A., Are Tau Aggregates Toxic or Protective in Tauopathies? *Front. Neurol.* **2013,** *4*, 114.

4. Shafiei, S. S.; Guerrero-Muñoz, M. J.; Castillo-Carranza, D. L., Tau Oligomers: Cytotoxicity, Propagation, and Mitochondrial Damage. *Front. Aging Neurosci.* **2017,** *9*, 83.

5. Lasagna-Reeves, C. A.; Castillo-Carranza, D. L.; Sengupta, U.; Clos, A. L.; Jackson, G. R.; Keyed, R., Tau Oligomers Impair Memory and Induce Synaptic and Mitochondrial Dysfunction in Wild-Type Mice. *Mol. Neurodegener.* **2011,** *6*, 39.

6. Kontsekova, E.; Zilka, N.; Kovacech, B.; Skrabana, R.; Novak, M., Identification of Structural Determinants on Tau Protein Essential for its Pathological Function: Novel Therapeutic Target for Tau Immunotherapy in Alzheimer's Disease. *Alzheimers Res. Ther.* **2014,** *6*, 45.

7. Kontsekova, E.; Zilka, N.; Kovacech, B.; Novak, P.; Novak, M., First-in-Man Tau Vaccine Targeting Structural Determinants Essential for Pathological Tau-Tau Interaction Reduces Tau Oligomerization and Neurofibrillary Degeneration in an Alzheimer's Disease Model. *Alzheimers Res. Ther.* **2014,** *6*, 44.

8. Novak, P.; Schmidt, R.; Kontsekova, E.; Zilka, N.; Kovacech, B.; Skrabana, R.; Vince-Kazmerova, Z.; Stanislav, K.; Fialova, L.; Prcina, M.; Parrak, V.; Dal-Bianco, P.; Brunner, M.; Staffen, W.; Rainer, M.; Ondrus, M.; Ropele, S.; Smisek, M.; Sivak, R.; Winblad, B.; Novak, M., Safety and Immunogenicity of the Tau Vaccine AADvac1 in Patients with Alzheimer's Disease: A Randomized, Double-Blind, Placebo-Controlled, Phase 1 Trial. *Lancet Neurol.* **2017,** *16*, 123-134.

9. Novak, P.; Schmidt, R.; Kontsekova, E.; Kovacech, B.; Smolek, T.; Katina, S.; Fialova, L.; Prcina, M.; Parrak, V.; Dal-Bianco, P.; Brunner, M.; Staffen, W.; Rainer, M.; Ondrus, M.; Ropele, S.; Smisek, M.; Sivak, R.; Zilka, N.; Winblad, B.; Novak, M., FUNDAMANT: An Interventional 72-Week Phase 1 Follow-Up Study of AADvac1, an Active Immunotherapy Against Tau Protein Pathology in Alzheimer's Disease. *Alzheimers Res. Ther.* **2018,** *10*, 108.

10. Novak, P.; Kovacech, B.; Katina, S.; Schmidt, R.; Scheltens, P.; Kontsekova, E.; Ropele, S.; Fialova, L.; Kramberger, M.; Paulenka-Ivanovova, N.; Smisek, M.; Hanes, J.; Stevens, E.;

Kovac, A.; Sutovsky, S.; Parrak, V.; Koson, P.; Prcina, M.; Galba, J.; Cente, M.; Hromadka, T.; Filipcik, P.; Piestansky, J.; Samcova, M.; Prenn-Gologranc, C.; Sivak, R.; Froelich, L.; Fresser, M.; Rakusa, M.; Harrison, J.; Hort, J.; Otto, M.; Tosun, D.; Ondrus, M.; Winblad, B.; Novak, M.; Zilka, N., ADAMANT: A Placebo-Controlled Randomized Phase 2 study of AADvac1, an Active Immunotherapy Against Pathological Tau in Alzheimer's Disease. *Nat. Aging* **2021,** *1*, 521-534.

11. Boado, R. J.; Zhou, Q.-H.; Lu, J. Z.; Hui, E. K.-W.; Pardridge, W. M., Pharmacokinetics and Brain Uptake of a Genetically Engineered Bifunctional Fusion Antibody Targeting the Mouse Transferrin Receptor. *Mol. Pharm.* **2010,** *7*, 237-244.

12. Lim, F.; Spingola, M.; Peabody, D. S., The RNA-binding Site of Bacteriophage Qβ Coat Protein. *J. Biol. Chem.* **1996,** *271*, 31839-31845.

13. Golmohammadi, R.; Fridborg, K.; Bundule, M.; Valegård, K.; Liljas, L., The Crystal Structure of Bacteriophage Qβ at 3.5 Å Resolution. *Structure* **1996,** *4*, 543-554.

14. Yin, Z.; Delaney, S.; McKay, C. S.; Baniel, C.; Kaczanowska, K.; Ramadan, S.; Finn, M. G.; Huang, X., Chemical Synthesis of GM2 Glycan, Bioconjugation with Bacteriophage Qβ, and the Induction of Anticancer Antibodies. *ChemBioChem* **2016,** *17*, 174-180.

15. Yin, Z.; Wu, X.; Kaczanowska, K.; Sungsuwan, S.; Aragones, M. C.; Pett, C.; Yu, J.; Baniel, C.; Westerlind, U.; Finn, M. G.; Huang, X., Antitumor Humoral and T Cell Responses by Mucin-1 Conjugates of Bacteriophage Qβ in Wild-type Mice. *ACS Chem. Biol.* **2018,** *13*, 1668-1676.

16. Braun, M.; Jandus, C.; Maurer, P.; Hammann-Haenni, A.; Schwarz, K.; Bachmann, M. F.; Speiser, D. E.; Romero, P., Virus-Like Particles Induce Robust Human T-Helper Cell Responses. *Eur. J. Immunol.* **2012,** *42*, 330-340.

17. Liu, M.; Sui, D.; Dexheimer, T.; Hovde, S.; Deng, X.; Wang, K.-W.; Lin, H. L.; Chien, H.-T.; Kweon, H. K.; Kuo, N. S.; Ayoub, C. A.; Jimenez-Harrison, D.; Andrews, P. C.; Kwok, R.; Bochar, D. A.; Kuret, J.; Fortin, J.; Tsay, Y.-G.; Kuo, M.-H., Hyperphosphorylation Renders Tau Prone to Aggregate and to Cause Cell Death. *Mol. Neurobiol.* **2020,** *57*, 4704-4719.

18. LeVine III, H., Quantification of β-Sheet Amyloid Fibril Structures with Thioflavin T. *Meth. Enzymol.* **1999,** *309*, 274-284.

19. Fishman, J. B.; Berg, E. A., Ammonium Sulfate Fractionation of Antibodies. *Cold Spring Harb. Protoc.* **2018**, doi:10.1101/pdb.prot099119.

20. Hassan, H. S.; Najam, A.; Parveen, G.; Ali, H.; Channa, R. A.; Adeel, S. S., An Optimized method of IgG's Precipitation with Ammonium Sulphate from Hyper Immune Horse Plasma for Snake Anti Venom Production. *Int. J. Mol. Biol. Open Access* **2020,** *5*, 166-169.

21. Sungsuwan, S.; Wu, X.; Shaw, V.; Kavunja, H.; McFall-Boegeman, H.; Rashidijahanabad, Z.; Tan, Z.; Lang, S.; Nick, S. T.; Lin, P.-H.; Yin, Z.; Ramadan, S.; Jin, X.; Huang, X., Structure Guided Design of the Bacteriophage Qβ Mutants as Next Generation Carriers for Conjugate Vaccines. *ACS. Chem. Biol.* **2022,** *XX*, XXXX-XXXX.

22. Ramsden, M.; Kotilinek, L.; Forster, C.; Paulson, J.; McGowan, E.; SantaCruz, K.; Guimaraes, A.; Yue, M.; Lewis, J.; Carlson, G.; Hutton, M.; Ashe, K. H., Age-Dependent Neurofibrillary Tangle Formation, Neuron Lass, and Memory Impairment in a Mouse Model of Human Tauopathy (P301L). *J. Neurosci.* **2005,** *25*, 10637-10647.

23. Yue, M.; Hanna, A.; Wilson, J.; Roder, H.; Janus, C., Sex Difference in Pathology and Memory Decline in rTg4510 Mouse Model of Tauopathy. *Neurobiol. Aging* **2011,** *32*, 590-603.

24. Tampi, R. R.; Forester, B. P.; Agronin, M., Aducanumab: Evidence from Clinical Trial Data and Controversies. *Drugs Context.* **2021,** *10*.

25. Yang, E. Y.; Shah, K., Nanobodies: Next Generation of Cancer Diagnostics and Therapeutics. *Front. Oncol.* **2020,** *10*, 1182.

26. Hamers-Casterman, C.; Atarhouch, T.; Muyldermans, S.; Robinson, G.; Hammers, C.; Bajyana Songa, E.; Bendahman, N.; Hammers, R., Naturally Occurring Antibodies Devoid of Light Chains. *Nature* **1993,** *363*, 446-448.

27. Messer, A.; Butler, D. C., Optimizing Intracellular Antibodies (Intrabodies/Nanobodies) to Treat Neurodegenerative Disorders. *Neurobiol. Dis.* **2020,** *134*, 104619.

28. Li, T.; Bourgeois, J.-P.; Celli, S.; Glacial, F.; Le Sourd, A.-M.; Mecheri, S.; Weksler, B.; Romero, I.; Couraud, P.-O.; Rougeon, F.; Lafaye, P., Cell-Penetrating Anti-GFAP VHH and Corresponding Fluorescent Fusion Protein VHH-GFP Spontaneously Cross the Blood-Brain Barrier and Specifically Recognize Astrocytes: Application to Brain Imaging. *FASEB J.* **2012,** *26*, 3969-3979.

29. Danis, C.; Dupré, E.; Zejneli, O.; Caillierez, R.; Arrial, A.; Bégard, S.; Mortelecque, J.; Eddarkaoui, S.; Loyens, A.; Cantrelle, F.-X.; Hanoulle, X.; Rain, J.-C.; Colin, M.; Buée, L.; Landrieu, I., Inhibition of Tau Seeeding by Targeting Tau Nucleation Core Within Neurons with a Single Domain Antibody Fragment. *Mol. Ther.* **2022,** *30*, 1484-1499.

30. Dupré, E.; Danis, C.; Arrial, A.; Hanoulle, X.; Homa, M.; Cantrelle, F.-X.; Merzougui, H.; Colin, M.; Rain, J.-C.; Buée, L.; Landrieu, I., Single Domain Antibody Fragments as New Tools for the Detection of Neuronal Tau Protein in Cells and in Mice Studies. *ACS Chem. Neurosci.* **2019,** *10*, 3997-4006.

31. Henry, K. A.; MacKenzie, C. R., Antigen Recognition by Single-Domain Antibodies: Structural Latitudes and Constraints. *MABS* **2018,** *10*, 815-826.

32. Fiedler, J. D.; Brown, S. D.; Lau, J. L.; Finn, M. G., RNA-Directed Packaging of Enzymes Within Virus-Like Particles. *Angew. Chem. Int. Ed.* **2010,** *49*, 9648-9651.

33. Sulima, A.; Jalah, R.; Antooline, J. F. G.; Torres, O. B.; Imler, G., H.; Deschamps, J. R.; Beck, Z.; Alving, C. R.; Jacobson, A. E.; Rice, K. C.; Matyas, G. R., A Stable Heroin Analogue That Can Serve as a Vaccine Hapten to Induce Antibodies That Block the Effects of Heroin and Its Metabolites in Rodents and That Cross-React Immunologically with Related Drugs of Abuse. *J. Med. Chem.* **2018,** *61*, 329-343.